Generation and Storage of Ultrashort Pulses Using Optical Fiber Devices

by

David John Jones

M. Phil., University of Cambridge (1994)

B.S., Swarthmore College (1993)

B.A., Swarthmore College (1993)

Submitted to the Department of Electrical Engineering and Computer Science
in partial fulfillment of the requirements for the degree of
Doctor of Philosophy in Electrical Engineering
at the
Massachusetts Institute of Technology
February 1999

Signature of Author _____
Department of Electrical Engineering and Computer Science October 7, 1998

Certified by _____
Hermann A. Haus.
Institute Professor
Thesis Supervisor

Certified by _____
Erich P. Ippen.
Elihu Thompson Professor of Electrical Engineering
Professor of Physics
Thesis Supervisor

Accepted by _____
Arthur Smith
Chairman, Departmental Committee on Graduate Students

Generation and Storage of Ultrashort Pulses Using Optical Fiber Devices

by

David John Jones

Submitted to the Department of Electrical Engineering and Computer Science on October 7, 1998 in partial fulfillment of the requirements for the degree of

Doctor of Philosophy in Electrical Engineering

Abstract

Three different types of optical fiber devices were investigated for this thesis: actively mode-locked fiber lasers, optical fiber ring buffers, and passively mode-locked fiber lasers. Intra-cavity soliton compression was employed in an actively mode-locked fiber laser to reduce the pulse width by a factor of 4.4 below the pulse widths predicted by standard active mode-locking theory. Stability regions for these solitons were mapped out and compared to theoretical predictions. In the second device the dynamics of a 5 Gbit/sec packet of ONES and ZEROS loaded into a phase-modulated optical fiber ring buffer were experimentally investigated. A new mode of operation was explored where the cavity length of the buffer was slightly detuned from the modulation frequency that was driving the phase modulator. An investigation into the conditions for successful loading and the storage behavior was performed. In addition, relaxation oscillations, which have affected the storage time of previous high-speed optical ring buffers, were nearly eliminated with a CW holding beam, and significantly enhanced storage times were obtained. Investigations of passively mode-locked fiber lasers included both soliton and stretched-pulse implementations. Two different versions using the soliton configuration were studied; in both cases a waveguide amplifier was used to provide gain, allowing short cavity lengths. A polarization additive-pulse-mode-locked version generated 116-fs, 130 pJ solitons at a repetition rate of 130 MHz. Preliminary work was also completed on a second short cavity soliton laser with a semiconductor saturable absorber mirror as the mode-locking mechanism. Using the stretched-pulse cavity design, an environmentally-stable fiber laser was demonstrated to generate 1.8 nJ pulses that were compressible to sub-100 fs. 980-nm pumping requirements for this laser were only 200 mW. Lastly, the first observation and characterization of resonant sideband formation in stretched-pulse fiber lasers was completed. Experimental results were evaluated in conjunction with numerical simulations and a theoretical analysis.

Thesis Supervisor: Hermann A. Haus
Title: Institute Professor

Thesis Supervisor: Erich P. Ippen
Title: Elihu Thompson Professor of Electrical Engineering
Professor of Physics

For Michelle

your presence, support, encouragement ... your love, patience ...Thank you Michelle

I cannot begin to express my gratitude and appreciation.

Acknowledgements

I am grateful to both Prof. Haus and Prof. Ippen for giving me the opportunity to work in their research group. Prof. Haus' enthusiasm is highly motivating. His insights are simply amazing and he patiently explained them to me until I understood his ideas. I admire Prof. Ippen's ability to analyze situations with clear and concise models. I have learned a considerable amount from Prof. Ippen's approach toward science. It has been exhilarating to work with both of them.

Dr. Katie Hall graciously lent me space in her lab to do some experiments and provided her advice and expertise when I was struggling to set-up a new experiment or to interpret some data. She even agreed to act as a reader for my thesis! I thank her for also being a great friend when I needed support.

Over the course of my thesis work, I have had the opportunity to work with a number of inspiring individuals from the Optics group. Lynn Nelson gave me a superb example on how to organize both the lab itself as well as my lab book. I became much more productive once I followed her lead and got organized. She was also a good friend, helping me through all of my qualifying exams. Thanks for your friendship Lynn. Last year, I had a productive time working with Shu Namiki just prior to his departure. Recently, I had the pleasure of working with Erik Thoen and Dr. Franz Kärtner. Erik showed me that he (and thus by extension, myself) could always be in a good mood, no matter what the situation. And I always seemed to learn something from Franz every time I spoke with him. Thanks to other past and present Optics group members as well: Dan Ripin, Dr. Brent Little, Pat Chou, Dr. Nanda Ramanujam, Dr. Brett Bouma, Boris Golubovic, and Igor Bilinsky (aka Guy).

Thanks to Cindy for always being willing to help me out. Her tireless work for everyone in the group is quite refreshing. Thanks to Donna as well. Marilyn Pierce in the Graduate Office has been a big help guiding me through the degree requirements, late registrations, and just listening to my various predicaments.

Prior to my arrival at MIT, there were four people who were highly influential in both getting me to MIT and finishing this degree: Mike Cole and Scott MacDonald cultivated an ethic of hard work and a desire for excellence within myself; Saul Benjamin pushed me, beyond what I found familiar and comfortable, into the unknown and toward a higher level; and Prof. Lynne Molter introduced me to optics and continually supported me through my struggles at Swarthmore College and MIT.

My immediate family has been supportive, including my brother Aaron and brother-in-law Ian both of whom could always show me the lighter side of life. Throughout everything over the 10 years, the one fundamental constant in my life has been my wife Michelle. Thank you for your tireless support, for believing in me when no one else did (including myself), and for sticking with me throughout. I am forever grateful.

Contents

List of Figures

Chapter 1

Introduction

The availability of low-loss optical fiber [1], combined with the development of diode-pumped optical fiber amplifiers operating at 1.5 μm [2], has revolutionized telecommunications. Researchers broke the 1 Tbit/s transmission capacity barrier early in 1998 using conventional technology [3], [4]. Work in optical transmission systems has spurred research in supporting devices such as all-optical switches, wavelength multiplexers, sources and receivers. Several semiconductor-based components have been successfully demonstrated including laser diode pump sources, high-speed laser diode signal sources [5], wavelength routers [6] and multi-wavelength sources [7] among others. Fiber-based devices utilizing passive fiber, erbium-doped fiber, and active semiconductor devices capable of performing high-speed all-optical switching [8], [9], wavelength conversion [10], 100 Gbit/s all-optical multiplexing and demultiplexing, [11], and rate conversion [12] have also been developed.

The focus of this thesis is upon three different types of optical fiber devices: harmonically mode-locked fiber lasers, passively mode-locked fiber lasers, and optical fiber storage rings. Harmonically mode-locked fiber lasers with pulse repetition rates ranging from 1 GHz to beyond 20 GHz are potential sources in both wavelength-division multiplexed (WDM) [13] and time-division multiplexed (TDM) [14] optical communication systems. Their low-jitter, high repetition rates pulse streams can also be used as a clock for high-speed sampling systems [15]. Passively mode-locked fiber lasers generally have much shorter pulse widths and significantly lower repetition rates (approximately 50 MHz) than harmonically mode-locked fiber lasers. As a result, their direct application to optical communication systems is limited although the broad spectrum of a short pulse fiber laser has been used as a spectrally-spliced source for a 206 channel WDM system [16]. Rather, the attributes of this type of mode-locked fiber laser, including low noise, high peak power (up 20 kW), broad bandwidths (nearly 80 nm), compactness, and diode-pumped nature,

make it a valuable diagnostic tool for development of devices for optical communications, such as those cited previously, as well as fundamental studies in both in the time domain [17] and spectral domain [18]. The third device investigated for this thesis was an all-optical storage fiber ring buffer capable of storing packets of high-bit rate data. This type of buffer is expected to play a key role in next-generation ultrafast TDM networks [14].

1.1 Overview of Thesis

The remainder of this thesis is organized as follows: an overview of some fundamental characteristics of optical fiber that are relevant to ultrashort pulses is given in Chapter 2 including gain from erbium-doped fiber and waveguides, group-velocity dispersion, self-phase modulation and the soliton effect. The next four chapters constitute the main body of this thesis. In Chapter 3, an experimental study of soliton compression in harmonically mode-locked fiber lasers is presented. Experimental results from this investigation are compared with theoretical predictions. This chapter also motivates work on harmonically mode-locked fiber lasers and provides background on previous work. An investigation of an asynchronously phase-modulated fiber ring buffer is reported in Chapter 4. By employing a CW holding beam to suppress relaxation oscillations, a 0.5 kbit, 5 Gbit/s packet could be stored for at least 160 μs. In addition, asynchronous phase modulation relaxed the cavity and modulation tolerances necessary for successful storage, yet still provided crucial noise cleanup. Next, two different types of passively mode-locked fiber cavities based on an erbium-ytterbium waveguide amplifier are discussed in Chapter 5. In the first cavity design, polarization additive-pulse mode-locking (P-APM) is used to generate 116-fs solitons from a ring cavity. Preliminary investigations on cavities employing semiconductor saturable absorbers as the mode-locking element are also reported. Chapter 6 contains two studies of stretched-pulse fiber lasers. First, an environmentally stable version of the stretched-pulse fiber laser is presented. With 980-nm diode-pumping levels of 200 mW, this laser was able to generate 1.2-nJ pulses with 50 nm of spectra that can be externally compressed to sub-100 fs. Pulse dynamics in this laser are also studied. In the latter portion of Chapter 6, the first observation of resonant sideband formation in a stretched-pulse fiber laser is reported. Experimental results are compared with theoretical predictions and numerical simulations. Finally, concluding remarks are given in Chapter 7.

Chapter 2

Review of Fundamentals for Optical Fiber Devices

In this chapter a few of the basic attributes of optical fiber and erbium-doped fiber are briefly reviewed. As this thesis reports work on ultrashort pulse optical fiber devices, these characteristics will be presented within the context of short pulses. For a more in-depth discussion on these topics, the reader is referred to a number of excellent references [19], [20], [21], and [22].

2.1 Erbium-Doped Fiber

Optical amplification in optical fiber was first demonstrated as early as 1961 with a neodymium-doped device [23]. Compared to present-day optical fiber, the fiber available at that time was quite lossy (1000 dB/km) which limited both the performance and possible applications from fiber lasers and other fiber devices. By 1970 improvements in the optical fiber fabrication process reduced the loss to 20 dB/km [24]. Accompanying work in fiber lasers resulted in a demonstration of a Nd-doped fiber laser pumped by a semiconductor diode laser source [25]. Following the realization of extremely low-loss (0.2 dB/km) optical fiber in 1979 [1], research into rare-earth-doped fiber lasers and fiber amplifiers increased at a dramatic pace. Driven by the demands of optical communications systems, the research focus shifted toward erbium-doped fiber (EDF) [2] as it provides gain at 1.5 μm, a wavelength region that is within the window of lowest loss for silica fiber. In this thesis, research was centered exclusively on devices operating at 1.5 μm using both erbium-doped fiber and erbium-ytterbium co-coped waveguide amplifiers.

Figure 2-1 illustrates the relevant energy levels, absorption transitions, and signal emissions of erbium doped into a silica host. EDF is typically pumped using one of two different absorption bands that are presently accessible by laser diode sources. InGaAsP devices are utilized for 1480-nm pumping transition while strained quantum well InGaAs devices provide a 980-nm pump source. Pumping with 980 nm offers higher gain and a lower noise figure as it is easier to reach

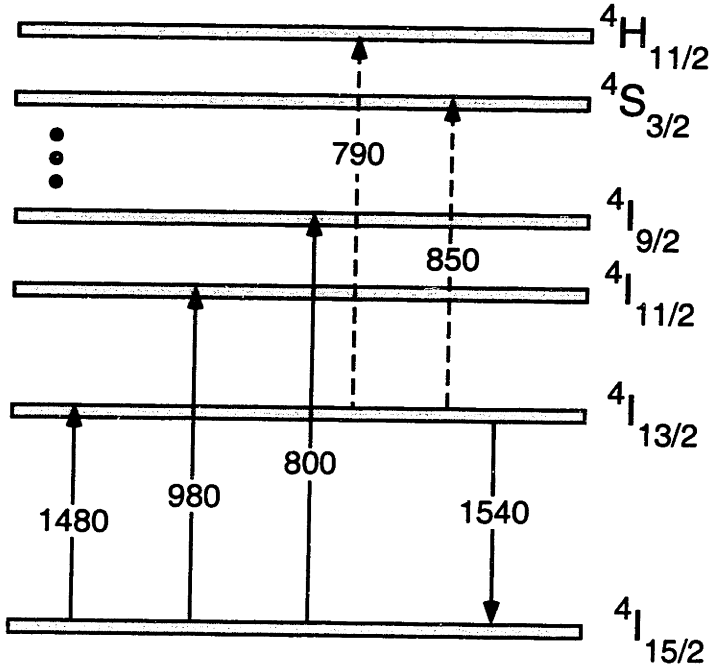

Figure 2-1: Energy transition levels in erbium-doped silica. All transitions are given in nanometers. Dashed lines indicated excited state pump absorption when an 800-nm pump is used.

inversion in a three level system as compared with a 1480-nm pumped two level system [19]. A third transition at 800 nm can be pumped using GaAlAs devices. Diode sources at this wavelength offer a number of practical advantages such as high power, established fabrication technology, and low cost. However, excited-state (pump) absorption from the $^4I_{13/2}$ level to the $^4S_{3/2}$ and $^4H_{11/2}$ levels significantly decreases the power conversion efficiency and this pumping transition is not normally utilized. For the devices reported in this thesis a 978-nm Master-Oscillator Power Amplifier (MOPA) laser diode was used as the pump source. The MOPA generated up to 1 W of power in free space with typically 65 to 70 % of the power coupled into a single mode fiber.

The 980-nm and 1480-nm diode sources discussed above normally have a single transverse mode for efficient coupling into fiber. This characteristic is a factor that limits the amount of available pump power for diode- and MOPA-pumped EDF. To address this shortcoming, two additional pumping techniques have been developed. By sensitizing the erbium with other rare-earth co-dopants, additional pumping transitions are created, thereby enabling absorption transitions at

wavelengths available from high-power solid-state lasers while still obtaining gain at 1.5 μm [22]. For example, ytterbium-sensitized erbium-doped fiber can be pumped with Nd:YAG at 1.064 μm or Nd:YLF at 1.053 μm. A second approach uses a double-clad guidance structure in the fiber itself [26]. An inner core is designed to be single mode at the signal wavelength, while an outer core supports multi-mode propagation at the pump wavelength. High-power diode arrays can then be efficiently coupled into this multi-mode (pump) core. Various outer core geometries have been studied in an effort to maximize the pump overlap with the signal [27]. Indeed the highest output power generated from a fiber laser has been produced by Nd-doped double-clad fiber lasers [28], [29].

2.2 Erbium-Ytterbium Codoped Waveguide Amplifier

An Er-Yb codoped planar waveguide amplifier fabricated by Dr. Denis Barbier of GeeO (Grenoble, France) was the second type of gain element used in this thesis. Due to the short length of the waveguide amplifier, a high erbium doping concentration is necessary to obtain a reasonable amount of gain. In this case an erbium doping concentration of 2.0 wt-% was used. At this concentration level, the ionic distribution usually becomes inhomogeneous and the ion-to-ion distance is reduced, allowing a type of ion-ion coupling known as cooperative energy transfer (CET) assisted up-conversion [22], [30]. In CET, neighboring erbium ions exchange energy through non-radiative transitions, significantly reducing the fluorescence lifetime at the 1.5 μm transition. This effect is also known as concentration quenching. As a result, the optical gain decreases abruptly after a certain erbium doping level (approximately 0.12 wt-% in a silica host).

Two steps were taken so that a significantly higher erbium concentration of 2.0 wt-% could be doped into the waveguide amplifier. First, phosphate (rather than silica) was used as the host in the waveguide which accepts a higher dopant concentration before the ionic distribution becomes inhomogeneous [31]. In addition, following a standard technique another rare-earth element, ytterbium, was also doped into the phosphate host. In this case, the ytterbium was included, not to enable additional pumping wavelengths as discussed in the previous section, but rather to reduce the erbium ion-ion interaction by physically surrounding them with ytterbium ions [32]. Surrounding the erbium ions with ytterbium has an additional advantage; ytterbium ions excited by 980-nm pump photons are able to transfer their energy (via a photon-assisted exchange) to the

erbium's $^4I_{11/2}$ energy level. The energy diagram for erbium-ytterbium is illustrated in Fig. 2-2. In

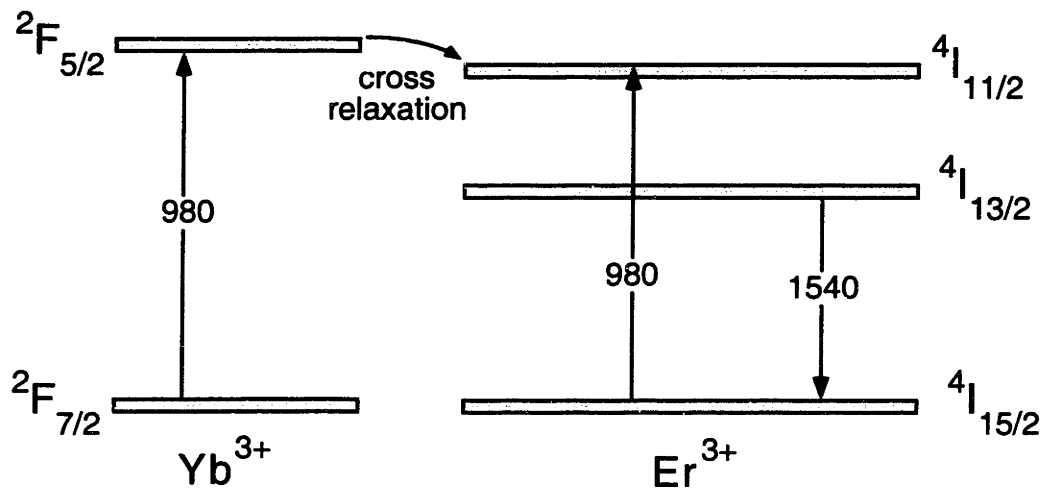

Figure 2-2: Energy levels of erbium-doped silica sensitized with ytterbium. All transitions are given in nanometers. Through cross-relaxation processes, the Yb^{3+} $^2F_{5/2}$ level transfers energy to the Er^{3+} $^2I_{11/2}$ level. In the waveguide amplifier discussed in Section 2.2, this codoped composition is used to take advantage of the additional pumping mechanism and to allow a higher Er^{3+} doping concentration.

comparison to erbium, ytterbium has an absorption cross-section at 980 nm that is 25 % larger [33]. This indirect pumping arrangement complements the direct pumping of erbium and enables excitation of a large percentage of erbium ions over a small pump interaction length. All of these attributes enable the 4.5 cm long waveguide to deliver a small signal gain of 14 dB with 120 mW of 980-nm pump power [34]. To obtain this level of gain from EDF a fiber length of least 1 m is usually necessary. The remaining details of the waveguide amplifier such as fabrication procedure and specific performance levels are discussed in Section 5.2

2.3 Group-Velocity Dispersion

Group-velocity dispersion (GVD) occurs when refractive index is a function of wavelength (or frequency). Physically, this causes different wavelengths to travel at different speeds. In optical fiber, there are two contributions to the total GVD: material (or chromatic) dispersion and waveguide dispersion. The material dispersion is caused by an interaction of the electromagnetic field with the bound electrons of the silica glass. In particular, oscillations of these electrons and their characteristic resonant frequencies result in a frequency-dependent response for the electro-

magnetic field. At frequencies far from resonance, the material dispersion can be accurately modeled using Selemeier equations [35]. Waveguide dispersion is the result of a wavelength-dependent propagation constant which is intrinsic to the guidance properties of a waveguide. The waveguide dispersion for optical fiber can be determined by finding the propagation constant of LP_{01} mode in a cylindrically symmetric waveguide [20].

To quantify the amount of dispersion, the propagation constant, β, is normally expanded in a Talyor series around a central frequency ω_o,

$$\begin{aligned}\beta(\omega-\omega_o) &= \beta_o+\frac{\partial\beta}{\partial\omega}(\omega-\omega_o)+\frac{1}{2}\frac{\partial^2\beta}{\partial\omega^2}(\omega-\omega_o)^2+\frac{1}{6}\frac{\partial^3\beta}{\partial\omega^3}(\omega-\omega_o)^3+\ldots \\ &= \beta_o+\beta'(\omega-\omega_o)+\frac{1}{2}\beta''(\omega-\omega_o)^2+\frac{1}{6}\beta'''(\omega-\omega_o)^3+\ldots\end{aligned} \tag{2-1}$$

where β' is the group velocity, β'' is the group-velocity dispersion and β''' is the third-order dispersion. In optical fiber β'' is usually quoted in units of ps^2/km. Dispersion can also be specified as D in units ps/nm/km. β'' and D are related by,

$$D = -\frac{2\pi c}{\lambda^2}\beta'' \tag{2-2}$$

where c is the speed of light in a vacuum and λ is the center wavelength of the pulse.

When a pulse propagates through a dispersive optical fiber, different spectral components travel at different speeds, causing the pulse to temporally broaden. Figures 2-3 (a) and (b) illustrate this effect. Normal (anomalous) dispersion occurs when the sign of β'' is positive (negative) and lower (higher) spectral frequencies are pushed to leading edge of the pulse. The frequency of the electric field becomes as a function of time delay across the pulse and thus the pulse acquires

a frequency chirp. In this spectral domain, the propagation equation can be solved exactly yielding,

$$a(\omega, z) = a(\omega, 0)\exp\left[-\frac{j}{2}\beta''\omega^2 z\right] \tag{2-3}$$

where $a(\omega, z)$ is the spectral envelope of the pulse measured from the carrier frequency ω_o.

Both the net cavity dispersion as well as the local dispersion are critical parameters when constructing short pulse fiber devices. The value of dispersion for various types of fiber used in this thesis were numerically calculated from fiber specifications (such as core size, index difference, etc.) using a Mathematica program written by Kohichi Tamura when he was a graduate student at MIT [36]. These theoretical values were then compared to an experimental measurement of the net dispersion in the fiber laser cavities. The experimental dispersion value was determined using method of Knox [37]. In this procedure the fiber laser is set to run in a CW operation. Next, the CW wavelength is tuned either by adjustment of an intra-cavity filter or waveplates. At each wavelength the change in repetition rate is measured by monitoring a higher-order cavity harmonic on an RF spectrum analyzer. From this data the net cavity dispersion can be determined from [37],

$$\frac{\partial T}{\partial \lambda} = L_c D \tag{2-4}$$

where L_c is the total cavity length and the roundtrip time T,

$$T = \frac{n}{\nu} \tag{2-5}$$

where n is the order of the cavity harmonic measured and ν is the harmonic frequency. All of the net cavity dispersion values quoted in this thesis were measured using this method. In order to remain consistent with commonly used notation, in the following chapters the net average dispersion of a cavity is denoted as $\Delta k''$ while the local fiber dispersion is expressed as k_o''.

It is also possible to introduce dispersion by a prism sequence or a set of grating pairs [38], [39]. In this case, the prisms and gratings are used to spatially separate different wavelengths and the dispersion originates from a physical path length difference for different wavelengths. In Chapter 6 prism sequences and grating pairs are used to add amounts of dispersion in both intracavity and external applications.

2.4 Kerr Effect in Optical Fiber

Fused silica has a centrosymmetric structure, so in optical fiber the lowest-order, non-zero nonlinear susceptibility is $\chi^{(3)}$. Through $\chi^{(3)}$ a number of nonlinear processes are possible including field-induced second harmonic generation, third harmonic generation and four-wave mixing. As all of these processes involve generation of new frequencies, specific measures to obtain phase-matching are normally required for their observation. However, a fourth nonlinear process known as the optical Kerr effect which is enabled by $\chi^{(3)}$ does not have any phase matching requirements. The Kerr effect which includes self-phase modulation (SPM) and cross-phase modulation (XPM), is the dominate nonlinear process in optical fiber. The Kerr effect causes the refractive index to become nonlinear,

$$n(\omega, t) = n_o(\omega) + n_2 I(t) \tag{2-6}$$

where n_o is the linear index of refraction, n_2 is the nonlinear index coefficient and the $I(t)$ intensity of the electric field. Recent measurements give $n_2 \approx 2.2 - 3.4 \times 10^{-20}$ m^2/W [19] for fused silica which is not particularly strong. However, two characteristics of optical fiber, the small mode-field size (roughly 30 μm^2), which creates high intensities, and a potentially long interaction length, enable the expression of the Kerr effect with reasonable pulse energies.

2.4.1 Self-Phase Modulation

Due the intensity dependent refractive index, a pulse that propagates through an optical fiber acquires a nonlinear phase shift,

$$a(t, z) = a(t, 0)\exp[-j\delta|a(t, 0)|^2 z] \tag{2-7}$$

with δ, the SPM coefficient, equal to,

$$\delta = \frac{2\pi n_2}{\lambda A_{eff}} \tag{2-8}$$

where λ is the free space wavelength and A_{eff} is the effective, cross-sectional area of the mode inside the fiber. Table 2-1 summarizes the parameters (including the SPM and GVD coefficients)

Table 2-1: Calculated parameters for various fibers used in this thesis at 1.55 μm. MFD, mode field diameter; A_{eff} effective mode area; δ, SPM coefficient; β'', group-velocity dispersion; β''', third order dispersion.

Fiber Type	MFD (μm)	A_{eff} (μm^2)	δ ($kW^{-1}m^{-1}$)	β'' (ps^2km^{-1})	β''' (ps^3km^{-1})
SMF-28	8.9	62.2	1.5	-22	+0.126
FlexCor 1060	5.4	22.9	4.2	-7	+.102
Er^{+3} (1128)	3.9	12.0	8.0	+75	-0.108
Er^{+3} (1128-2)	3.1	7.5	12.8	+105	-0.235

for the different types of fiber used in this thesis.[1]

Note in eqn. (2-7) as the pulse propagates through an optical fiber, the pulse remains invariant in magnitude and temporal shape. However, the phase of the pulse acquires a time-dependent frequency (or chirp) due to a variation in the pulse intensity. Figure 2-3(c) illustrates this effect. The sign of n_2 in optical fiber causes the pulse to obtain a positive chirp.

2.4.2 Solitons

Under proper conditions the negative chirp due to anomalous dispersion can be exactly balanced with the positive chirp caused by SPM and a pulse can propagate with a static temporal envelope and zero chirp. This type of pulse is known as a soliton [41], [42] and its existence in optical fiber was first predicted in 1973 by Hasagawa and Tappert [43]. The first experimental

1. These fiber parameters were compiled by Lynn Nelson [40].

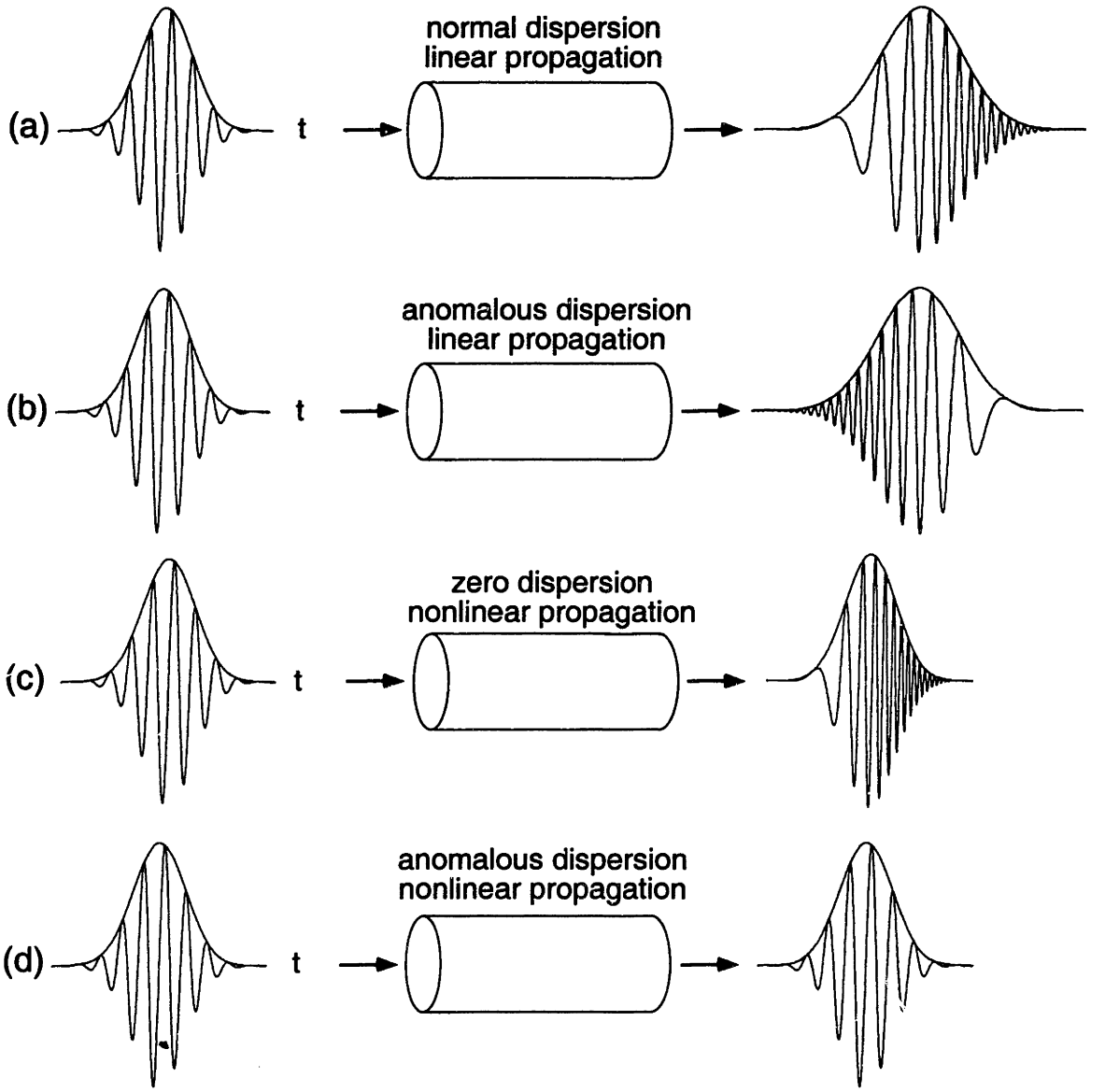

Figure 2-3: Pulse after traveling through a fiber with (a) linear propagation and normal dispersion (causing temporally broadening and a positive frequency chirp); (b) linear propagation and anomalous dispersion (causing temporally broadening and a negative frequency chirp); (c) nonlinear propagation and no dispersion (causing a positive frequency chirp); (d) nonlinear propagation and anomalous dispersion. In this last case, the chirps induced by anomalous dispersion and nonlinearity can balance each other allowing a soliton to exist.

observation of a soliton in optical fiber was made in 1980 by Mollenauer [44]. Mathematically, the solution of the propagation equation,

$$-j\frac{\partial a}{\partial z} = \frac{\beta''}{2}\frac{\partial^2 a}{\partial t^2} - \delta|a|^2 a \tag{2-9}$$

yields the specific pulse shape of a optical fiber soliton,

$$a(t, z) = A\,\mathrm{sech}\left(\frac{t}{\tau_s}\right)\exp\left[j\frac{\beta''}{2\tau_s^2}z\right] \tag{2-10}$$

where τ_s the soliton pulse width ($1.76\tau_s = \tau_{FWHM}$). The soliton area theorem relates the pulse characteristics to parameters of the fiber,

$$A\tau_s = \sqrt{\frac{|\beta''|}{\delta}} \tag{2-11}$$

Solitons have a number of other mathematical attributes and the reader is referred to an extensive set of references [45], [46] and [47]. Similar to solitons in long-distance transmission systems [48], solitons generated by mode-locked fiber lasers behave under an "averaged" soliton model which is slightly different from the precise mathematical definition of a soliton. In this thesis, additional characteristics of solitons that are relevant to mode-locked fiber lasers are discussed in Chapter 3 and Chapter 5

2.5 Polarization Additive-Pulse Mode-Locking

In most of the passively mode-locked fiber lasers reported in this thesis, the mode-locking mechanism employed was polarization additive-pulse mode-locking (P-APM). P-APM uses nonlinear polarization rotation in optical fiber to create an artificial saturable absorber. In this section a overview of the physics behind P-APM will be presented. For a more mathematical analysis the reader is referred to a number of thorough treatments of P-APM [36], [49].

The optical Kerr effect in optical fiber causes nonlinear polarization rotation when the initial polarization state is elliptical [50]. The polarization ellipse can be resolved into a basis of right-

and left-hand circular polarization components with different intensities. These two circular components then accumulate different nonlinear phase shifts due to the nonlinear intensity dependence of the refractive index as the signal propagates down the fiber. This phase differential between the orthogonal components leads a rotation of the polarization ellipse while the ellipticity and handedness are maintained. The angle of rotation is proportional to,

$$\Phi(t) \propto \delta l I(t) \tag{2-12}$$

where l is the length of propagation, δ is the SPM coefficient, and $I(t)$ is the intensity.

In the case of a pulse, there is an inhomogeneous polarization ellipse rotation across the pulse, resulting from the variation in the intensity of the pulse itself. Figure 2-4 illustrates how intensity-

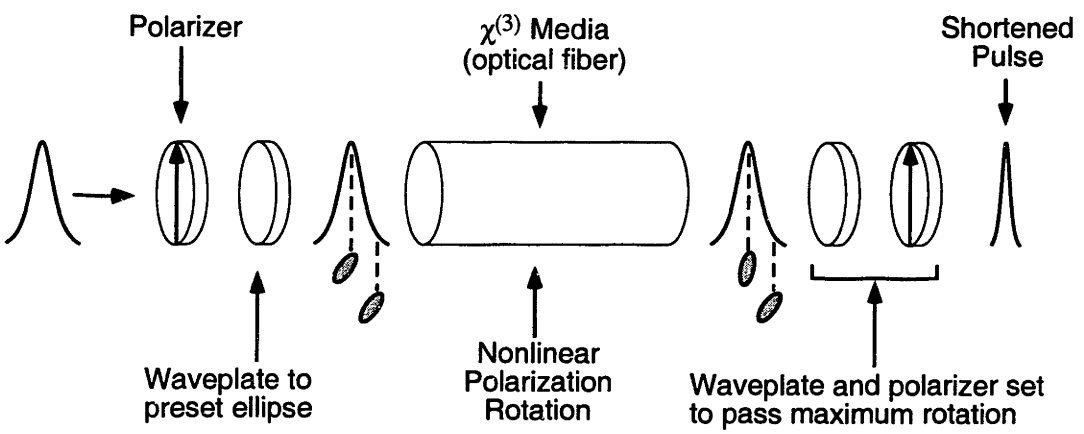

Figure 2-4: Construction of a saturable absorber using nonlinear polarization rotation.

dependent ellipse rotation can be used in conjunction with polarization optics to create an artificial saturable absorber, an element that absorbs low intensities but is bleached by and transmits high intensities. Early proposals utilized this functionality as an intensity discriminator to clean up pulse pedestals from a fiber soliton compressor [51] and as an optical soliton limiter [52]. By incorporating this mechanism directly into a fiber laser cavity, a mode-locked fiber laser can be created [53], [49]. As it relies on a coherent addition of two pulses which have a nonlinear differential phase shift, this mode-locking technique is a form of additive-pulse mode-locking (APM) [54], [55] hence the name polarization APM (P-APM).

In addition to P-APM, passively mode-locked fiber lasers have also been demonstrated using nonlinear amplifying loop mirrors (NALM) [56], [57] and semiconductor saturable absorbers [58], [59]. A NALM is typically used in a so-called figure-8 cavity where two loops of fiber are connected with a coupler. The lower loop has an isolator and thus is unidirectional, while the upper section is used as a Sagnac fiber interferometer. A length of EDF is placed asymmetrically inside the Sagnac section which causes the two counter-propagating pulses to pick up a differential phase shift (via SPM). After circulating through the Sagnac loop, the pulses interfere at the connecting coupler. With a proper bias the NALM reflects high intensities into the proper direction of the isolator in the lower loop. Pulses as short as 98 fs have been obtained from a fiber laser using a NALM [60]. A review of the work using semiconductor saturable absorbers in fiber lasers is given in Section 5.4.

Chapter 3

Soliton Stability in Actively Mode-locked Fiber Lasers[2]

Actively mode-locked fiber lasers are leading candidates for sources in optical communication systems because high quality pulses centered at 1.55 μm can be locked to a master clock at high repetition rates (> 1 GHz) with low timing jitter. Mode-locking is generally achieved using a high-speed intra-cavity electro-optic modulator and typical cavity lengths are usually > 1 meter due to the limited doping concentrations of Er^{+3} in silica fiber. Accordingly, to obtain a high pulse repetition rate, the modulator must be driven at a harmonic of the round-trip cavity frequency to produce multiple pulses in the cavity. If the fundamental cavity frequency is Ω_c and the modulation frequency is $\Omega_M = N\Omega_c$, the laser is mode-locked at the Nth harmonic with N pulses in the cavity. This means that an axial mode is locked to every Nth mode falling within the gain bandwidth, forming a so-called supermode [63].

Early work on harmonically mode-locked fiber lasers revealed two major difficulties: fluctuations in the pulse energy and stabilization requirements of the cavity length. In this chapter both of these characteristics are reviewed along with various solutions reported in the literature. Pulse widths generated by these lasers are typically 2 to 20 ps in duration. In order to shorten the pulses, a number of researchers have pursued intra-cavity pulse compression using soliton effects with varying degrees of success. In Sections 3.2 and 3.3 of this chapter the stability region for soliton generation in an actively mode-locked fiber laser is experimentally mapped out and compared with theoretically predictions.

---

2. Portions of this chapter appear in [61] and [62].

3.1 Review of Harmonically Mode-locked Fiber Lasers

3.1.1 Pulse Energy Stabilization

Actively mode-locked fiber lasers were first demonstrated using Nd^{+3}-doped fiber [64], [65] and Er-Yb-doped fiber [66] with pulse widths > 70 ps at the fundamental cavity repetition rate. Harmonic mode-locking was achieved by [67], [68] but the lasers suffered from pulse-to-pulse energy fluctuations. This unfortunate result is caused by the slow ≈ 10 msec relaxation time of the Er^{+3}-gain, which does not respond rapidly enough on the time scale of the pulse spacing (≈ 1 nsec) to stabilize pulse energy variations. Pulse energy fluctuations are equivalent to a simultaneous oscillation of more than one supermode and can be diagnosed by examining the RF spectrum of the pulse train. A supermode suppression of greater than 45 to 50 dB is generally considered acceptable for optical communication sources. Bit-error-rate testers can also be used to examine the uniformity of the pulse trains.

Stabilization of pulse energies is clearly required before harmonically mode-locked fiber lasers can be used in optical communication applications. One solution is the introduction of a sub-cavity with a free spectral range that matches the modulation frequency [69], [70]. Energy stabilization is achieved because a portion of each pulse in injected into successive pulses, injection locking the pulse train optically. The major disadvantage of this method is that it requires interferometric stabilization of the sub-cavity with respect to the modulation frequency and the main cavity.

A second, more appealing approach uses a passive, fast intensity-dependent loss mechanism. In this technique, an intra-cavity nonlinear element causes more intense pulses to experience higher loss. As long as the nonlinearity can recover to its initial state before the next pulse arrives (i.e., it is fast), the pulse intensities become clamped to a common value.

The first application of this technique used nonlinear polarization rotation [71]. As described in Section 2.5, APM in fiber lasers uses nonlinear polarization rotation to create an artificial fast saturable absorber. By suitable adjustment of the APM (interference) bias, it is possible to impose intensity limiting on the pulses, or Additive-Pulse-Limiting (APL). In the initial demonstration, APL was used to stabilize a 1-GHz pulse train, producing a supermode suppression of roughly 50

dB. APL is dependent on the nearly instantaneous Kerr effect, so it could be safely scaled to much higher repetition rates.

Recently, a second technique using self-phase modulation (SPM) and spectral filtering to obtain a fast intensity-dependent loss was reported [72], [73]. In this case a more intense pulse generates a broader spectrum through SPM. An intra-cavity spectral filter then causes a higher-intensity pulse (with wider spectrum) to experience greater loss than a lower intensity. In this manner an optimum pulse bandwidth, and thus a standard pulse intensity, is imposed on the pulse train. As this method does not rely on polarization effects, it can be used in polarization-maintaining (PM) fiber lasers.

3.1.2 Frequency and Cavity Stabilization

Another remaining difficulty with harmonically mode-locked fiber lasers is thermal drift of the cavity length. The variation of the refractive index with respect to temperature in silica fiber is,

$$\frac{\partial n}{\partial T} = 1.1 \times 10^{-5}/^{\circ}C \tag{3-1}$$

With a typical fiber laser length of 50 m, a ring cavity length will fluctuates by 0.55 mm/$^{\circ}C$. If the modulation is at the $N = 2000th$ harmonic, this translates to a cavity frequency fluctuation of around 60 kHz/$^{\circ}C$ about an 8-GHz modulation frequency. Accordingly, slight thermal variations are able to cause the pulses to lose synchronism with the modulator. Typically for stable operation the mismatch between the modulation and cavity frequencies must be < 5 kHz. A number of techniques have been reported to compensate for thermal drift.

The most obvious stabilization scheme is a dynamic adjustment of the cavity length [74]. A portion of the fiber in the cavity is wound around a piezo-electric drum. By driving the drum with the correct feedback signal, the cavity length can be adjusted to keep the cavity frequency synchronous with the fixed modulator drive frequency. A second solution uses regenerative feedback where the modulation frequency is derived directly from the pulse train [75]. Any change in the cavity length automatically adjusts the modulation frequency to maintain pulse-modulator synchronism. In a third solution the modulation frequency is fixed and the cavity dispersion is suffi-

ciently high such that the pulses can remain synchronous with the modulator by shifting in wavelength [76].

An alternate approach abandons the requirement of pulse-modulator synchronism [77]. Anomalous dispersion fiber is used throughout the cavity in this fiber laser to provide strong soliton shaping, and the active mode-locking element is a phase modulator that is purposely detuned from a cavity harmonic. When mode-locked, the resulting pulse train has a repetition rate that deviates 15 to 30 kHz from the modulation frequency. Asynchronous phase modulation produces a sinusoidal frequency shift [78], which normally would destroy any pulses. Solitons, however, are able to fight the frequency shift [79] and remain intact. This type of asynchronous modulation is described in more detail in Section 4.3.2.

3.2 Intra-cavity Soliton Pulse Compression

Sources of subpicosecond pulses are being evaluated for two primary ultra-high bit rate communication systems applications: Time-Division Multiplexing (TDM) and Wavelength-Division Multiplexing (WDM). Pulse widths of approximately 1 ps are inherently required in 100 Gbit/s TDM systems [14]. For a WDM architecture, the broad spectrum of a subpicosecond pulse can be used as a high-repetition-rate, spectrally-sliced source [13]. As determined by Kuizenga and Siegman [80], the pulse width produced by active mode-locking is inversely proportional to the geometric mean of the mode-locking frequency and the bandwidth of the medium (or filters) in the resonator. Using typical parameters of fiber lasers, this expression predicts pulses widths to be 2 to 20 ps. Pulses generated from stabilized harmonically mode-locked fiber lasers confirmed this prediction [70]. For harmonically mode-locked fiber lasers to be used in either ultra-high bit rate TDM or WDM applications, the pulse widths must be reduced.

In order to shorten the pulses the fiber medium naturally invites the use of self-phase modulation (SPM) [81] or the soliton effect through a combination of SPM and anomalous group velocity dispersion (GVD) [82]. Pulse shortening with SPM was first demonstrated in an actively mode-locked Nd^{+3}-doped fiber laser [83]. Soliton shaping was initially demonstrated in an Er^{+3}-doped fiber ring laser [67]. Similar results were also attained in Er^{+3}-doped fiber lasers with an InGaAsP semiconductor amplifier [84] and with phase modulators [85], [86]. The theoretical results of [81]

were extended by Kärtner *et al* [87] (and indirectly in [88]) who showed that a sufficiently large amount of anomalous GVD and SPM should suppress the normal mode-locked state enough to allow formation of a solitary pulse that is considerably shorter than the normal actively mode-locked pulse. The central idea is that the soliton parameters of the cavity, rather than the modulator characteristics, determine the pulse width.

Successful shortening of actively mode-locked pulses by soliton compression must satisfy the following two conditions: 1) The solitons must be successfully re-timed on each round trip. 2) There must be discrimination between the soliton state and the normal actively mode-locked state. The former condition of pulse re-timing is a practical matter of maintaining synchronism between the modulator and the pulse train and is addressed in the previous section on cavity drift. Following the analysis in reference [88], the latter condition can be quantified by calculating the loss of the soliton and the loss of a fundamental Gaussian pulse, which is the eigen-solution of the active mode-locking equation (with no nonlinearity) [80]. If the soliton state is to remain stable, the Gaussian pulse (the eigen state of linear active mode-locking) must possess a higher loss than that of the soliton. The resulting condition is,

$$\frac{\pi^2}{24}M\Omega_m^2\tau_s^2+\frac{1}{3L_c\Omega_f^2\tau_s^2}<\mathrm{Re}\sqrt{\frac{1}{2}M\Omega_m^2\left[\frac{1}{L_c\Omega_f^2}-j\frac{\Delta k''}{2}\right]} \tag{3-2}$$

where M is the modulation index per unit length, Ω_m is the modulation frequency, τ_s is the soliton pulse width, Ω_f is the filter bandwidth, L_c is the cavity length, and $\Delta k''$ is the average group velocity dispersion of the cavity. On the left side is the loss experienced by the soliton, and on the right side is the loss of the Gaussian mode-locked pulse.

In addition, the modulation must not drive the soliton unstable. From soliton perturbation theory [89], energy fluctuations of the soliton are damped if,

$$\frac{\pi^2}{8}M\Omega_m^2\tau_s^2<\frac{1}{L_c\Omega_f^2\tau_s^2} \tag{3-3}$$

After fulfilling these two conditions, the pulse width is now specified by the soliton condition,

$$\tau = \frac{2|\Delta k''|}{W\delta} \tag{3-4}$$

where W is pulse energy and δ is the SPM coefficient defined in Section 2.4.1.

3.3 Experimental Investigation of Soliton Stability

The fiber laser used to investigate soliton compression of actively mode-locked pulses is shown in Fig. 3-1. The laser was constructed entirely of PM fiber, including the WDM coupler and out-

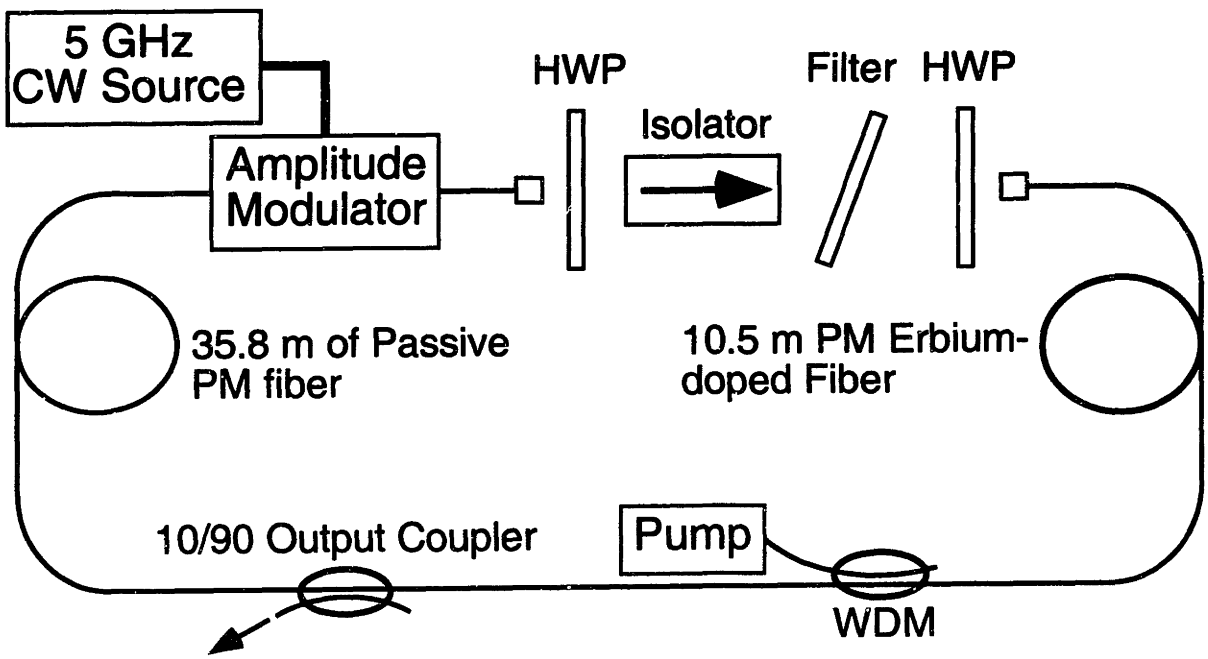

Figure 3-1: Actively mode-locked fiber laser using all polarization-maintaining fiber. WDM, wavelength division multiplexer; PM, polarization maintaining; HWP, half-wave plate.

put coupler, to eliminate any nonlinear polarization rotation, *thereby excluding any artificial saturable absorber action (APM/APL) that could contribute to the pulse shortening and soliton stability.* The average dispersion $\Delta k''$ of the cavity was measured to be -10 ps^2 km^{-1}. Approximately 500 mW of a 978-nm MOPA pump was coupled into the WDM. An open air section in the

ring facilitated placement of different optical filters in the cavity. A fiber-pigtailed $LiNbO_3$ waveguide amplitude modulator was the active mode-locking element.

When the modulation strength was adjusted to satisfy both eqns. (3-2) and (3-3), a soliton pulse train was generated. The optical spectra of the solitons for various filter bandwidths in this operating regime are displayed in Fig. 3-2. The shortest soliton observed was 634 fs; it was

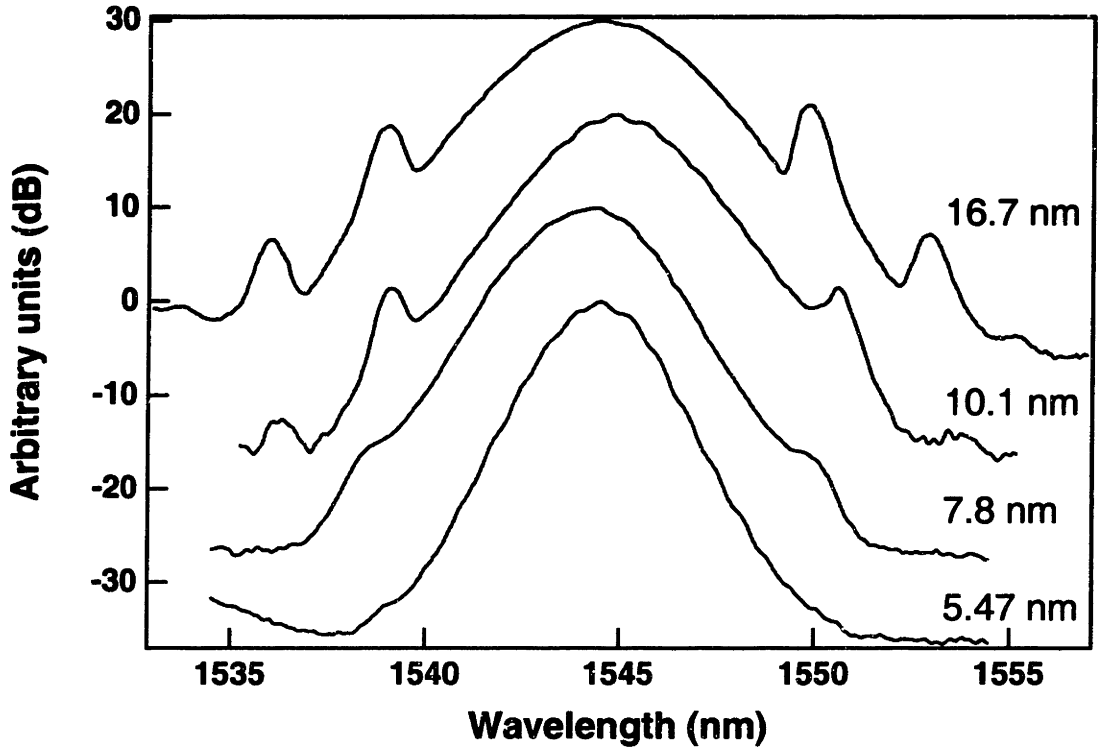

Figure 3-2: Series of soliton spectra generated by the actively mode-locked fiber laser shown in Fig. 3-1 using four different filter bandwidths. The pronounced resonant sidebands (see Section 5.1.1) confirm the pulses are indeed solitons.

obtained with 7.8-nm filter, a filter bandwidth that is narrow enough to loosen the pulse-width clamping effects of resonant sidebands (see Section 5.1.1) but not too narrow to limit the overall spectra bandwidth [90]. An intensity autocorrelation of these solitons is shown in Fig. 3-3. The 634-fs pulse width represented a pulse width shortening by a factor of 4.4 over the standard active mode-locked pulse width and these pulses are the shortest actively harmonically mode-locked pulses generated directly from a fiber laser to date.

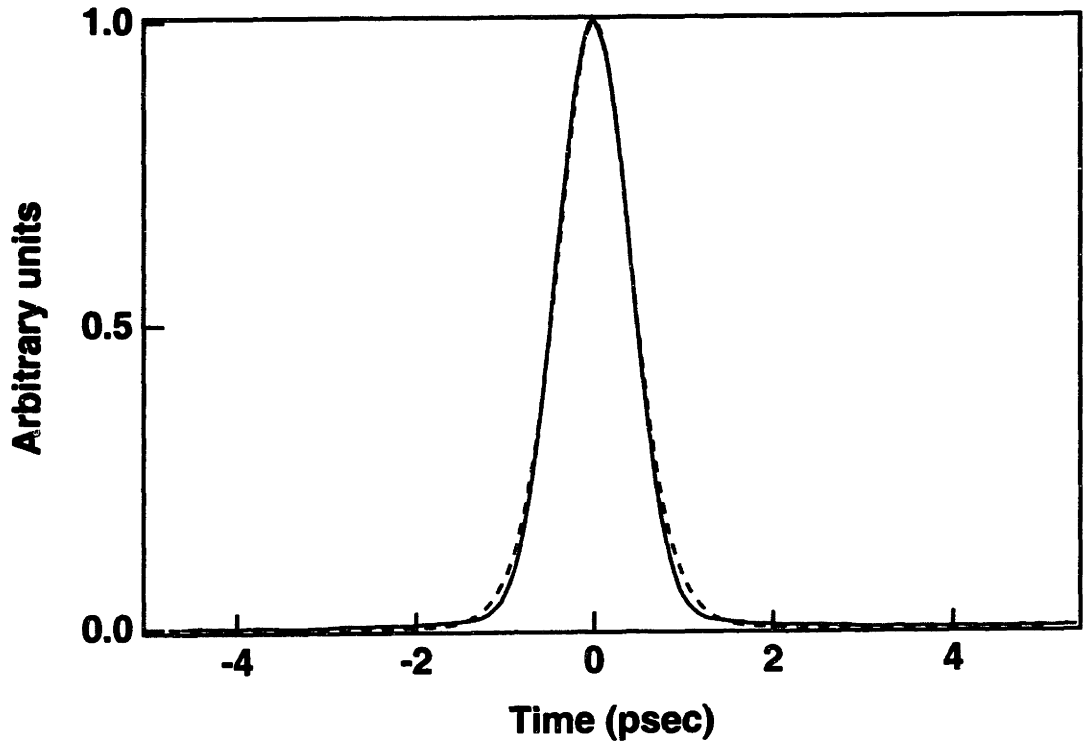

Figure 3-3: Intensity autocorrelation of a pulse train generated by active mode-locked fiber laser shown in Fig. 3-1 with a 7.8-nm filter. A sech fit (dashed curve) to the trace gives a FWHM pulse width of 634 fs.

Kärtner et al [87] has presented a theory quantifying the possible soliton compression of a pulse in an actively mode-locked laser. An expression for the possible pulse shortening factor can be found by rewriting eqn. (3-2),

$$\xi^2 - 3\mathrm{Re}\left\{\sqrt{1-j|\Delta k''|L_c\Omega_f^2}\right\}\xi + \frac{\pi^2}{4} < 0 \qquad (3\text{-}5)$$

with $\xi = (\tau_a/\tau_s)^2$ where τ_a is the 1/e intensity width of the unchirped Gaussian pulse width and τ_s is the soliton (sech) pulse width. ξ is a measure of the possible pulse width reduction. A direct comparison of the full-width at half-maximum pulse width is,

$$R = \frac{1.66}{1.76}\sqrt{\xi} \tag{3-6}$$

Using the parameters of this fiber laser, eqns. (3-5) and (3-6) predict a maximum pulse shortening factor of $R = 2.2$ while the experimentally observed compression factor was $R = 4.4$. This latter value was found by comparing the shortest soliton produced (634 fs at $\Omega_m = 5$ GHz, a filter bandwidth of 7.8 nm, $L_c = 46$ m, $\Delta k'' = -10$ ps^2, and $M = 0.25$) with the theoretically calculated pulse width [87] for an unchirped Gaussian pulse using these parameters. The disagreement between the theoretical and experimental pulse reduction factor is most likely due to uncertainties in the experimental parameters.

There is a simple physical viewpoint describing the shortening process. Increasing the dispersion serves to spread out (via a frequency chirp) any low-level pulse in the time domain. The broadened pulse is then is clipped by the modulation envelope. In this manner, the loss for the Gaussian pulse grows as dispersion is increased. A pulse with high enough peak power experiences the nonlinearity, allowing it remain chirp-free (and remain narrow) via the soliton effect. Consequently, it is able to pass through the modulator with lower loss. In this manner, the loss for the solitary pulses is not affected by the dispersion, allowing them to become the preferred (lowest loss) state of the system. It is important to realize the laser initially needs to produce pulses with high enough peak power so the pulses are affected by the nonlinearity and then can evolve into (shorter) solitary pulses.

As described above, the stability region for the solitons lies between the two curves of eqns. (3-2) and (3-3) and is shown in Fig. 3-4. For experimental observation of this regime, a series of different interference filters with varying bandwidths (5.47, 6.18, 7.80, 10.1, 11.0, 12.2, and 16.7-nm) were placed inside the cavity. The horizontal lines represent the explored regions at particular filter bandwidths. Autocorrelation traces for specific operating points, indicated by circles and

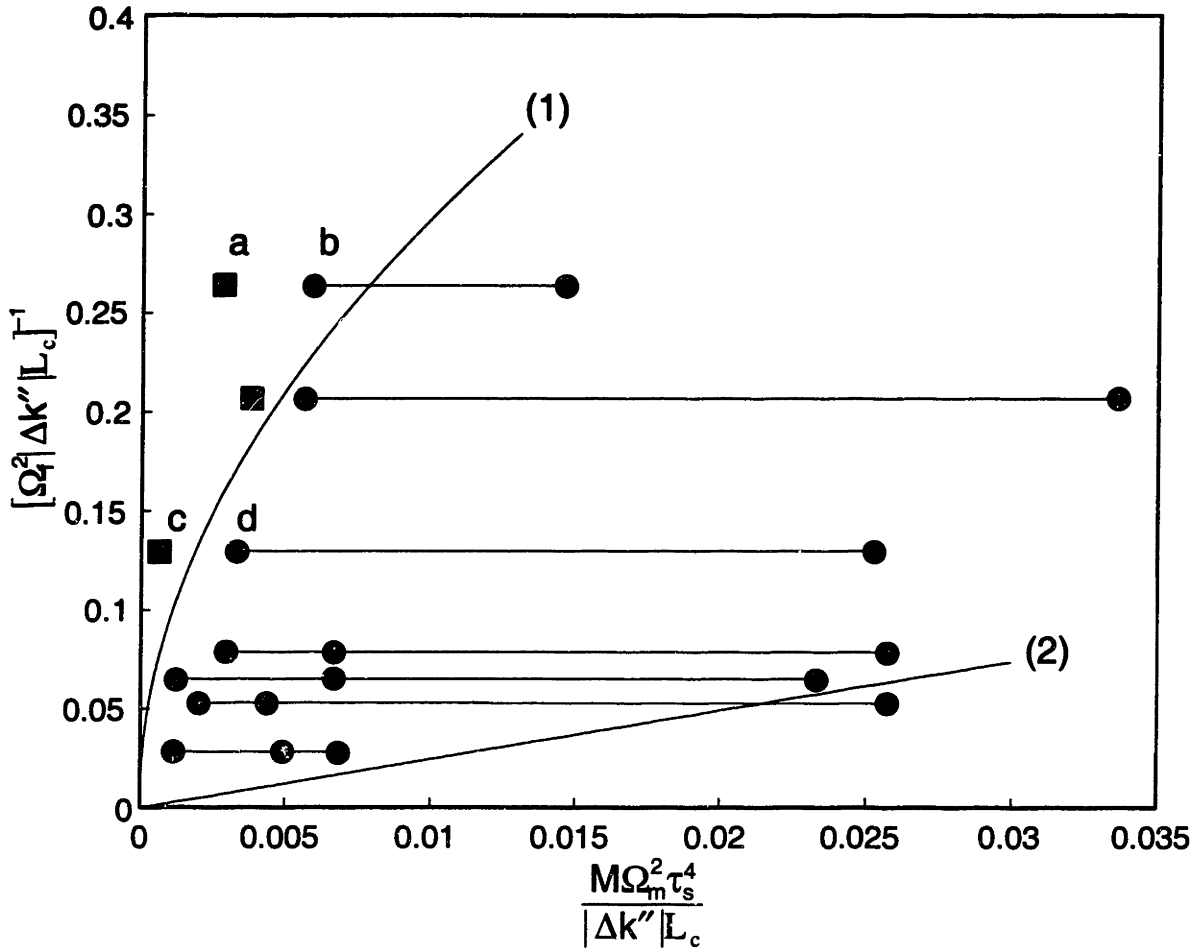

Figure 3-4: Stability region of solitons with the boundary curves (1) and (2) predicted by eqns.(3-2) and (3-3), respectively. The explored operating regions at different filter bandwidths are given by horizontal lines. The circles signify clean soliton operation. The squares indicate a mixture of solitons and Gaussian (mode-locked) pulses.

squares, are shown in Fig. 3-5. The circles represent operating points where clean solitons circulated in the cavity. No pedestal was observed on the autocorrelation trace at these points. The abscissa contains the soliton pulse width to the fourth power. Hence for every filter bandwidth each point on the plot was located by using the value of the modulation strength and experimentally observed soliton pulse width under constant cavity dispersion. The pulse widths varied between 635 fs and 1.2 ps depending on the filter bandwidth and the modulation strength. The squares represent operating points that showed a mixture of Gaussian pulse shapes and solitons.

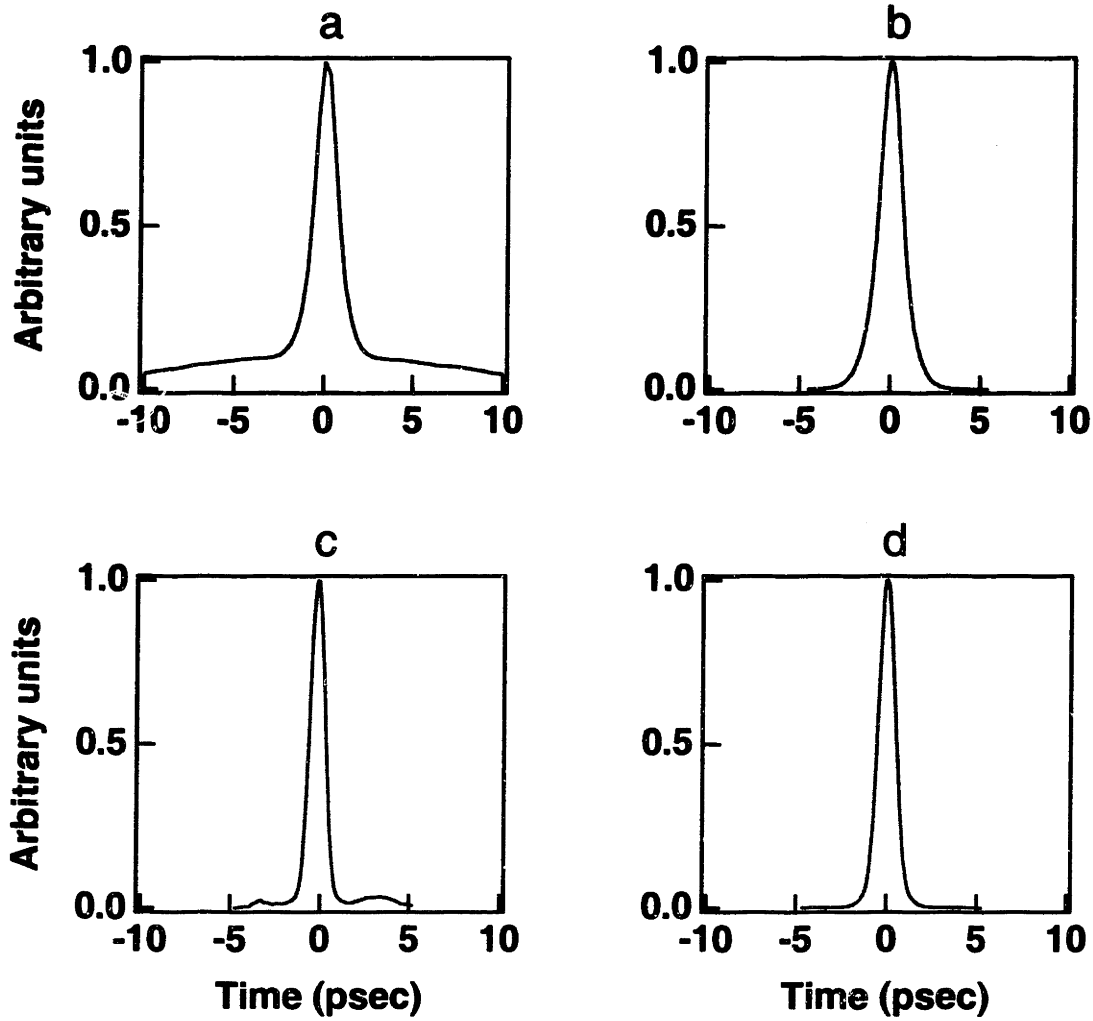

Figure 3-5: A series of autocorrelation traces referenced in Fig. 3-4 showing the transition between normal mode-locked pulses and solitons. Note the pedestals due to the competing Gaussian pulses in traces (a) and (c).

These points were unstable according to the stability criterion predicted by eqn. (3-2) because there was too little discrimination between the Gaussian pulse and the soliton.

A typical RF spectrum of the pulse train is given in Fig. 3-6 displaying a supermode suppression of only 15 dB. As discussed in Section 3.1.1, this level of supermode suppression indicates variation of the pulse energies in the pulse train and is not acceptable for optical communication sources. In the present laser, soliton parameters serve to quantize the pulses, so poor supermode

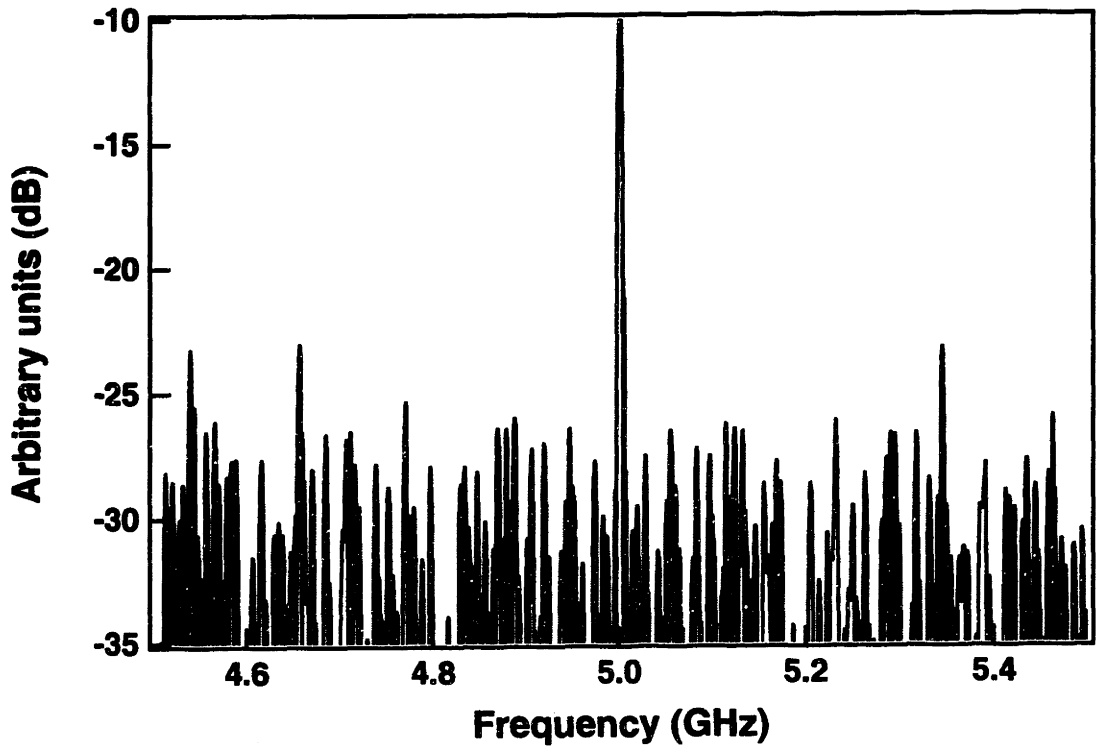

Figure 3-6: RF spectrum of soliton pulse train. The supermode suppression of only 15 to 20 dB indicates variations in pulse energies along the pulse train.

suppression actually means that the available gain was not sufficient to place a soliton in every available time slot. A calculation with the estimated intra-cavity power and the soliton energy indicates that approximately one-half to two-thirds of the time slots were filled with soliton pulses.

Chapter 4

Asynchronous Phase-modulated Optical Fiber Ring Buffer[3]

It is expected that a key component for ultra high-speed optical time-division multiplexed (OTDM) networks will be an optical buffer capable of storing packets of high bit-rate (10 to 100 Gbit/sec) data [14]. Packet storage at the (high-speed) bus rate before hand-off to lower speed electronics offers a number of networking advantages. In these types of applications the maximum amount of storage time is expected to be < 1 ms. An optical fiber ring utilized as a storage device could be capable of fulfilling these storage requirements and, due to its fiber nature, offers easy integration into an optical network.

In this chapter recent progress in the development of this type of optical fiber buffer is reviewed in Section 4.1. Limits in the packet storage time of this type of buffer as well as synchronization requirements are described in Section 4.2. Experimental results from a new buffer design are reported in Section 4.3. Significantly enhanced storage times are obtained by employing a CW holding beam to control relaxation oscillations and a new mode of operation is explored where the cavity round-trip frequency of the buffer is slightly detuned from the frequency driving the intracavity phase modulator.

4.1 Previous Demonstrations of Optical Fiber Ring Buffers

One of the simplest designs for an optical fiber ring buffer is a loop containing only an optical amplifier and an input/output coupler. Such an implementation was reported to store a 312 bit, 622 Mbit/sec Non-Return to Zero (NRZ) packet for a maximum of 100 circulations (0.8 ms) [92].

3. Portions on this chapter appear in [91].

After 40 circulations, bit error rates (BER) on the stored packets exceeded BER $>10^{-9}$. These errors were most likely caused by buildup of ASE in the ZERO time slots.

In 1992 it was shown theoretically that a fiber ring of net anomalous dispersion containing gain, an amplitude modulator and a filter could maintain indefinitely a Return to Zero (RZ) bit-pattern of ONES (solitons) and ZEROS (empty time intervals) [88]. Figure 4-1 illustrates a typical

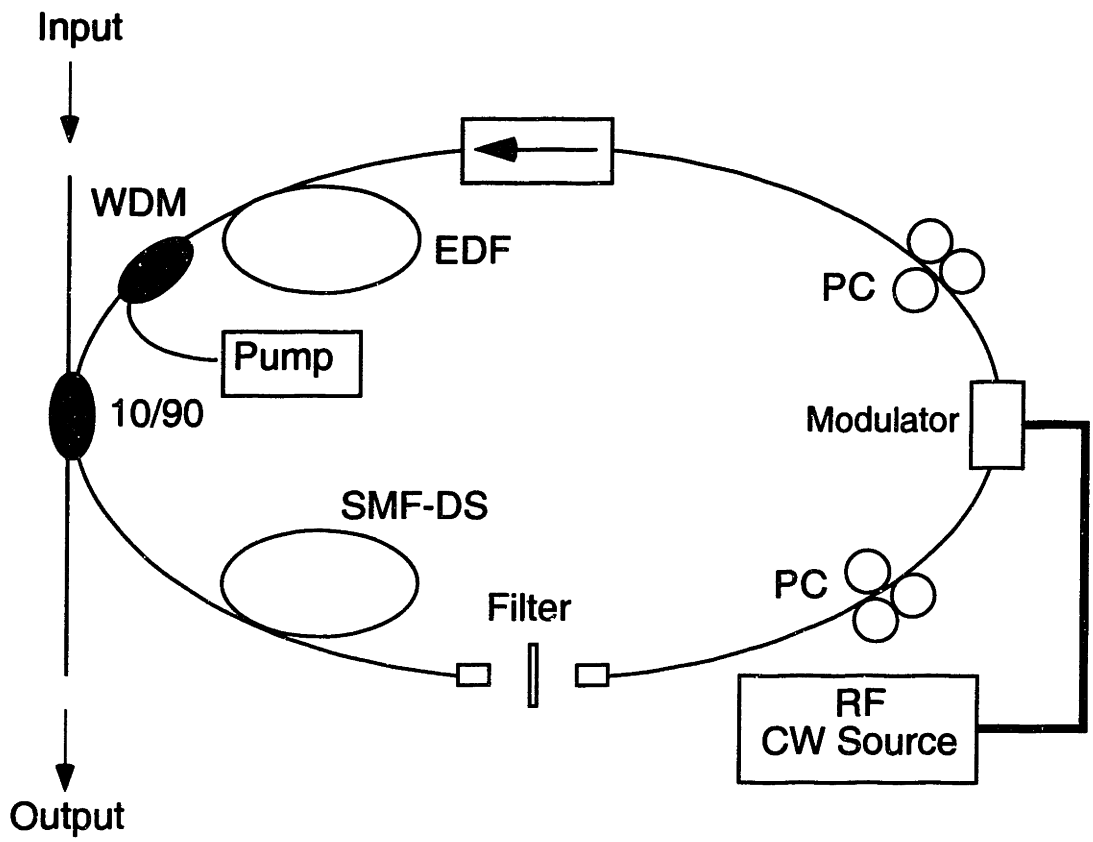

Figure 4-1: Typical design of optical fiber ring buffer. Packets are loaded into buffer via a 10/90 passive coupler (this could also be a 2x2 electro-optic switch). The output is taken from this same coupler after every packet circulation. The net dispersion of the cavity is chosen to be slightly anomalous. EDF, erbium-doped fiber; SMF-DS single mode fiber dispersion-shifted; WDM, wavelength-division multiplexers; PC, polarization controller.

experimental construction for this type of optical fiber ring buffer. Packets of data are loaded into the buffer via an input/output passive coupler or a 2x2 electro-optic switch. The packets then circulate around the cavity and the stored data can be accessed at each round-trip. Due to filtering and amplitude modulation, the ONES (or solitons) in the packet require a certain amount of excess

gain to be preserved. Under the proper combination of dispersion, filtering, and modulation this amount of excess gain is not enough to compensate the loss experienced by the linear noise. As a result, the linear-level radiation in the ZERO time slots can remain attenuated while, simultaneously, the solitons (ONES) are sustained. The stability region for successful pattern storage (when the buffer uses an amplitude modulator) is identical to the soliton stability regime discussion in Section 3.2 and shown in Fig. 3-4. The combination of these two conditions predicts the possibility of long-term storage of high-speed bit packets and was first confirmed experimentally in a 1 Gbit/sec system with a 66 bit storage capacity [93] and a storage time on the order of minutes. Attempts to scale the data rate to 50 Gbit/sec and increase the storage capacity to 4 kbits have been successful [94], [95], although storage times in these high-speed buffers have not exceeded approximately 31.5 μs or 320 circulations. It should be noted that in these experimental implementations (and subsequent work discussed below) the benefits of P-APM (described in Section 2.5) are utilized which greatly assist in noise clean-up in the ZERO time slots.

4.2 Attributes of Current Designs

Two characteristics of previous optical fiber ring buffer designs that have limited their storage times and might limit their possible implementation in high-speed optical networks are relaxation oscillations and synchronization requirements. With reference to the former limitation, this type of buffer is, in essence, an actively mode-locked fiber ring laser which is held below threshold so that pulses can not be created spontaneously. However, if pulses, seeded by ONES in an input packet, are able to build up and survive while suppression of ZEROS is maintained, the buffer can successfully store the packet. Viewed in this light, it is not surprising that loading of packets into the buffer induces relaxation oscillations (RO) [20], a coupled interaction between the intra-cavity optical intensity and the gain of the buffer's erbium-doped fiber amplifier. Initially, when there is no pattern in the buffer, the optical gain is large as it is unsaturated. After a packet is injected into the buffer and begins to circulate, the gain becomes increasingly saturated and steadily decreases from its initial value. The reduced gain, in turn, causes the amplitude of the packets to diminish. The gain then responds by increasing as it becomes less saturated and the process repeats itself. As a consequence, the packets' intensity is modulated as it circulates around the cavity and follows a damped oscillatory trajectory. The RO time constant is the geometric mean of the upper-state lifetime of the erbium-dopant (in the silica host) and the photon life-time in the resonator and

is equal to approximately 1 to 10 μs. This time constant is significantly longer than the round-trip time (100 ns) of a typical buffer. If the RO-induced modulation causes the amplitude of the packets' ONES to fall below a critical level, the discrimination between the ONES and ZEROS is lost and the buffer loses the stored packet. Due to this effect, relaxation oscillations are believed to be one of the main limitations of the storage time for high-speed buffers. As described in Section 4.3.1, significantly enhanced storage times were observed by utilizing a CW holding beam to pin the gain to a steady-state value and reduce RO.

A second possible limitation of optical fiber ring buffers can also be identified from their similarity to actively mode-locked fiber ring lasers. In optical buffers investigated previously, storage is possible only when the modulation drive to the amplitude modulator is adjusted to match a cavity harmonic (or integral sub-harmonic in the case of rational harmonic modulation [95]) to within 1 kHz. This requirement is akin to the requisite frequency and cavity stabilization of harmonically mode-locked fiber lasers that is discussed in Section 3.1.2. Buffers have two additional synchronization requirements: first, both a cavity harmonic and the modulator drive frequency must be equal to the bit-rate of the incoming packet; second, the packets must be loaded into the buffer with the proper phase with respect to the modulation drive.

Recently, the cavity length stabilization requirements of optical storage rings using amplitude modulators has been addressed by replacing the amplitude modulator with pulsed parametric gain [96], although introduction of pulsed phase-sensitive gain introduces its own set of difficulties. This design has been theoretically shown to provide time restoration and amplitude stabilization of the solitons while cleaning up the noise in the ZERO time slots [97]. Using this approach a 32 bit, 29 Mbit/sec packet was stored for 600 circulations (1 ms). A second option, pursued in this thesis, employs a phase modulator, in place of an amplitude modulator, that is driven slightly asynchronously with respect to a cavity harmonic. An asynchronous drive to a phase modulator is able to harmonically mode-lock a fiber laser [77], [78], suggesting that a similar, asynchronous mode of operation should be possible with an optical buffer. When applied to optical buffers, asynchronous phase modulation relaxes the cavity and frequency stabilization requirements and allows the packets to be injected in the buffer at any point in the intra-cavity modulation cycle. Results obtained using this approach, along with its advantages over synchronous modulation, are discussed in Section 4.3.2.

4.3 Optical Fiber Buffer Using a CW Holding Beam and Asynchronous Phase Modulation

The experimental setup used to investigate relaxation oscillations and asynchronous phase modulation is shown in Fig. 4-2. The optical buffer is enclosed within the dotted box while the remaining equipment (described below) is used for packet generation and detection. As in previous optical buffers, additive-pulse mode-locking/additive pulse limiting effects obtained via nonlinear polarization rotation produced a higher loss for the ZEROS than for the ONES, thereby helping to preserve the individual bit amplitudes in the packet. The phase modulator, coupled with a 7.8 nm filter, also served to discriminate between ZEROS and ONES.

A 5 GHz pulse train (with a pulse width of 9 ps) emitted from an actively mode-locked external cavity semiconductor laser (λ_o=1550 nm) was externally modulated by an electro-optic modulator (driven by a pattern generator) to generate 5 Gbit/sec packets with alternating lengths of 250 bits and 500 bits. After a packet was produced, the pattern generator did not produce another packet until the loaded packet propagated in the loop for 1600 circulations. At each round-trip a portion of the packet emerged from the fourth port of the coupler (see Fig. 4-2) and was detected by a high-speed (3-dB bandwidth of 45-GHz) photo-diode. The output signal from the photo-diode was then displayed on either a high-speed (3-dB bandwidth of 50-GHz) sampling oscilloscope to monitor the individual bits in the packet or a lower speed (3-dB bandwidth of 1-GHz) analog oscilloscope to display the packet envelope as it circulated in the buffer.

4.3.1 Reduction of Relaxation Oscillations

The variation in the average power of the circulating packets due to RO can be minimized by optically injecting a CW holding beam [98]. With this technique, either the packet or a CW signal is launched into the buffer. By correctly adjusting the power of the CW signal relative to the average packet power, the injected photon number is conserved, thereby inhibiting any RO. In this experiment a holding beam was generated by driving a gain-switched semiconductor (GSSL) (λ_o=1543 nm) with a square wave that had a period of approximately 160 μs. The phase of the square wave was set using an optical fiber delay line so that just after the holding beam is turned off, a packet is loaded. The holding beam remained off for 80 μs, while the packet circulated in the buffer, and then the holding beam was activated for 80 μs. When the holding beam was acti-

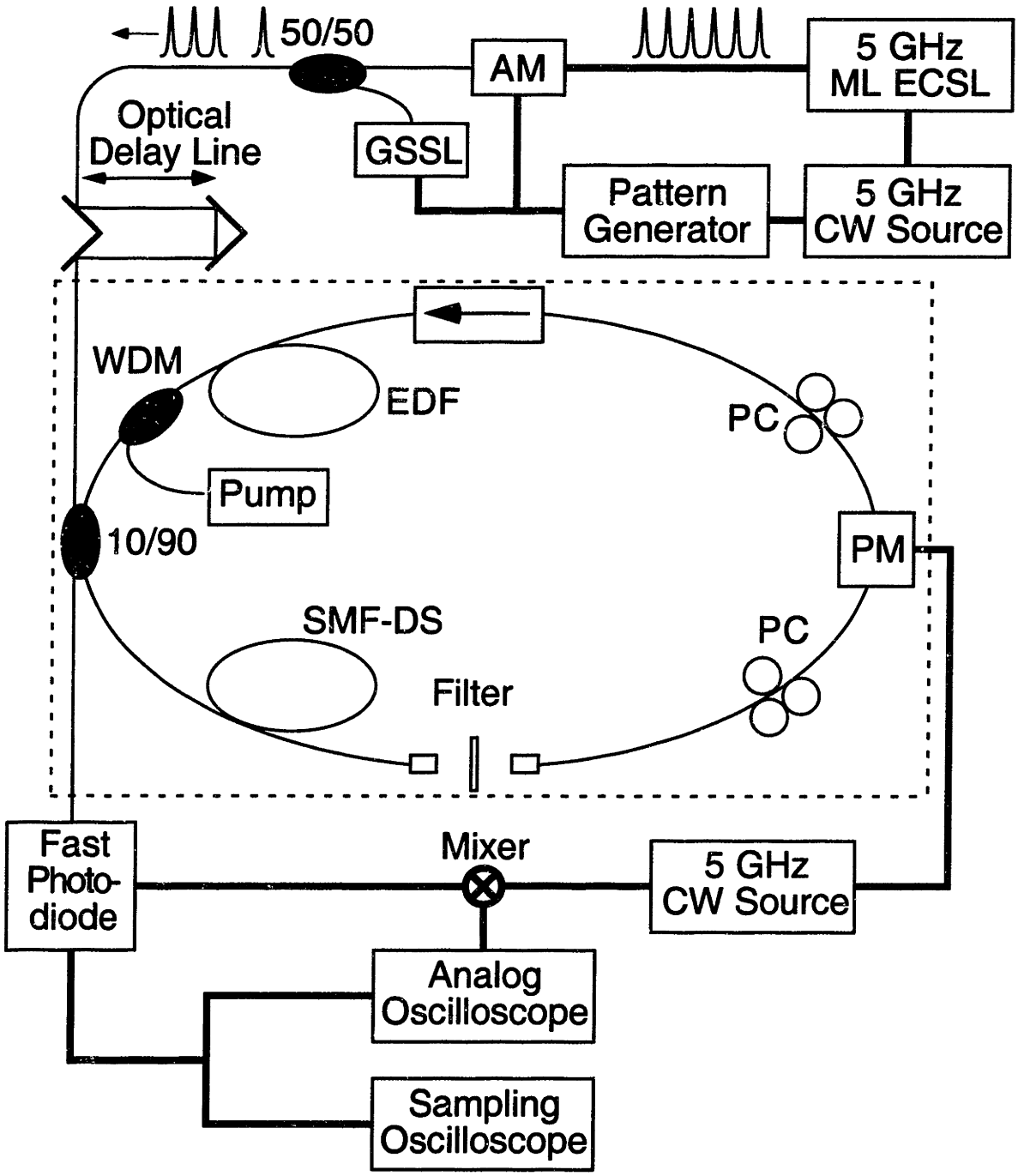

Figure 4-2: Experimental setup for evaluating an asynchronous phase modulated buffer. The buffer is shown in dotted box. Packets of data were placed on pulse train, derived from a mode-locked external-cavity semiconductor laser (ML ECSL), by an amplitude modulator (AM) which was driven by a pattern generator. Packets were loaded into the buffer via the 10/90 coupler. The gain-switched semiconductor laser (GSSL) was utilized as a CW holding beam. EDF, erbium-doped fiber; SMF-DS single mode fiber dispersion-shifted; PM, phase modulator; PC, polarization controller.

vated, the buffer was erased and there was no packet storage during this interval. This input time sequence is illustrated in Fig. 4-3 while the buffer output is shown in Fig. 4-4.

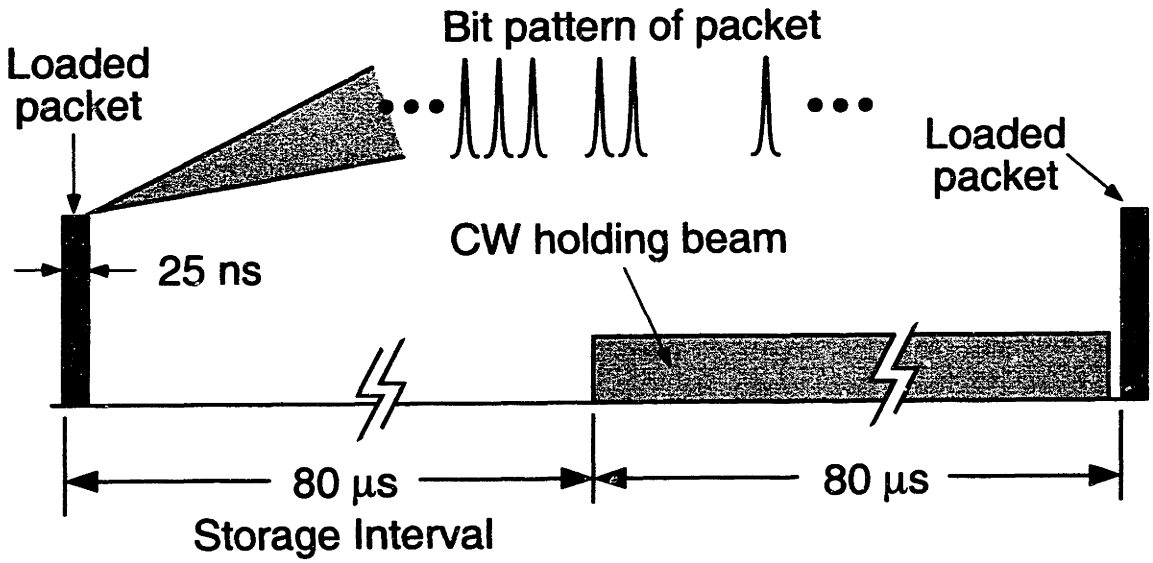

Figure 4-3: Input to buffer showing sequence of packet loading and activation of CW holding beam.

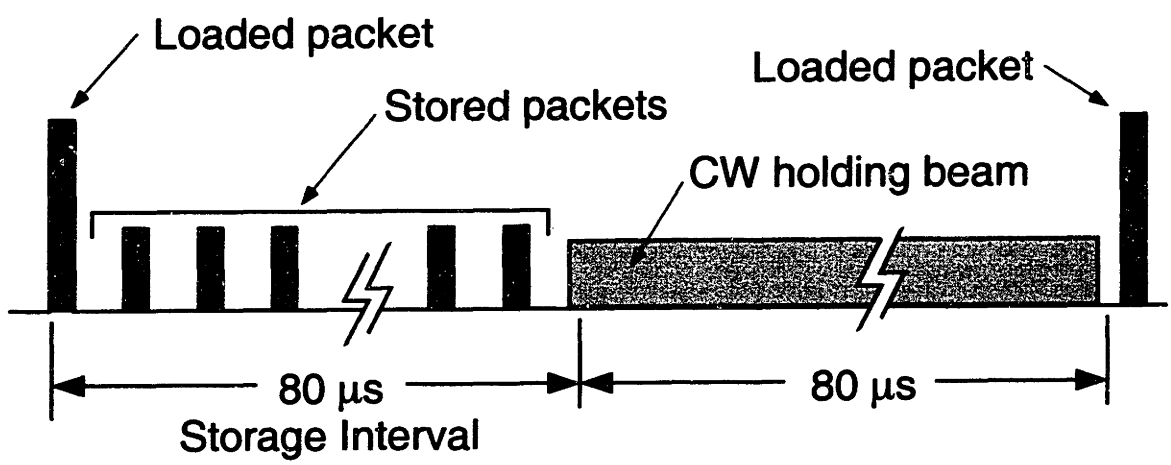

Figure 4-4: Output of buffer displaying one storage interval, followed by activation of CW holding beam. Stored packets emerge from the output port after every circulation. See Fig. 4-5 for actual data illustrating storage behavior.

After proper adjustment of the polarization controllers, the buffer was able to store the loaded packets. Typical storage behavior is given in Fig. 4-5. This photograph was taken from a 1-GHz

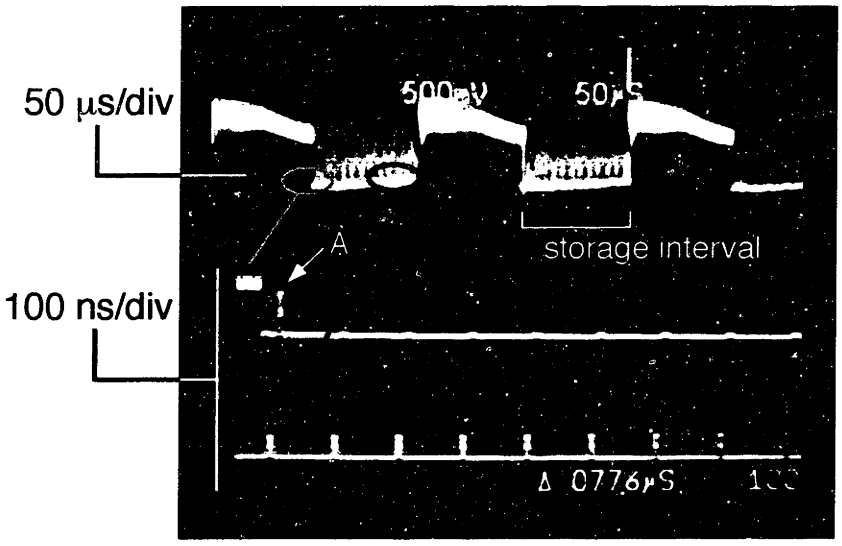

Figure 4-5: Dynamics of stored packets shown on the 1-GHz analog scope with a delaying time-base. Top trace shows long term packet evolution on a 50 μs/div scale. The middle trace, starting from the left, shows the falling edge of the CW holding beam, a packet loading event (point A) and subsequent packet circulations on 100 ns/div scale. The bottom trace is 78.7 μs (800 circulations) after the loading event (again on a 100 ns/div scale). Variations in the packets' amplitude during the storage interval are caused by filtering and asynchronous phase modulation. This attribute is discussed in detail in Section 4.3.2.

analog scope with a delaying time-base. The top trace shows the long-term packet behavior at 50 μs/div with loading events approximately every 160 μs. The square waveform of the holding beam is clearly evident. The holding beam appears much larger than the circulating packets because the holding beam was detected with only 10% tapped off into the loop, while only 10% of the circulating packets were coupled out to the detector. An expanded view is given in the lower two traces at 100 ns/div. As the round-trip time of the buffer was approximately 100 ns, sequential packet circulations can be clearly seen on this time scale. The middle trace displays a packet loading event. At the extreme left the holding beam turns off and 50 ns later a packet was loaded (point A) and begins to circulate in the loop. For the same reason cited above as well as intra-cavity losses, the first packet (point A) is larger than the following, stored packets. The bottom trace (on the same scale) shows the packet envelope after circulating for 78.7 μs (800 round-trips). Clearly, despite the CW holding beam, there is still some amplitude modulation on the

packets during the storage interval. As described in Section 4.3.2, the amplitude fluctuations are caused by a combination of asynchronous phase modulation and filtering. In Fig. 4-5 the envelope of stored packets in the top trace was not as intense as the base-line because the 1-GHz analog scope was attempting to resolve the individual bits in the packet which dispersed the top of the packet envelope.

Compared to earlier high-speed large-capacity buffers [94], the CW holding beam substantially reduced the RO-induced packet modulation and the storage time was significantly expanded. Extending the storage time to 157 μs (1600 round-trips) produced results similar to Fig. 4-5. In this case a strong packet envelope was still present just before the holding beam was activated so storage times longer even than 157 μs seem possible. However, a longer storage time could not be studied because the analog scope was triggered by the packet loading event and it could not operate with a longer trigger period or in a self-triggered mode. In theory the storage time is indefinite, but practical issues such as matching the packets' bits characteristics (such as pulse width) to the natural pulse qualities of the buffer may impose a limit on the total storage time.

Although storage of the packet envelope has been observed for at least 157 μs, it is important to verify maintenance of the individual bits in the packet. A 10 bit portion of the loaded packet displayed on a high-speed sampling scope is given in Fig. 4-6(a), while Fig. 4-6(b) shows the same 10 bit portion after 450 round-trips (44.3 μs). To obtain the trace in Fig. 4-6(b) the sampling oscilloscope was triggered at the loading event and the delay was set to 44.3 μs. The apparent widening of the pulses in Fig. 4-6(b) was caused by oscilloscope timing jitter due to the long time delay after the trigger event. Jitter was confirmed as the source by programming the pattern generator to generate an initial packet and a second packet after a delay of 44.3 μs and then observing the optical output of the amplitude modulator driven by the pattern generator (see Fig. 4-2) on the sampling oscilloscope. This procedure bypassed the buffer but still had an equivalent trigger delay. In this case the packet at zero-time delay was similar to Fig. 4-6(a) while a trace of second (delayed) packet is displayed in Fig. 4-7. Clearly there is pulse broadening similar to Fig. 4-6(b), verifying oscilloscope jitter as the origin of the pulse broadening. In addition, the oscilloscope failed to hold its trigger beyond this time delay, preventing an observation of a high-speed stored packet trace past a storage time of 44.3 μs.

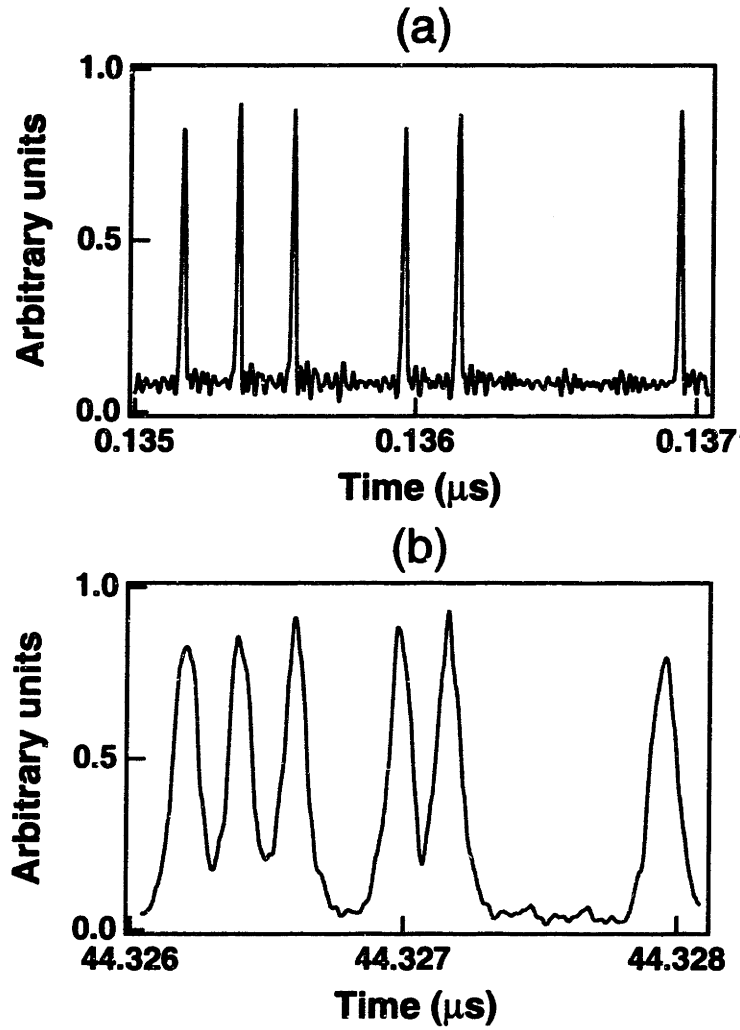

Figure 4-6: High-speed sampling oscilloscope trace showing a portion of (a) the initial, loaded packet; (b) after the 450 circulations. Pulse broadening in the stored packet was caused by jitter from the sampling oscilloscope (see Fig. 4-7).

4.3.2 Asynchronous Phase Modulation

In previous storage rings (except for buffers utilizing rational harmonic modulation [95]), the RF frequency driving the modulator is equal (to within 1 kHz) to a harmonic of the cavity frequency. In this case, known as synchronous modulation, all of the pulses in the packet normally are located under a peak of a modulation cycle after each round-trip. If a pulse or group of pulses become mistimed due to random cavity fluctuations, the modulator envelope is usually able to retime the pulses and move them back to the stable position under a modulation peak. Under asyn-

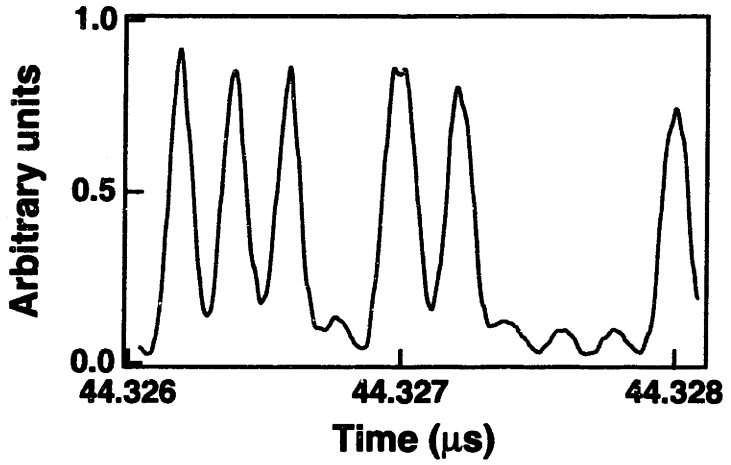

Figure 4-7: High-speed sampling oscilloscope trace of a packet generated by the pattern generator after a delay of 44.3 μs. A packet at zero-time delay looked similar to Fig. 4-6(a). This result confirmed that pulse broadening was caused by oscilloscope timing jitter, rather than by processes internal to the buffer.

chronous modulation, the modulation frequency is detuned from a cavity harmonic by at least 100 kHz. Due to the frequency detuning, there is a deterministic and continuous sliding of the pulses in the packet relative to the modulation cycle. If amplitude modulation is used, the pulses would not survive this sliding. Under asynchronous phase modulation the pulses receive a time-varying phase shift (due to the sliding) which corresponds to a sinusoidal shift in the pulses' carrier frequency [78]. Normally, this effect would also destroy the pulses as they would be frequency shifted into the wings of the optical filter. However, if the pulses are solitons they can fight the frequencies shifts through their nonlinear ability to generate new frequencies. As a result, the frequency swings into the filter are reduced and the solitons can survive the detuned modulation. The response of solitons and linear pulses to asynchronous phase modulation is illustrated in Fig. 4-8. As low-level (linear) noise is shifted further into the filter than the solitons, the linear noise experiences a higher degree of loss. The behavior of solitons and linear noise under asynchronous modulation is similar to sliding-guiding filters studied in long-distance soliton transmission experiments [79].

In the case of asynchronous harmonically mode-locked fiber lasers and optical fiber ring buffers placed in transmission nodes, the characteristic of a sinusoidal shift in center wavelength caused by asynchronous phase modulation makes them unsuitable for telecommunication appli-

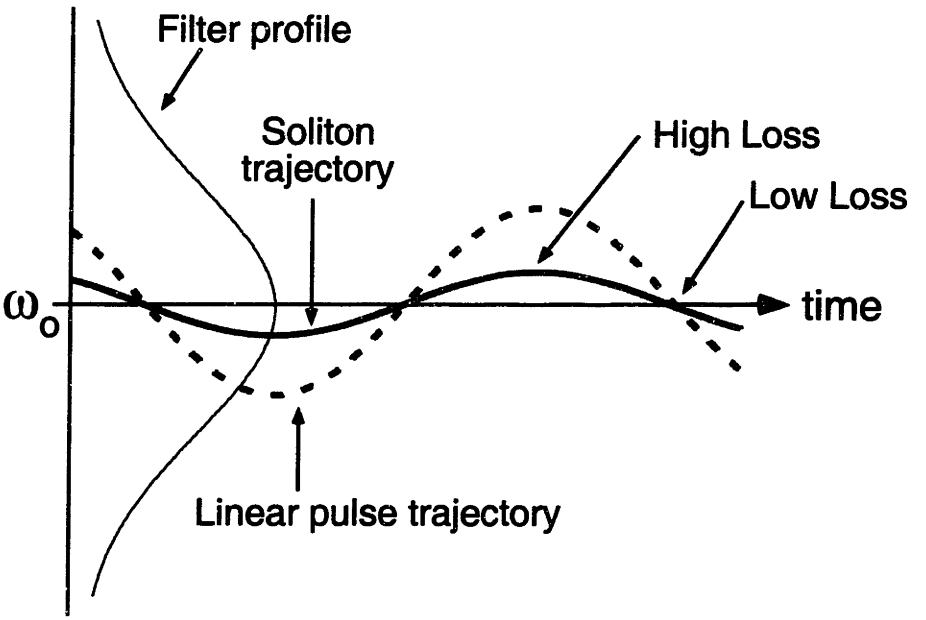

Figure 4-8: Behavior of solitons and linear pulses under asynchronous phase modulation. The deterministic sliding of modulation envelope with respect to the pulse train imparts a time-varying frequency shift to the pulse train. Through their nonlinearity, solitons are able to fight the frequency shift and thus experience less loss as compared to linear signals. Regions of high loss and low loss for both linear pulses and solitons are also labeled. ω_0, carrier frequency

cations. However, when buffers are used in receiver nodes, the wavelength shift might not be as debilitating because the packets will be directly detected rather than transmitted. In these applications the asynchronous mode of operation offers several possible advantages over synchronous buffers. The central wavelength of the packet does not need to exactly match the wavelength of the buffer and drifts in the cavity length can be tolerated. Furthermore, the packets' bits slide though the modulation envelope so there is no definition of relative phase between the modulator and the packet. Thus, in theory, the packets could be injected at any position relative to the modulation of the buffer. This is perhaps most important advantage of asynchronous operation as incoming packets could be injected into the buffer without regard to the phase of the intra-cavity modulation cycle.

In all of the previous results discussed in Section 4.3.1, including the results given in Figs. 4-5 and 4-6, the buffer was operated with asynchronous modulation. In this case the modulation frequency was detuned between 70 to 110 kHz from the 500th cavity harmonic at approximately 5

GHz. The asynchronous nature of the buffer can be examined by mixing the packet signal from the high-speed photo-detector with a tap from the modulation drive. When low-pass filtered by the 1-GHz analog scope, the mixed signal is a sinusoid with an amplitude proportional to the amplitude of the bits in the packet and a frequency equal to the difference between the modulation drive frequency and the packet round trip frequency (i.e. the cavity harmonic closest to the modulation drive). Mathematically, after being low-pass filtered, the signal is equal to,

$$v(t)_{mixed} = A_1 A_2 \cos[(\Omega_1 - \Omega_2)t + \phi_o] \tag{4-1}$$

where A_1 is the amplitude of the modulation drive, A_2 is the amplitude of the bits in the packet, Ω_1 is the modulator drive, Ω_2 is the nearest harmonic of the packet round trip (cavity) frequency, and ϕ_o is the relative phase between the modulation drive and the packet bit-rate. Note that in the experiment, the modulation drive and packet bit-rate were equal. Experimentally, the relative (initial) phase ϕ_o could be adjusted by changing the optical delay line shown in Fig. 4-2 while Ω_2 was adjusted by changing the cavity length of the buffer. Figure 4-9 displays the mixed signal dur-

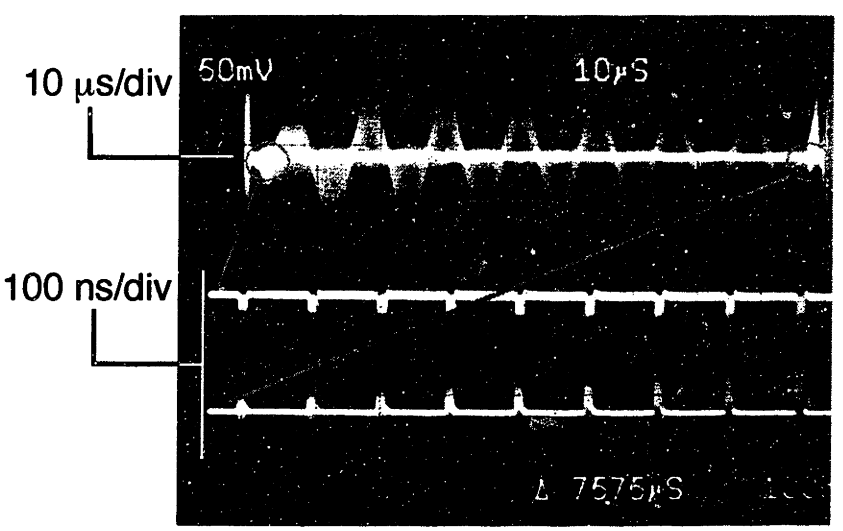

Figure 4-9: Output of mixer (see Fig. 4-2) displayed on a 1-GHz analog oscilloscope using a delaying time-base. Top trace at 10 µs/div spans the entire storage interval. The middle and bottom traces show the mixed signals at the beginning and the end of the storage interval at 100 ns/div. The sinusoidal form of the mixed signal confirms that the cavity frequency (and thus the packets' round-trip frequency) is detuned from the modulation frequency.

ing the 80-μs storage interval (when the CW holding beam was turned off) using a 1-GHz analog oscilloscope and a delaying time-base. The top trace, at 10 μs/div, spans the entire storage interval, while the middle and bottom traces, at 100 ns/div, show the mixed signal just after a packet was loaded and just before activation of the CW holding beam, respectively. The sinusoidal form of the mixed signal confirmed $\Omega_1 \neq \Omega_2$ and thus the packets were modulated asynchronously. The enhanced base-line in the top trace was due to a non-zero mixed signal being generated only when a packet is present.

Further confirmation of the packets' asynchronous modulation appears in the series of traces in Fig. 4-10 again showing the mixed signal on a 1-GHz analog oscilloscope. In this case the detun-

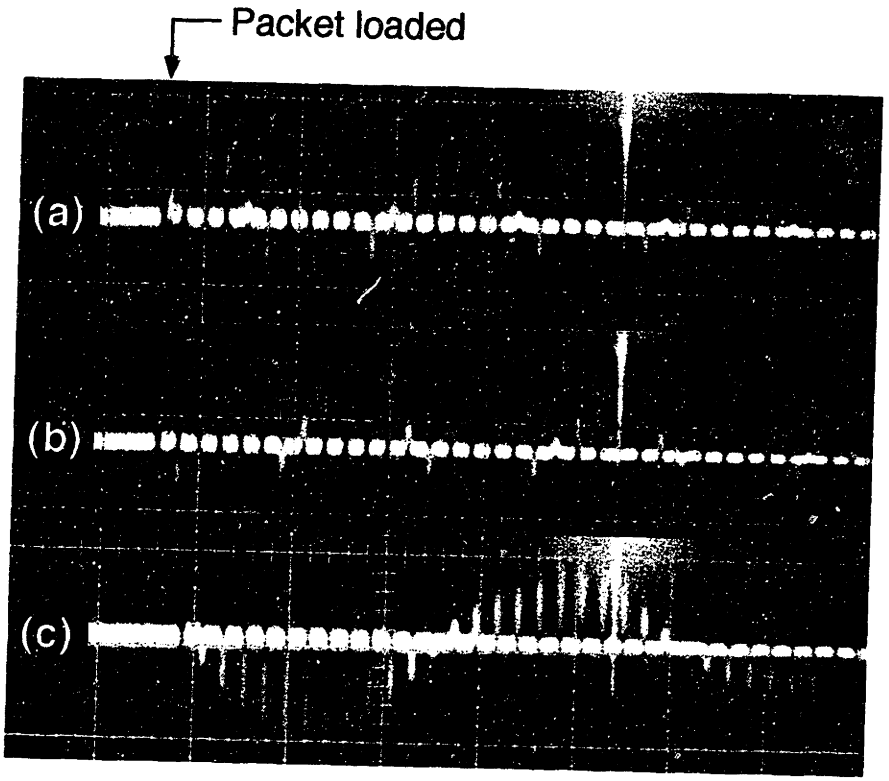

Figure 4-10: Series of 3 traces showing the mixed signal on a 1-GHz analog oscilloscope with a 500 ns/div time scale under 3 different operating conditions. (a) cavity was detuned roughly 1 MHz from the modulation frequency. (b) same detuning as (a), but an extra delay of 100 ps was added to a delay line before the packets are injected into the buffer. As expected, the added delay corresponds to a change in phase of the mixed signal. Specifically, the mixed signal was shifted in phase by π. (c) detuning was decreased to 400 kHz by adjusting the cavity length which increased the period of the mixed signal by approximately a factor of 2.

ing was increased to approximately 1 MHz and the mixed signal is shown on a 500 ns/div time scale so that changes in the period and phase of the signal can be easily observed. On this time scale only the first 35 circulations are shown. In the top trace (a) the packet was loaded slightly out of phase and the mixed signal was initially positive as the packets begin to circulate. In the middle trace (b) an extra delay of 100 ps was added to the optical delay line which increases ϕ_o in eqn. (4-1) by roughly π. As expected, the mixed signal in trace (b) was shifted in phase by approximately π due to the added delay. In the bottom trace (c) the cavity detuning was reduced to approximately 400 kHz which increased the period of the mixed signal by a factor of approximately 2.

In spite of the asynchronous modulation, the phase modulator still provides noise clean-up and was crucial to the storage of packets. If the phase modulator was turned off, the buffer could only store a packet for 6.3 μs (60 circulations). Beyond a detuning of 100-110 kHz the buffer could not reliably store a packet for 800 circulations. If the cavity length was detuned by a much greater amount, around 1 MHz (as in Fig. 4-10), the storage time was reduced to 12.7 μs (120 circulations). In this case the relatively rapid sliding between the bits and the modulation envelope greatly reduced the modulator's effect.

Asynchronous modulation also had an effect on the packets' amplitude. The top trace in Fig. 4-11 is the envelope of the packet during a storage interval while the bottom trace in Fig. 4-11 displays this mixed signal during the same time frame. This data was taken with the buffer detuned to roughly 70 kHz and operated under conditions identical to Fig. 4-9. Clearly, there is amplitude modulation on the packets with a period equal to two times the mixed signal. As discussed previously, asynchronous phase modulation imparts a sinusoidal frequency shift on the packets (with a period identical to the mixed signal). As shown in Fig. 4-8, when this frequency shift is combined with a filter, a sinusoidal loss is produced that has a period equal to two times the detuning frequency. It is likely this loss is responsible for remaining modulation on the packets, although, in spite of the CW holding beam, relaxation oscillations could also be a contributing factor.

As mentioned previously, perhaps the most important advantage of asynchronous operation for a buffer is elimination of phase matching for the injected packet (with respect to the modulation frequency). Experimentally, the initial position of packet in the asynchronous modulation cycle

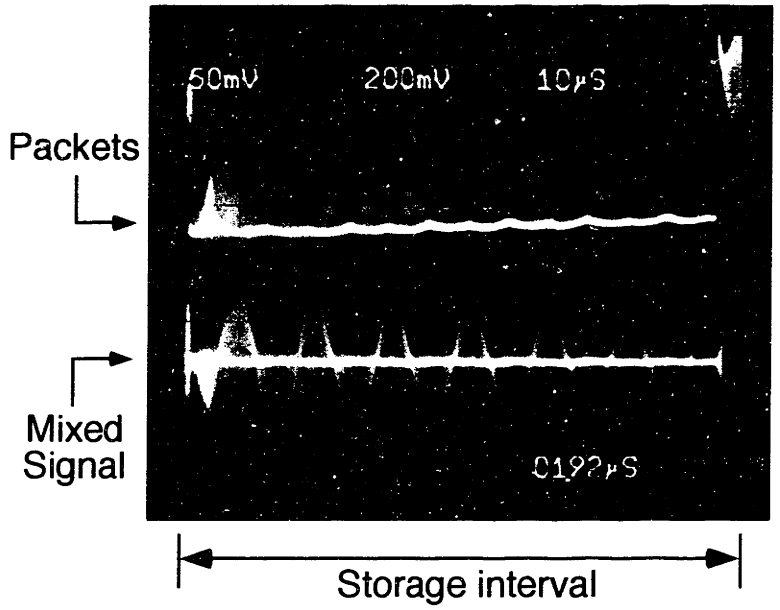

Figure 4-11: The packet envelope (top trace) and the mixed signal (bottom trace) shown during a storage interval at 10 μs/div. The modulation on the packets' amplitude was due to a combination of filtering and asynchronous modulation as illustrated in Fig. 4-8.

could be varied by changing the optical delay line shown in Fig. 4-2. The window of initial position where successful storage was observed varied with input packet energy; a packet with higher energy had a larger injection position tolerance. Such a dependence is easily understood by noting that different injection positions have different amounts of initial loss depending on the position of the injected packets' bits relative to the modulation envelope (see Fig. 4-8). A packet with an average bit energy of 14 pJ (the highest packet energy that could be generated) had an injection tolerance of 100 ps or 50 % of the modulation period. It is interesting to consider why a phase tolerance of $+\pi$, but not $-\pi$ was observed. There are two possible reasons for this condition. First, the center wavelength of the injected packets could have been offset from the center wavelength of the filter, thereby initially causing one sliding direction to have a higher amount of loss. Experimentally, this condition is a strong possibility. Second, a different amount of loss between up sliding and down sliding with solitons in long-distance transmission systems using sliding-guiding filters was found [99] and a similar condition probably also occurs with asynchronous phase modulation. Both of these characteristics break the degeneracy of equal loss when loading out of

phase with a delay of $+\pi$ or $-\pi$. With higher bit energies to overcome the additional loss, it is expected that packet loading could be successful at any phase relative to the modulation cycle.

Chapter 5

Soliton Fiber Lasers Incorporating Waveguide Amplifiers

Following the development of erbium-doped fiber (EDF) a number of different designs have been reported for short pulse fiber lasers operating in the 1.5 μm region [62], [100], and [101]. Each of these cavity designs has utilized EDF or Er-Yb codoped-fiber as the gain element. Due to the limited erbium-doping concentrations in silica fiber, the shortest cavity length obtained from P-APM fiber lasers is roughly 4 m, giving a fundamental repetition rate of 50 MHz. Mode-locked fiber lasers with shorter cavities are desirable for a number of reasons. Higher fundamental repetition rates could be obtained and, as described below in Section 5.1, the limitations of pulse energy and pulse width inherent in soliton fiber lasers could also be deferred, significantly reducing the shortest obtainable pulse width.

Typically, the P-APM fiber lasers cited previously required at least 0.5 m of EDF because a limit on the erbium doping concentration requires a minimum EDF length for the necessary amount of gain. One fiber laser design that obtained 270-fs pulses at a fundamental repetition rate of 290 MHz used an Er-Yb codoped-fiber with a high pump absorption cross-section [102]. The length of Er-Yb codoped-fiber (EYDF) was minimized by constructing a low-loss cavity and utilizing a semiconductor saturable absorber as the mode-locking element. An alternative to using EDF or EYDF in short cavity fiber lasers is an Er-Yb codoped planar waveguide amplifier [34], [103], and [104]. In the work of GeeO [34] the gain per unit length of waveguide amplifiers is considerably higher than EDF or EYDF because the Er-Yb is doped into a phosphate host which allows higher doping concentrations (and thus higher gain per unit length) before the debilitating effects of CET occur [31]. With a typical length of 4.5 cm this integrated optical amplifier is able to deliver 14 dB of single-pass, small-signal gain at 1.53 μm with 980 nm pump powers of 130 mW. The noise figure of these amplifiers varies from 6 to 8 dB.

A fundamental advantage of replacing EDF with a waveguide amplifier in a mode-locked fiber laser is a sharp reduction in the cavity length which, in turn, yields a number of benefits. A decrease in the cavity length increases the fundamental repetition rate of the pulses, possibly to rates which could be useful in telecommunications or other applications. In P-APM fiber lasers, a shortened cavity length simultaneously reduces two parasitic effects that have limited the performance for this type of soliton fiber laser: resonant sideband formation [105], [106] and saturation of the P-APM mechanism [62]. In the following chapter, the advantages, operating characteristics, and performance of two types of mode-locked soliton fiber lasers using a waveguide amplifier as the gain element are discussed.

5.1 Inherent Limitations of Soliton Fiber Lasers

5.1.1 Resonant Sideband Formation in Soliton Fiber Lasers

Investigations in both long-distance soliton transmission systems [48] and fiber soliton lasers [107] have found a resonant instability which produces a distinct sideband structure in the pulse spectrum as shown in the lower half of Fig. 5-1. The existence and location of these sidebands can be explained by a phase-matching condition. As the soliton circulates in the cavity, various perturbations cause it to emit radiation as it readjusts itself back to the steady-state. The spectral content of the radiation spans the bandwidth of the soliton. Coherent superposition of this radiation on successive round-trips occurs when the round-trip phase delays of the soliton and of the radiation produced at perturbation points are modulo 2π. The linear radiation experiences a per-round-trip phase dispersion of,

$$\phi_{lin} = \frac{1}{2}|\Delta k''|\Delta\omega^2 L_c \tag{5-1}$$

where $\Delta k''$ is the average net dispersion of the cavity, $\Delta\omega$ is the offset from the center frequency, and L_c is the cavity length. An averaged soliton with net anomalous dispersion obeys an area theorem [19],

$$A_o\tau_s = \sqrt{\frac{|\Delta k''|}{\delta}} \tag{5-2}$$

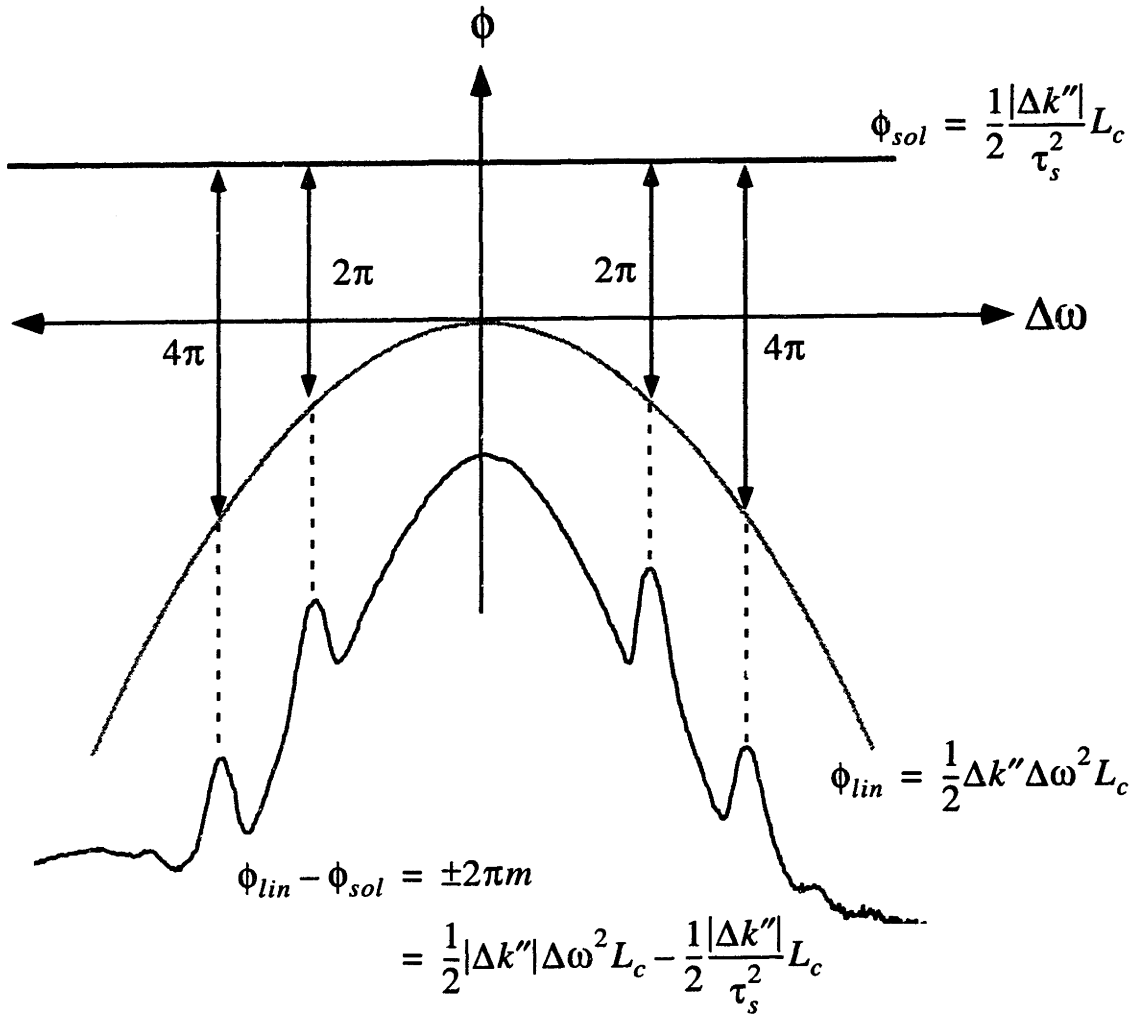

Figure 5-1: Phase-matching diagram for resonant sideband formation. Sidebands are formed at discreet spectral components that have a round-trip phase difference between the linear, dispersive waves and the soliton in multiples of 2π. The optical spectrum of an actual soliton exhibiting sidebands is shown in the lower half of the figure.

where A_o is the amplitude, τ_s is the soliton pulse width, and δ is the nonlinear Kerr coefficient. The soliton energy is,

$$W = 2|A_o|^2\tau_s = 2\frac{|\Delta k''|}{\delta\tau_s} \tag{5-3}$$

From the area theorem the nonlinear phase shift per round-trip can be calculated to be,

$$\phi_{sol} = \delta|A_o|^2 L_c = \frac{1}{2}\frac{|\Delta k''|}{\tau_s^2} L_c \tag{5-4}$$

Sidebands are formed when the phase difference between the phase shift of the soliton and the radiative (linear) waves is a multiple of 2π. The resonant condition is shown graphically in Fig. 5-1,

$$\begin{aligned} \phi_{lin} - \phi_{sol} &= \pm 2\pi m \\ &= \frac{1}{2}|\Delta k''|\Delta\omega^2 L_c - \frac{1}{2}\frac{|\Delta k''|}{\tau_s^2} L_c \end{aligned} \tag{5-5}$$

Positions of the sidebands are found by solving for $\Delta\omega$,

$$\Delta\omega = \frac{1}{\tau_s}\sqrt{m\frac{4\pi\tau_s^2}{|\Delta k''|L_c} - 1} = \frac{1}{\tau_s}\sqrt{m\frac{8Z_o}{L_c} - 1} \tag{5-6}$$

where Z_o is the soliton period. For a fixed cavity length and dispersion, as the pulse width is reduced, the sidebands move toward the spectral peak of the soliton ($\Delta\omega \rightarrow 0$) and grow in amplitude. However, a shorter soliton requires more energy. At some point the soliton's energy, and hence the pulse width, becomes clamped due to gain competition with the sidebands. Experimentally, the pulse width of soliton fiber lasers is limited by sideband generation when the cavity length $L_c \approx Z_o - 3Z_o$ [90]. If the pump power is increased after the quantization point is reached, the laser will usually shift into a multi-pulsing regime where 2 or more, untimed pulses circulate in the cavity simultaneously. Clearly, from eqn. (5-6) the quantization point can be delayed by reducing the $|\Delta k''|$ or L_c. Decreasing the net dispersion is not an optimal solution because the pulse energy scales in direct proportion to $|\Delta k''|$. Nakazawa *et al.* [60] followed this approach and reported production of 98-fs solitons from a figure-8 cavity. However, this laser operated with multiple, untimed pulses in the cavity. As demonstrated experimentally in Section 5.3, a significant reduction in L_c by employing a waveguide amplifier as the gain element, led to a substantial

decrease in the shortest obtainable pulse width from a soliton fiber laser while still maintaining single pulse operation.

5.1.2 P-APM Saturation

An additional effect that limits the peak power (and hence the pulse energy) of a soliton fiber laser is saturation of the P-APM mechanism. This condition occurs due to the interferometric nature of P-APM which has a sinusoidal dependence of transmission with peak power. At high pump powers (typically 85 mW for ring cavities similar to [108]) the peak power for a single soliton reaches a saturation point and the single pulse breaks up into multiple pulses. This type of energy quantization was observed in early work on soliton fiber lasers [109], [110] which had typical cavity lengths of 18 to 180 m. The P-APM mechanism is derived from nonlinear polarization rotation (NPR), which in turn, is directly proportional to the fiber length in the cavity. Thus, by reducing the cavity length the peak-power saturation level can be increased. Following this approach, a 4.8-m cavity produced 450 fs solitons with single pulses in the cavity [108]. Replacing the erbium-doped fiber with a waveguide amplifier offers an opportunity to further shorten the cavity and generate high-energy, 100-fs solitons without having the laser slip into a multi-pulse state.

5.2 Characteristics of the Waveguide Amplifier

The waveguide amplifier used in these experiments is similar to devices used in amplifier modules for long-distance transmission trials [111]. The 4.5 cm long waveguide was fabricated[4] in a 2.0 wt-% erbium, 4.0 wt-% ytterbium-doped phosphate glass by a two-step ion exchange process shown in Fig. 5-2. An aluminum mask was applied to the glass wafer. Next, an ion exchange (driven by diffusion) replaced Na^+ ions with Ag^+ ions in the unmasked region, thereby defining a semicircle-shaped waveguide core. In the second step, a field-assisted exchange procedure was performed by applying a high-voltage source. This moved the waveguide core to a depth of roughly 4 μm. Due to diffusion, this process also changed the core shape to be slightly elliptical.

An asymmetric core indicates the waveguide probably has a linear birefringence, meaning that there are two distinct eigen modes of propagation for linearly polarized light. Each mode experi-

4. The waveguide amplifier was fabricated by Dr. Denis Barbier of GeeO.

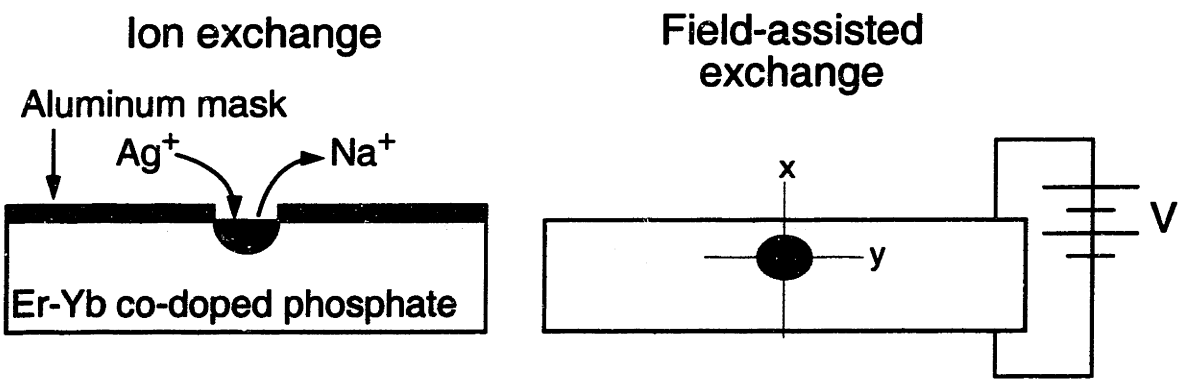

Figure 5-2: Two-step ion exchange fabrication process of the waveguide amplifier used in this thesis. In the first step an aluminum mask was applied to an Er-Yb codoped phosphate substrate and an ion exchange process defined a waveguide core. Next, the waveguide core was driven to a depth of 4 μm by applying a constant high-voltage. The finished waveguide was slightly elliptical, and the resulting birefringent axes are shown in a schematic of the finished waveguide.

ences a different, effective refractive index, depending on whether the linear polarization of the light is parallel or perpendicular to a symmetry line drawn through the waveguide. These two directions are known as birefringent axes of the waveguide. If linearly polarized light is launched exclusive along either axis, the polarization state of the light will be maintained as it propagates. A polarization state that initially excites both axes will not be maintained. Instead, due to a difference in the propagation constants between the two axes, the two eigen states will pick-up a relative phase that is z-dependent. As a result, the overall polarization state (a super-position of the two eigen states) will periodically change from linear, to circular, to elliptical, back to linear, and so on.

A polarization beat length is defined as the distance over which the relative phase between the two propagation modes becomes 2π,

$$(k_x - k_y)L_b = 2\pi \tag{5-7}$$

where k_x and k_y are the propagation constants along the two birefringent axes. Solving for L_b gives,

$$L_b = \frac{\lambda}{n_x - n_y} = \frac{\lambda}{\delta n} \tag{5-8}$$

where δn is index difference between the two birefringent axes.

When constructing a fiber laser around a waveguide amplifier, the amount of linear birefringence is important in two regards. If P-APM is used as the mode-locking mechanism, the birefringence can disrupt mode-locking by reducing the amount of nonlinear polarization rotation [40]. Additionally, if a pulse does not enter the waveguide polarized solely along one birefringent axis, portions of the pulse that are projected on each birefringent axes will temporally walk-off from one another due to the index difference δn. This walk-off can also be a hindrance in obtaining a CW mode-locked state.

The birefringence of the waveguide can be measured by constructing a birefringent filter [112]. If broad-band, linearly-polarized light is launched into a birefringent medium so both birefringent axes are excited, the output will have, in general, a wavelength-dependent polarization ellipse due to wavelength-dependent beat length shown in eqn. (5-8). By placing a polarizer at the output, an optical filter is created. The transfer function of this birefringent filter can be shown to be,

$$T(\lambda) = 1 + 2\cos^2\theta \sin^2\theta [\cos(\Delta\phi) - 1] \tag{5-9}$$

where θ is the angle between the birefringent axis and the input polarization (normally $\theta = \pi/4$ for highest discrimination) and the phase change $\Delta\phi$,

$$\Delta\phi = \frac{2\pi}{\lambda}\delta n L \tag{5-10}$$

where L is the propagation distance through the birefringent medium. The free spectral range (FSR) of the filter separates two adjacent wavelengths of maximum transmission. From eqn. (5-9) FSR occurs when $\Delta\phi(\lambda_1) - \Delta\phi(\lambda_2) = 2\pi$. Solving for FSR gives,

$$\text{FSR} = \lambda_1 - \lambda_2 = \frac{\lambda_1 \lambda_2}{\delta n L} \tag{5-11}$$

From this expression, the index difference δn can be determined by experimentally measuring the FSR.

Figure 5-3 illustrates the experimental set-up used to find the birefringence of the waveguide.

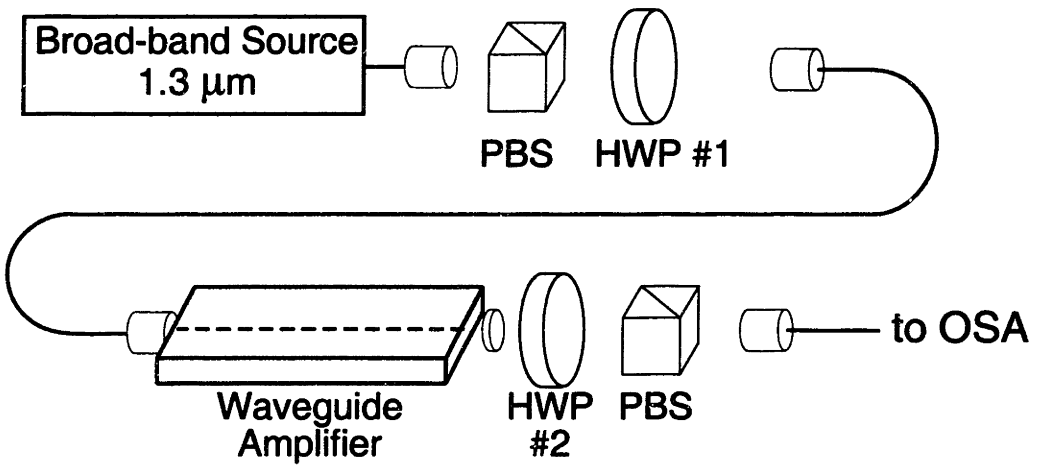

Figure 5-3: Experimental set-up to measure the birefringence of the waveguide amplifier. The waveguide was placed between two polarizers, forming a birefringent filter. By launching 1.3 μm broad-band light off-axis, the index difference between the two eigen modes (birefringent axes) was determined by measuring the free spectral range (FSR) of the transmitted signal. HWP, half-wave plate; PBS, polarizing beam splitter; OSA, optical spectrum analyzer.

A broad-band (full-width half-maximum of 40 nm) source at 1.3 μm was linearly polarized and then launched into the waveguide. 1.3 μm was chosen as the center wavelength as it is not absorbed by the waveguide. As described above, a filter was formed by placing a second polarizer at the output. By rotating HWP #1 the orientation of the input polarization with respect to the birefringent axes can be varied, thereby turning the filter on or off. The output spectra for these two states are given in Fig. 5-4. The FSR was determined by measuring the spacing between

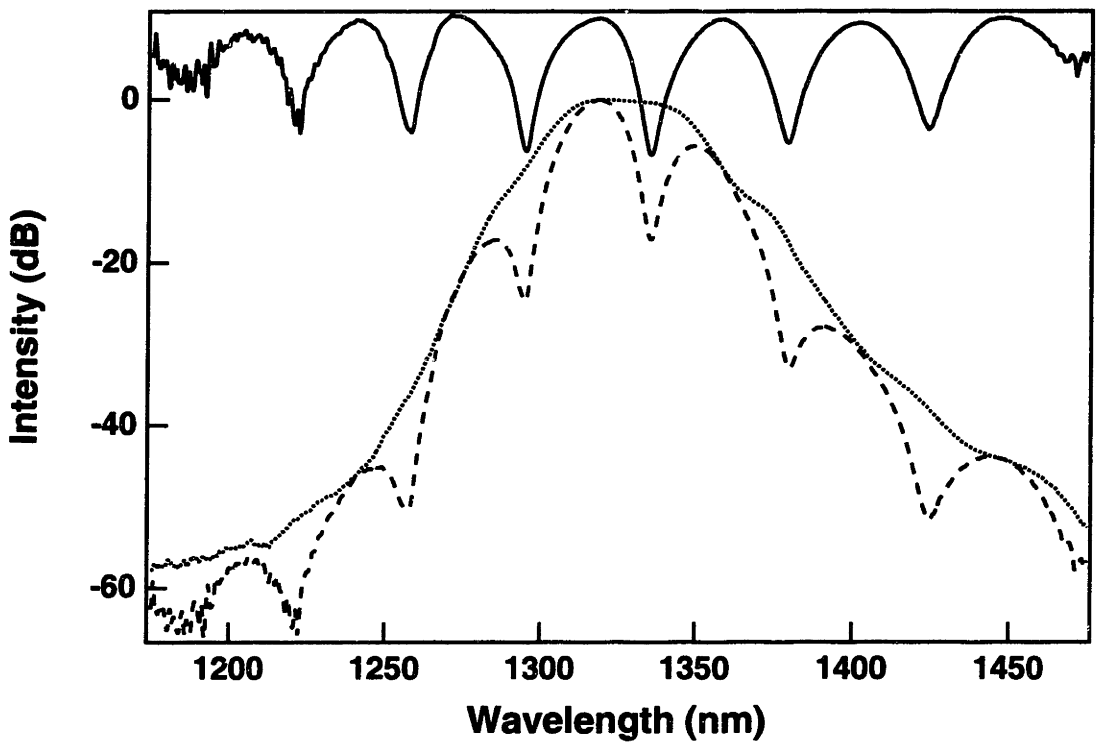

Figure 5-4: Spectral output of the 1.3 μm broad-band source after passing through a birefringent filter composed of the waveguide and polarizers (see Fig. 5-3). By rotating HWP #1 the filter can be turned on (dashed line) and off (dotted line). The ratio of these two curves is the solid line. By measuring FSR from this last trace and using eqn. (5-11), the index difference δn was found.

adjacent peaks from the ratio of these two states. The ratio was taken to reduce the amount of distortion due to the slope of the input spectrum. When this technique is used to measure the birefringence of polarization-maintaining fiber (PM), the length of fiber under test is chosen so that the FSR is approximately 2 to 5 nm. In present case the length of the waveguide was not adjustable, fixing the FSR to approximately 30 nm. Using eqn. (5-11) and the FSR obtained from Fig. 5-4, the index difference δn was found to be $8.29\times10^{-3} \pm 0.05$ making the beat length L_b = 1.6 mm at λ_o = 1.55 μm. This amount of birefringence is significant; typical high-birefringent or PM fiber has a $\delta n \approx 5 \times 10^{-3}$ and a beat length of L_b = 3.0 mm at λ_o = 1.55 μm.

5.3 P-APM Soliton Lasers Incorporating Waveguide Amplifiers[5]

To evaluate the performance of the waveguide amplifier in a mode-locked fiber laser, a cavity design similar to previous soliton ring fiber lasers which used EDF as the gain medium was studied initially. A self-starting ring cavity was formed by butt-coupling fibers (with index-matching oil) on both sides of the waveguide.[6] Facets of the waveguide and coupling fibers were angle-polished at 6 degrees to reduce back reflections. The coupling efficiency was measured to be approximately 75 % using a 1.3 μm diode. The resulting cavity is illustrated in Fig. 5-5. The cavity

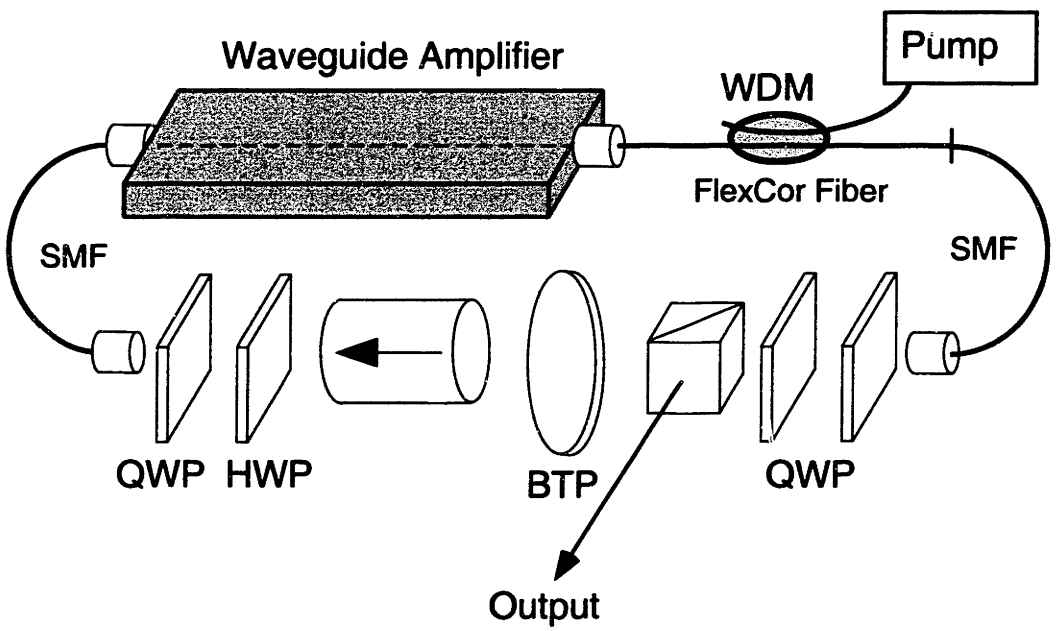

Figure 5-5: Cavity diagram of mode-locked fiber laser using a waveguide amplifier. QWP, quarter-wave plate; HWP, half-wave plate; BTP, birefringent tuning plate; WDM, wavelength-division-multiplexer; SMF, single-mode fiber.

consisted of 0.86 m of Corning FlexCor fiber, 2.83 m of Corning SMF-28 fiber and open air section of 0.20 m, giving a repetition rate of 52 MHz. The average dispersion was estimated to be -17 ps^2/km. Apart from a slightly higher average dispersion (-17 vs. -15 ps^2/km) and slightly shorter total length (3.69 m vs. 4.51 m) this cavity was nearly identical to the soliton erbium-

5. Work reported in this section was performed in collaboration with Dr. Shu Namiki and portions of this section appear in [113] and [114].
6. The waveguide amplifier used in this section is slightly different than the waveguide used in Sections 5.2 and 5.4. The main difference was the length (4.5 cm vs. 5.2 cm, respectively) and a smaller core size in the latter to increase the gain of the amplifier.

doped fiber laser reported in [90]. Both cavities have a similar dispersion allocation. With proper adjustment of the waveplates and a pump power of 200 mW, a self-starting mode-locked state was obtained with a pulse width of 230 fs. An autocorrelation trace and the corresponding spectrum are given in Fig. 5-6. The output was obtained from an intra-cavity 10/90 output coupler that is not shown in Fig. 5-5. For these results the birefringent filter (BTP) was turned off by rotating the c-axis to be parallel with the input polarization. This pulse width is somewhat shorter than the comparable EDF soliton laser due to the different gain spectrum (i.e. benefits of filtering [90]) and a shorter cavity length. The pedestal caused by the resonant sidebands contains roughly 18 % of the total pulse energy. The average output power (when pulsing) was 1.76 mW (from the 10/90 coupler) making the output pulse energy 33 pJ (including the pedestal). Single pulse operation was verified by long-range autocorrelations and a sampling oscilloscope with a 100 ps rise-time.

As described in Section 5.1, the main benefit of using a waveguide amplifier in a mode-locked fiber laser is the reduction in the cavity length to decrease the pulse width clamping effects of resonant sidebands. P-APM saturation is also curtailed, thereby avoiding the laser's tendency to produce multiple pulses. To investigate these benefits, a second cavity was constructed that consisted of 0.83 m of Corning FlexCor fiber, 0.47 m of Corning SMF-28 fiber, and a free-space section of 0.26 m. The repetition rate was 130 MHz and the average dispersion was roughly -8 ps^2/km. Again, Fig. 5-5 illustrates the cavity construction. In this cavity design the output was taken from the P-APM rejection port of the PBS. The shortened cavity design produced the 116-fs soliton shown in Fig. 5-7, a 52 % pulse width reduction over the longer cavity. An average output power of 21 mW (a pulse energy of 130 pJ, excluding pedestal) was obtained from the P-APM rejection port which represented approximately 30 to 50% of the intra-cavity power [115]. An additional (and unwanted) effect of a shorter cavity was an increased self-starting pump threshold due to a reduction in the nonlinearity per pass. For the 130-MHz cavity, the pump threshold increased to approximately 290 mW for self-starting mode-locked operation. Note that, due to approximately 75 % coupling efficiency of the butt-coupling to the waveguide, the pump power actually delivered (coupled) to the waveguide amplifier in this case was roughly 220 mW. For the pulse shown in Fig. 5-7, a pump power of 490 mW was launched into the WDM.

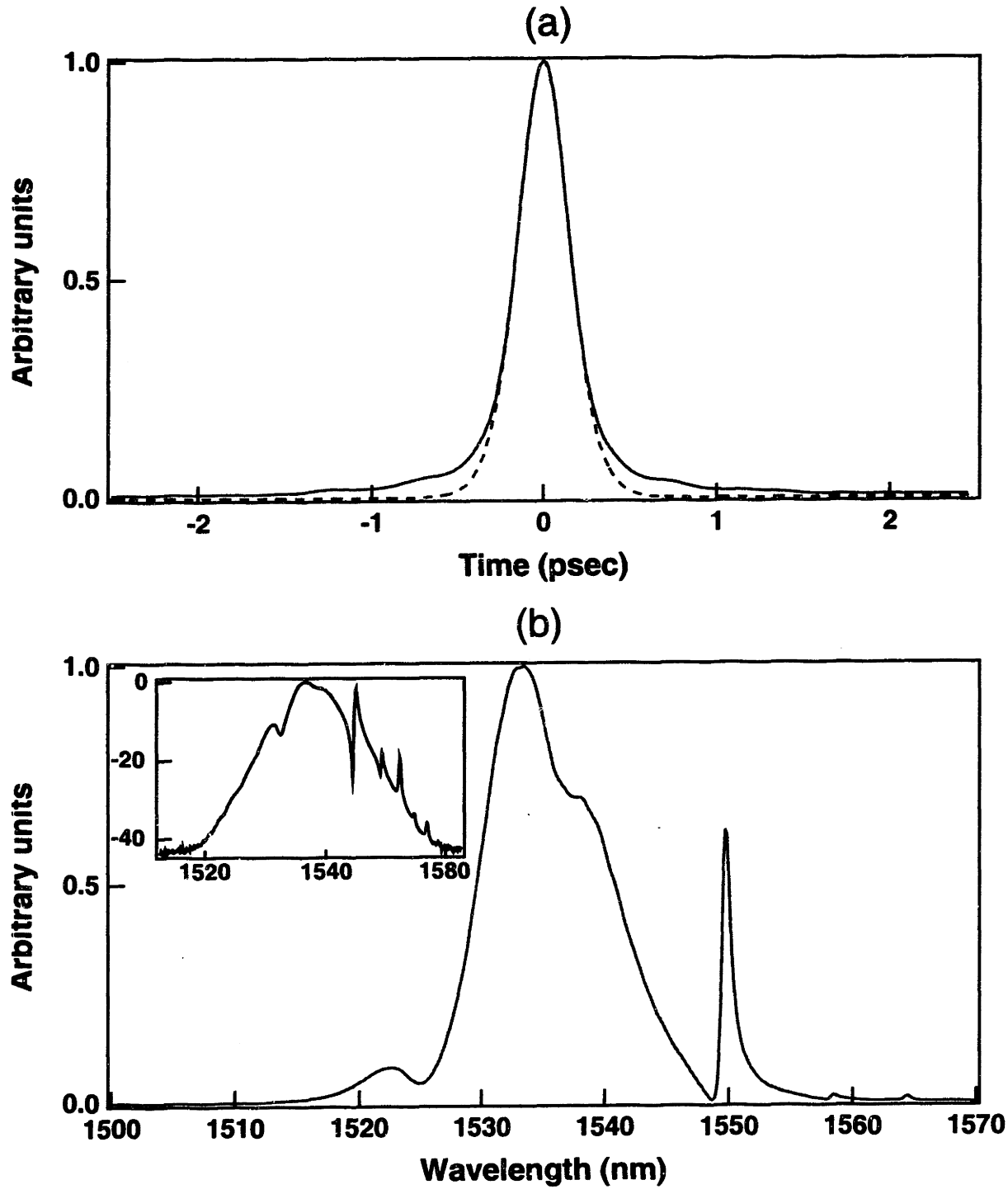

Figure 5-6: (a) Intensity autocorrelation with sech-fit (dashed line) of 52 MHz cavity. The pulse-width is 250 fs. (b) Optical spectrum. Inset in (b) is the spectrum plotted on a dB scale. Output was taken from an intra-cavity 10/90 fiber output coupler not shown in Fig. 5-5.

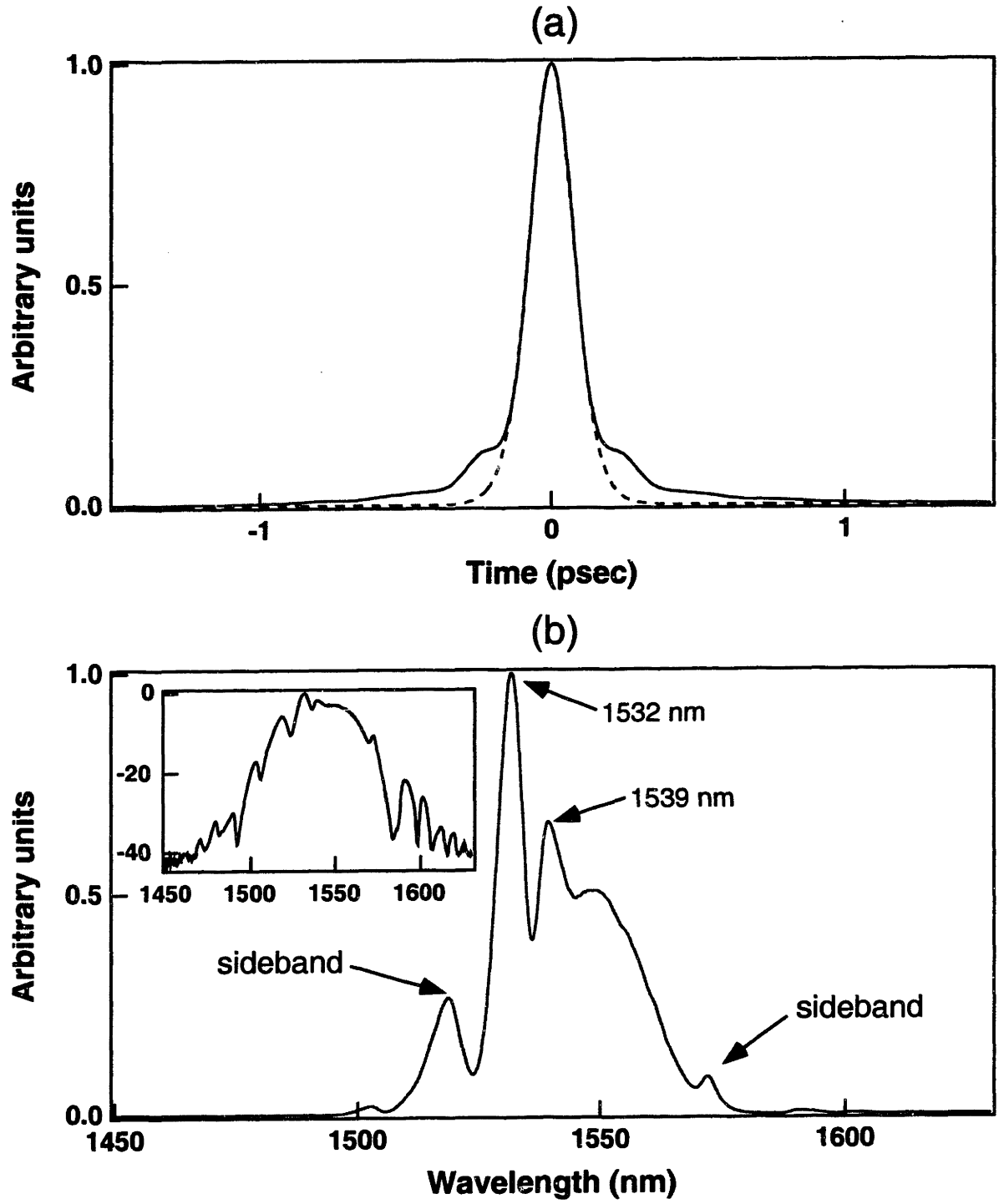

Figure 5-7: (a) Intensity autocorrelation with sech-fit (dashed line) of 130 MHz cavity. The pulse-width is 116 fs. (b) Optical spectrum. Inset in (b) is the spectrum plotted on a dB scale. Output is taken from the P-APM rejection port.

The results presented in Fig. 5-7 were obtained with a 10 T birefringent filter set to produce a modulation depth of 4 dB with a bandwidth of approximately 30 nm. In theory, a stronger filter could reduce the sidebands (and pedestal) present in Fig. 5-7 while maintaining the pulse width [90]. A second method to minimize the pedestal is illustrated in Fig. 5-8. When the launched

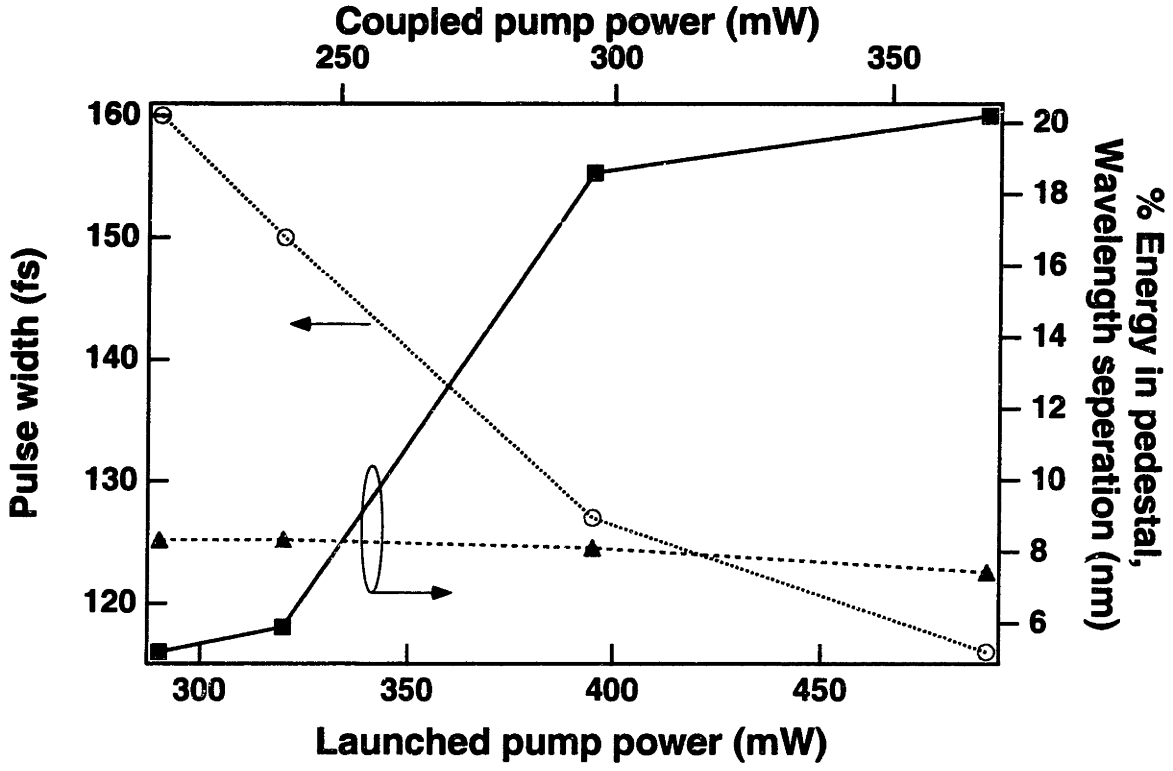

Figure 5-8: Variations in pulse width (dotted line, circles), % of energy in pedestal (solid line, squares), and relative peak separation in spectra (dashed line, triangles) as a function of pump power in the 130 MHz cavity.

pump power was reduced to 290 mW, causing the soliton energy to decrease, the pulse width increased to 156 fs. The sidebands then moved away from the spectral peak and decreased in amplitude. As a result, the pedestal energy content diminished to 5 %.

In addition to the sidebands, the pulses generated by the 130 MHz cavity also contained a double-peaked spectrum with peaks at 1531 nm and 1539 nm. An estimate of the sideband positions based on the soliton parameters of the laser indicated these peaks were most likely not resonant sidebands. Due to the approximately 100-fs pulse width, this structure could have been caused by the soliton self-frequency shift (SSFS) [19]. However, behavior summarized in Fig. 5-8 does not

support this conclusion. As the launched pump power was increased from 290 mW to 490 mW, the pulse width decreased from 156 fs to 116 fs. The SSFS scales as τ^{-4}, so over this pump range if the SSFS were responsible for the structure we would expect a change in the separation between the two peaks in Fig. 5-7. As shown as the dashed line in Fig. 5-8, the relative separation remained virtually unchanged as the pump was varied. Rather, a reduction in the spectral width was observed and the short wavelength peak at 1531 nm became nearly extinguished. The pulse spectrum at the two pumping extremes are shown in Fig. 5-9. The relative amplitude of the peaks

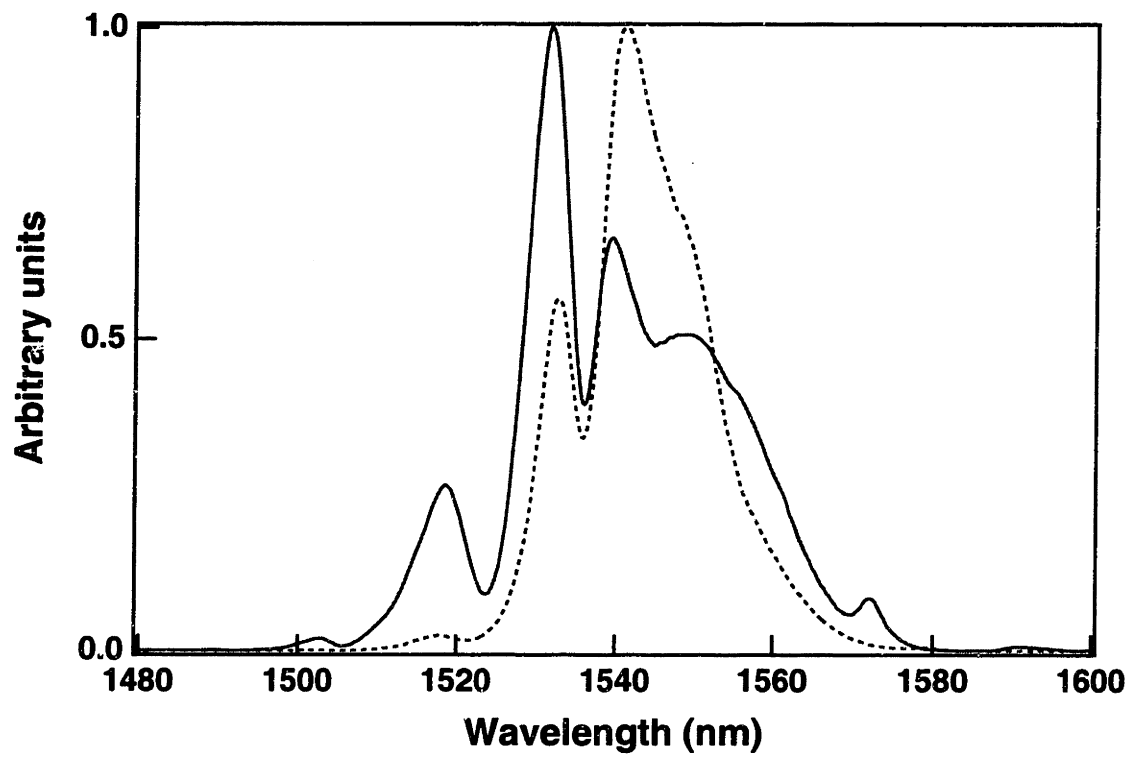

Figure 5-9: Pulse spectra with 290 mW (dashed line) and 490 mW (solid line) of launched pump power in the 130 MHz cavity.

also changed when the filter was tuned. These characteristics suggest the 1531 nm peak might be caused by the collective filtering of the gain spectrum and the sinusoidal wavelength response of the BTF.

Unlike previously reported soliton lasers, we rarely observed multi-pulsing behavior, even at high pump powers. There are a few possible reasons for this condition. As discussed previously,

the short fiber length in the cavity avoided the pulse energy limiting effect of P-APM saturation. It is also possible that under these conditions the waveguide amplifier could not provide enough gain to support more than one pulse in the cavity. Indeed, the trends in Fig. 5-8 indicate higher gain would produce an even shorter pulse. Only when the pulse width becomes clamped will the laser shift into a multi-pulsing regime.

5.4 Work Towards an Ultra-Compact Mode-Locked Laser Using a Waveguide Amplifier[7]

Although the performance of P-APM soliton ring lasers has benefited by replacing EDF with a waveguide amplifier, the clear design direction using a waveguide amplifier is construction of an ultra-compact cavity, roughly 5 to 10 cm in length. As the length of fiber in this short of a cavity precludes using P-APM, it is necessary to employ semiconductor saturable absorbers as the mode-locking element. In this section preliminary work on a soliton laser using with this cavity design is reported.

Demonstration of a mode-locked fiber laser using a semiconductor saturable absorber was first reported in 1991. In this experiment an absorber with 80 quantum wells was used in transmission inside a ring cavity and produced transform-limited, 1.2 ps pulses [58]. In a subsequent experiment a 2-μm thick bulk layer absorber was mounted (i.e. glued) directly to a mirror to form one end of a linear cavity [59]. This design produced 320-fs, 60-pJ pulses. Refinements in the growth of quantum wells over the past several years has enabled precise control over various characteristics of the absorber such as the band-edge and time-constants. Advances in fabrication technology has also provided the ability to grow these absorbers in conjunction with highly reflective Bragg reflectors which have engineerable phase responses. These types of devices, known as semiconductor saturable absorber mirrors (SESAM) [116] or saturable Bragg reflectors (SBR) [117] have successfully mode-locked a number of different solid-state lasers such as Ti:Sapphire, Nd:YLF, Nd:YAG and Cr:LiSAF among others. SESAM devices have also mode-locked a neodymium-doped fiber laser, producing 260-fs pulses [118] and an erbium-ytterbium codoped-fiber laser [102].

---

7. Work reported in this section was done in collaboration with Erik Thoen, Dr. Franz Kärtner and Elisabeth Marley-Koontz.

In this thesis preliminary work was completed on two compact, mode-locked cavities shown in Fig. 5-10 which contain a waveguide and a SESAM. The waveguide was angle-polished at 8° on

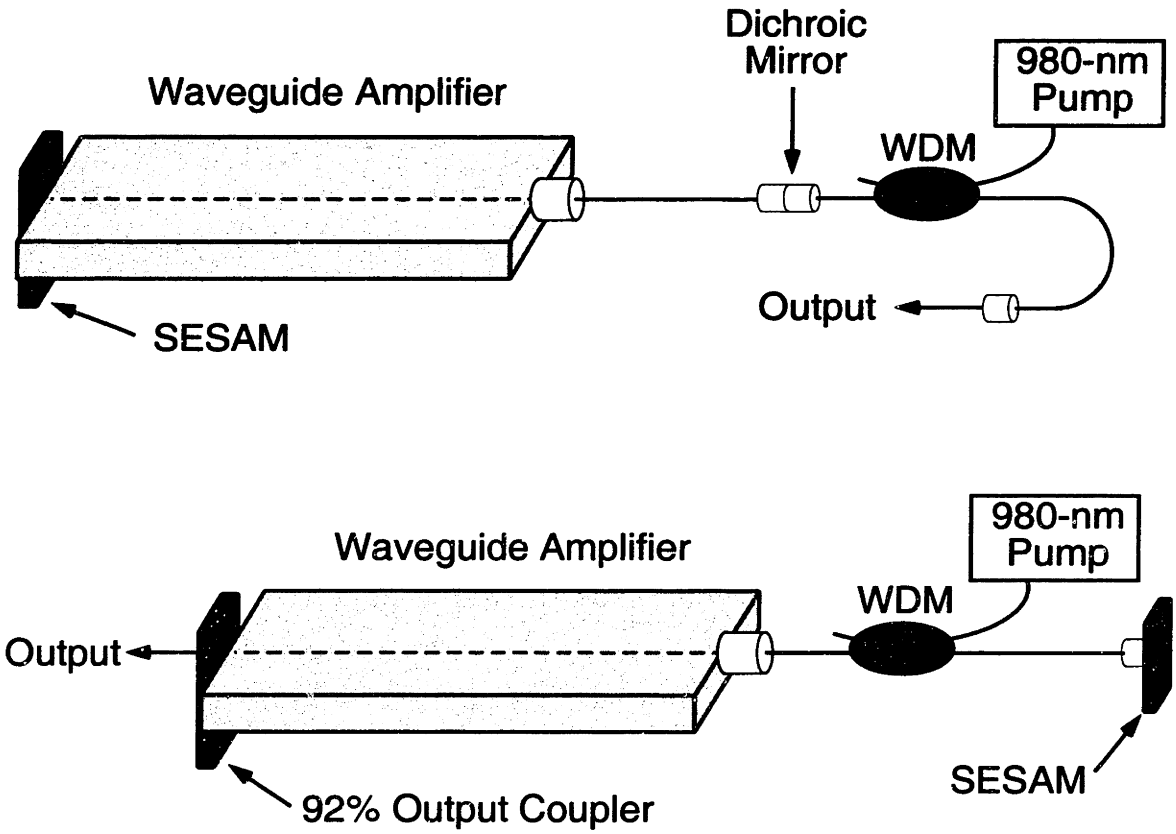

Figure 5-10: Two ultra-compact cavity designs using a waveguide amplifier and a semiconductor saturable absorber mirror (SESAM). The dichroic mirror in the upper cavity was deposited on an FC/PC fiber connector. Its reflectivity at 1550 nm was roughly 98 %.

one end and flat polished on the other end. The SESAM was mounted either on the fiber or waveguide by first applying a small amount of index-matching oil and then placing a small (typically 2 mm by 2 mm) cleaved piece of the SESAM. Various cavity lengths and dispersion allocations were investigated with lengths ranging from 0.5 to 2.0 m. Due to the birefringence of the waveguide it was necessary to include a polarization controller in the cavity so that the pulse had a self-consistent polarization after every round-trip. There are advantages to each cavity design shown in Fig. 5-10. In the upper cavity, the cavity length can be significantly shortened and the 0.4 dB insertion loss of the WDM loss (at 1.55 μm) can also be avoided by placing the WDM outside the cavity. However, there are benefits if the WDM is located inside the cavity (as shown in

the lower half of Fig. 5-10). By placing the SESAM behind the WDM, no unabsorbed pump light can hit the SESAM, a condition which could affect its absorption characteristics. In addition, this design does not suffer from back reflections of 980-nm pump off the dichroic mirror. Experimentally, these back reflections were found to significantly influence the MOPA pump source. Note that both of these aspects can be potentially corrected in the first design by depositing a 980-nm high-reflection coating on the SESAM and using a 980-nm isolator in the pump beam path. Both cavities were investigated; the results shown in Figs. 5-13 and 5-14 were obtained with the upper cavity design shown in Fig. 5-10.

A diagram of the two basic SESAM structures[8] used in this thesis is shown in Fig. 5-11. In

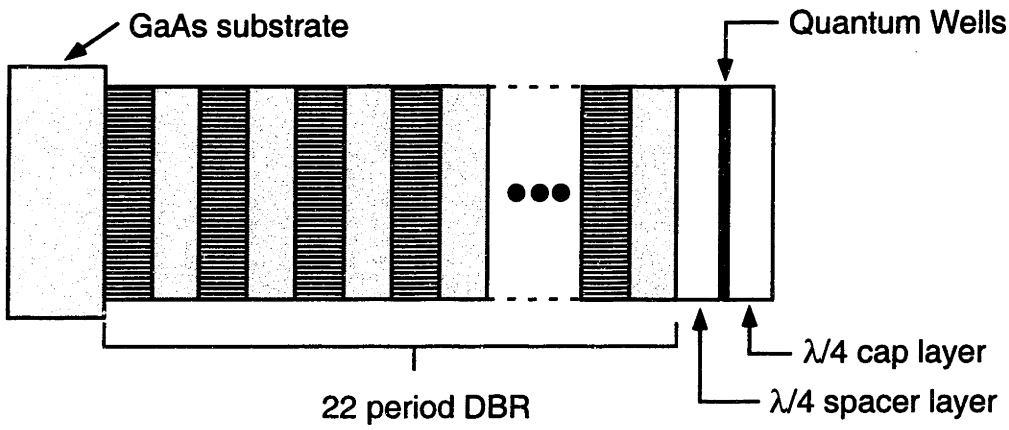

Figure 5-11: Construction of the SESAM devices used in this thesis. The distributed Bragg reflector (DBR) consists of alternating quarter-wave layers of GaAs and AlAs. The quantum wells were placed a quarter-wave from the top surface of the SESAM so that they were located at the peak of the standing-wave field for maximum absorption. For SESAM device III, two quantum wells with a band-edge of 1.545 μm were grown at this location. In device IV four quantum wells with a band-edge of 1.53 μm were grown.

both structures a 22-pair stack of GaAs/AlAs formed a 99.8 % distributed Bragg reflector (DBR) centered at 1.55 μm with a bandwidth of 200 nm. A measurement of the linear reflectivity before the absorber quantum wells were grown is shown in Fig. 5-12. In device III two quantum wells with an estimated band-edge of 1.545 μm were located a quarter-wavelength from the surface (and a quarter-wavelength from the top of the DBR). At this location the peak of the reflected opti-

8. Elisabeth Marley-Koontz designed and grew the SESAM devices and performed the photo-luminescence measurements used to estimate the band-edge of the quantum wells.

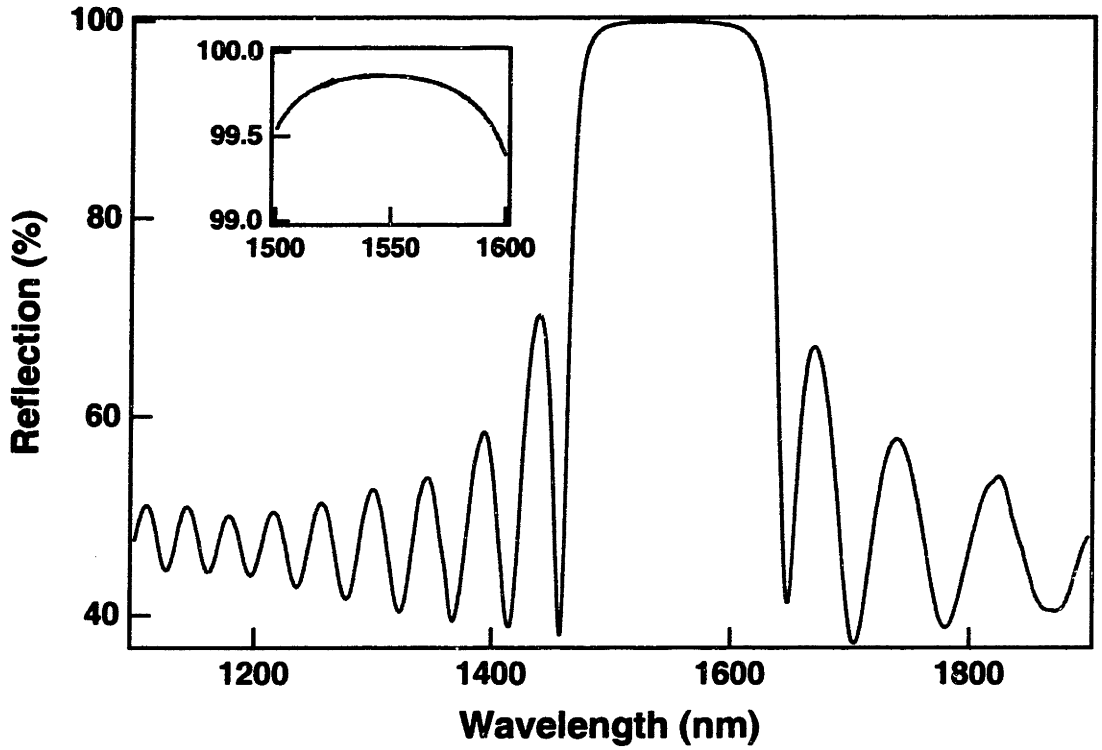

Figure 5-12: Reflectivity of the distributed Bragg reflector (DBR) mirror in the SESAM devices III and IV before growth of absorber quantum wells. Inset shows transmission at peak.

cal field, which is a standing wave, is a maximum and the quantum wells were placed at this location in an attempt to maximize their absorption. The band-edge of the quantum wells was determined by photo-luminescence measurements. The composition of device IV is identical to device III, except that a set of four quantum wells (with an estimated band-edge of 1.53 μm) were placed a quarter-wavelength from the surface. A linear transmission absorption measurement on similar quantum wells for each structure yielded comparable values for the band-edge.[9]

Despite placement of the quantum wells in the peak of the standing wave, attempts to measure their absorption were not very successful due to the small magnitude; the maximum absorption was estimated to be approximately 1 %.[10] As the round-trip losses in the waveguide laser were estimated to be 50 to 60 %, this amount of nonlinear loss was too small of a perturbation to ini-

9. The linear absorption measurements were performed by Erik Thoen.
10. These measurements were completed by Dr. Gunter Steinmeyer.

tiate CW mode-locked operation. In an effort to increase the absorption of the existing SESAM devices, two different coatings were deposited on top of the structures.[11] The basic idea was that, by increasing the strength of the field inside the absorber (normalized to the external field), an enhancement of the saturable loss could be obtained. The first coating was a simple anti-reflection (AR) coating that consisted of a single quarter-wave layer of Al_2O_3. It was estimated that this coating increased the field inside the absorber, relative to the field on the outside, by 1.5 times. A saturation energy measurement[12] at λ_0=1.53 μm of the AR-coated device III determined the saturable loss to be 2.5 %, while in device IV it was 4.3 %. Additionally, in order to further increase the absorption a second, resonant coating was designed using a 5 layer structure of Al_2O_3 and Si. This coating was calculated to increase the internal-to-external field ratio by a factor of 3 (compared to an uncoated SESAM). The saturable loss in resonant-coated SESAM was measured to be 2.8 % at 1.50 μm and 15 % at 1.53 μm. The wavelength-dependent saturable loss was due to the resonant character of the coating.

The saturation fluence E_{sat} was obtained from a fitting of the incident pulse energy vs. saturable loss with the following function,

$$R(E_p) \sim 1 - \frac{R_o}{1 + E_p \S E_{sat}} \tag{5-12}$$

11. Both coatings were designed by Dr. Franz Kärtner and Erik Thoen. The coating runs were done at Lincoln Laboratories by Chris Cook.
12. All of the saturation energy measurements were performed by Erik Thoen.

where E_p is the pulse energy density incident on the absorber. Table 5-1 summarizes the parame-

Table 5-1: Measured parameters of the SESAM devices used in this thesis.

SESAM sample number	Saturable loss (%)	E_{sat} (μJ/cm^2)
III AR-coated	2.5	10.5
IV AR-coated	4.3	10.5
III Resonant-coated	not measured	not measured
IV Resonant-coated	2.8 (at 1.50 μm) 15.0 (at 1.53 μm)	11.2 (at 1.50 μm) 1.86 (at 1.53 μm)

ters of the various SESAM devices used in this thesis.

Initially, a cavity with an internal WDM (lower design shown in Fig. 5-10) was investigated. First, the fiber to the angled-polished side of the waveguide was carefully coupled to obtain approximately 1 dB single-pass coupling loss. After placing a SESAM in the cavity, there was a strong tendency for the laser to operate in a pure Q-switched or Q-switched mode-locked regime [119], an expected characteristic given the long upper-state lifetime of the Er-Yb codoped phosphate glass. In fact, only after careful adjustment of polarization, waveguide coupling, pump power, and position of the SESAM on the waveguide was it possible to eliminate Q-switching, and obtain an unstable "mode-locked" state. In this state there is one pulse per round-trip with a slight (< 1dB) long-term (10 μs period) modulation which was most likely due to relaxation oscillations. A trace of the pulse train from an analog oscilloscope is shown in Fig. 5-13. An autocorrelation was attempted but the pulse train was too unstable to produce any meaningful data. From the RF spectrum the cavity modes appeared clean and locked together although at the first several cavity harmonics there were a couple of relaxation oscillation sidebands roughly 25 dB down compared to the harmonic. With the proper setting of the polarization controller and optimized waveguide coupling, this state was self-starting down to a launched pump level of 100 mW. At this lower limit an output power of 0.8 mW was obtained from the 92 % output coupler. Both AR-coated devices III and IV were used in this cavity and similar results were obtained for both structures.

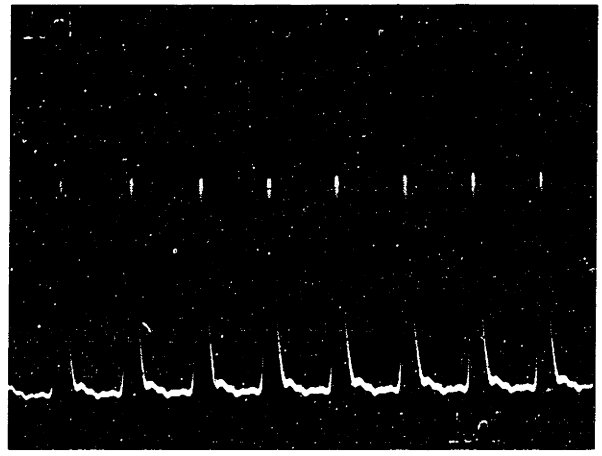

Figure 5-13: Trace from analog oscilloscope showing the unstable "mode-locked" state. This result was obtained from the lower cavity in Fig. 5-10 at 130 mW of 980-nm pump power using AR-coated device III. The cavity repetition rate is 100 MHz and there is one pulse per round-trip.

An examination of the optical spectrum clearly indicated the unstable nature of this state. Fig. 5-14. displays a series of 5 spectra taken over roughly a 30 second time span. It is apparent this is not a steady-state condition. There are a number of possibilities why this cavity could not successfully stabilize the pulse train. One reason could be the amount of self-phase modulation experienced by the pulse. As the WDM is inside the cavity, there was approximately 0.5 m of Corning FlexCor 1060 fiber while the remaining 0.5 m length of fiber was Corning SMF-28. The relatively small Mode-Field Diameter of FlexCor fiber (see Table 2-1) enhances the amount of self-phase modulation and reduces the local dispersion which accordingly to numerical simulations could be a factor preventing the laser from reaching a stable mode-locked state.[13]

To remove most of the FlexCor from the cavity, the upper cavity illustrated in Fig. 5-10 was explored. The WDM was placed outside the cavity and the 980-nm pump was coupled via a dichroic-coated fiber connector. This cavity had 0.05 m of FlexCor fiber and roughly 0.90 m of SMF-28 fiber. Again, after suitable adjustment of the waveguide coupling, polarization controller and pumping level, a state close to mode-locking was obtained with AR-coated devices III and IV. Qualitatively, this cavity operated with a higher degree of stability. However, as in the previous case, the absorbers could not stabilize the pulse train. When the resonant versions of both SESAM

13. These simulations were completed by Dr. Franz Kärtner

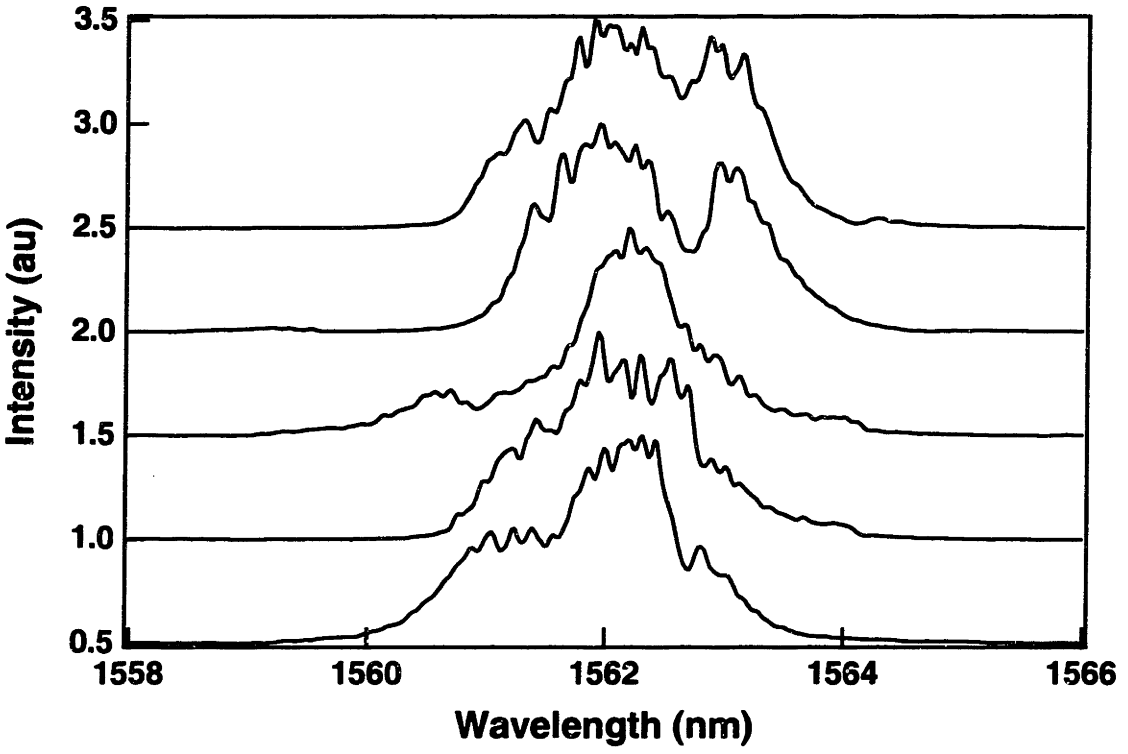

Figure 5-14: A series of optical spectra taken over a time span of 30 seconds when the waveguide laser is operating in an unstable mode-locked state. The corresponding time domain is shown in Fig. 5-13. The rapidly fluctuating pulse spectrum clearly indicates the SESAM could not successfully stabilize the mode-locked pulse train.

structures where tested, the laser did not leave the Q-switched regime. In this case filtering caused by the wavelength-dependent absorption and a fairly low saturation fluence could be a factor in prohibiting the laser from operating in either a stable or unstable mode-locked state.

A second possible characteristic of this laser which could inhibit a stabilization of the mode-locked pulses with the AR-coated SESAM devices is the magnitude of pulse energy density hitting the SESAM relative to its saturation fluence. A major motivation for working on this type of fiber laser is development of an ultra-compact cavity. Toward this end, the absorbers were butt-coupled against either the waveguide or fiber as indicated in Fig. 5-10. Due to the small diameter (approximately 5 μm) of the core, the energy density incident on the absorbers was 500 to 1000 $\mu J/cm^2$, which is nearly 100 times larger than the saturation fluence. An overly saturated SESAM cannot stabilize a pulse train because amplitude fluctuations in the pulse do not significantly

change the reflectivity. In solid state lasers the pulse energy density is typically chosen to be five to ten times larger than the saturation fluence of the SESAM. Due to the fixed spot size emerging from the waveguide (or fiber) the pulse energy density incident on the SESAM was a function only of the intra-cavity pulse energy. The pulse energy (and hence the energy density) was adjustable by changing the cavity length and the pump power. Unfortunately, this amount of adjustment was not enough. In contrast, the incident energy density on absorbers used in solid state laser cavities can be easily adjusted over a much larger range with focussing optics. With this extra degree of freedom, the energy density incident can be usually adjusted to the proper value, relative to the saturation fluence, to obtain a stable CW mode-locked condition. As this adjustment was not available in the ultra-compact cavities shown in Fig. 5-10, the fabrication tolerances on a SESAM capable of supporting CW mode-locking become much tighter.

Presently work is continuing on this project with an short-term goal of determining the incident energy density necessary for CW mode-locking by building a simple linear all-fiber cavity. By temporary replacing the waveguide amplifier with erbium-doped fiber, the waveguide's associated difficulties such coupling and birefringence can be deferred until a more complete understanding of the SESAM characteristics are obtained. Once an all-fiber cavity is successfully mode-locked and a parameter range is established, new absorbers will be designed and fabricated that have a saturation fluence and saturable absorption capable of supporting mode-locked pulses in the waveguide cavities illustrated in Fig. 5-10.

Chapter 6

Studies of Stretched-pulse Fiber Lasers

As discussed in Chapter 5, P-APM fiber lasers operating in the soliton regime are limited in pulse width and pulse energy by resonant sideband generation and saturation of the P-APM mechanism. In 1993 Kohichi Tamura developed a cavity design known as the stretched-pulse laser which can overcome some of these limitations [120]. With this type of fiber laser, routine production of high energy, femtosecond pulses from erbium-doped fiber lasers is now possible from a compact source. These characteristics make the stretched-pulse fiber laser an attractive source for a number of applications including chirped-pulse wavelength-division multiplexing [121] and optical coherence tomography [18] as well as a seed for solid-state regenerative amplifiers [122], [123].

In this chapter the stretched-pulse concept is reviewed in Section 6.1. Next, two aspects of stretched-pulse lasers investigated for this thesis will be reported. An environmentally-stable version of the stretched-pulse fiber laser will be discussed in Section 6.2. With 980-nm diode-pumping levels of 200 mW, this laser is able to generate 1.2 nJ pulses with 50 nm of spectra that can be externally compressed to sub-100 fs. In addition the effects of high output coupling (> 80 %) and pump configuration on output performance and intra-cavity pulse dynamics are also studied. In Section 6.3, the initial, experimental observation of resonant sidebands in stretched-pulse lasers is presented. Via a theoretical model, the differences between sideband generation in stretched-pulses and soliton lasers are described. Finally, findings from numerical simulations are also compared with theory and experimental results.

6.1 Overview of The Stretched-pulse Laser

The stretched-pulse fiber laser is normally constructed as a ring resonator containing lengths of both normal dispersion erbium-doped fiber and anomalous dispersion passive fiber. Figure 6-1

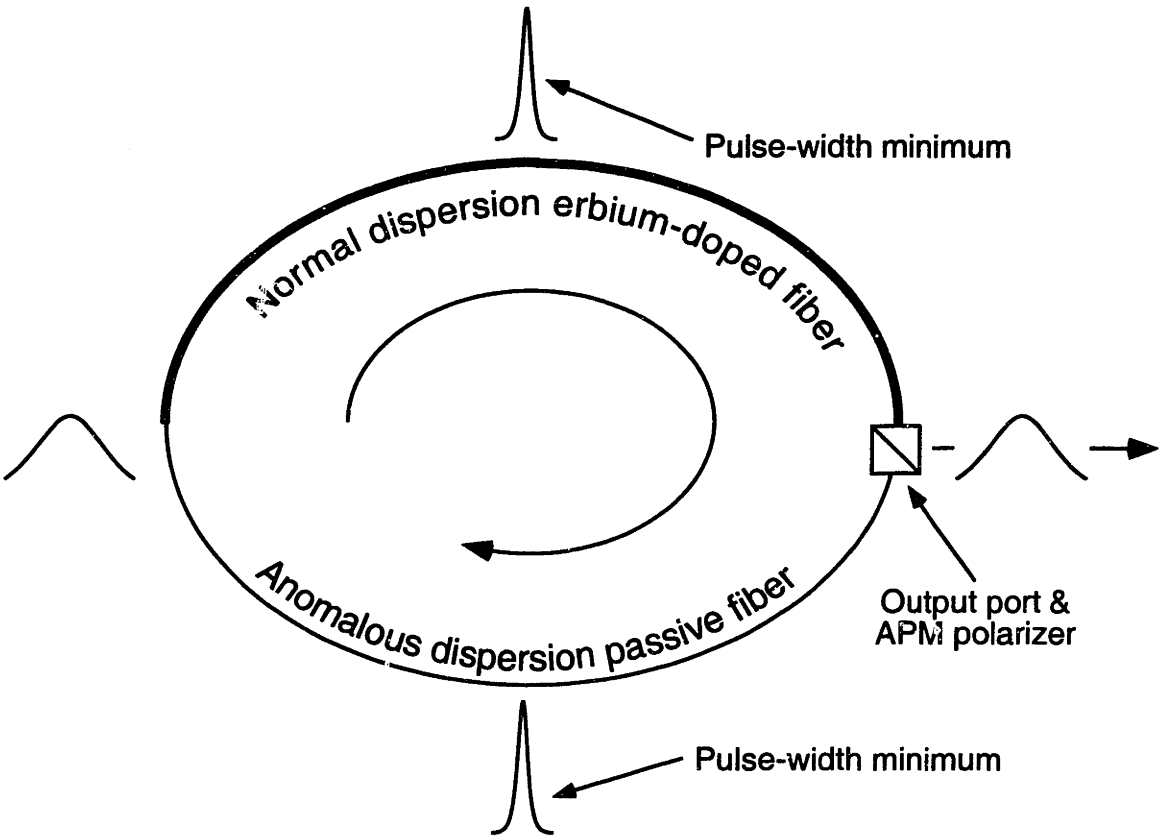

Figure 6-1: Configuration of a stretched-pulse fiber ring laser. Also shown is a first-order approximation of the pulse-width-minimum locations and the pulse stretching and compressing, due to fiber segments with opposite signs of dispersion, as the pulse circulates around the cavity.

illustrates the cavity configuration. The dispersion per unit length for each segment is large so that the dispersion map is the dominant characteristic of the cavity, causing the pulse to periodically stretch and compress (typically by a factor of 10 to 20) as it propagates around the cavity. To a first approximation, the nonlinearity is maximized when the pulse compresses to a transform-limited width at the midpoint of each fiber segment and disperses to maximum width at the interface between each type of fiber. For reasons discussed in Section 6.2, the output is normally taken just after the pulse emerges from the normal dispersion fiber where it has a positive linear chirp. The stretching ratio increases with a larger pulse bandwidth (i.e. a smaller minimum pulse width). Therein lies the advantage of this system over the soliton laser. Normally, for a given pulse energy, a shorter pulse has a higher peak intensity and thus experiences a greater nonlinearity. But in a

stretched-pulse laser, this is true only to a point. The shorter the pulse gets, the more rapidly it spreads, which limits the nonlinearity experienced by the pulse. Hence some of the limits on pulse width and pulse energy imposed by nonlinear effects such as sideband generation and saturation of the P-APM mechanism are significantly reduced.

Initial work on a stretched-pulse ring fiber laser reported self-starting pulses, with 56 nm of bandwidth and 90 pJ of energy, that were compressed to 77 fs [120]. The stretched-pulse technique has yielded the shortest, pulses from an erbium-doped fiber laser (63 fs) [124], while an optimized high-power design produced 100 fs pulses with 2.7 nJ of energy [125]. This pulse energy is nearly three orders of magnitude greater than that generated from femtosecond soliton fiber lasers.

6.2 Stretched-pulse Sigma Fiber Laser[14]

Previous stretched-pulse lasers have been passively mode-locked via P-APM in a self-starting ring cavity with non-Polarization Maintaining (non-PM) fiber. Such a configuration is sensitive to mechanical and temperature variations which may induce drifts in the bias of the P-APM and thus affect the laser's environmental stability. Previously reported environmentally-stable soliton fiber lasers [128] have used a standing wave topology and a Faraday mirror (FRM) to eliminate P-APM bias drift caused by environmentally induced polarization perturbations [129]. As a step towards obtaining high powers and broader spectra with a diode pump, an alternate cavity design was developed for this thesis that was environmentally stable, yet still generated nanojoule pulses with 50 nm of spectrum. The pulses from this laser were compressible to sub-100 fs and required 980-nm diode-pumping levels of only 200 mW. This was the first stretched-pulse fiber laser which could be pumped by conventional laser diodes.

The cavity layout is shown in Fig. 6-2 and is the so-called sigma cavity used by Carruthers *et al* [130], [131] as an environmentally-stable high-repetition-rate, short pulse source. PM fiber was used in the ring section while a Faraday mirror at the end of the linear section allowed use of non-PM erbium-doped fiber while retaining environmental stability. The 1-m piece of erbium-doped fiber had an approximate total dispersion of 0.105 ps^2. The ring section was composed of

14. Portions of this section appear in [126] and [127].

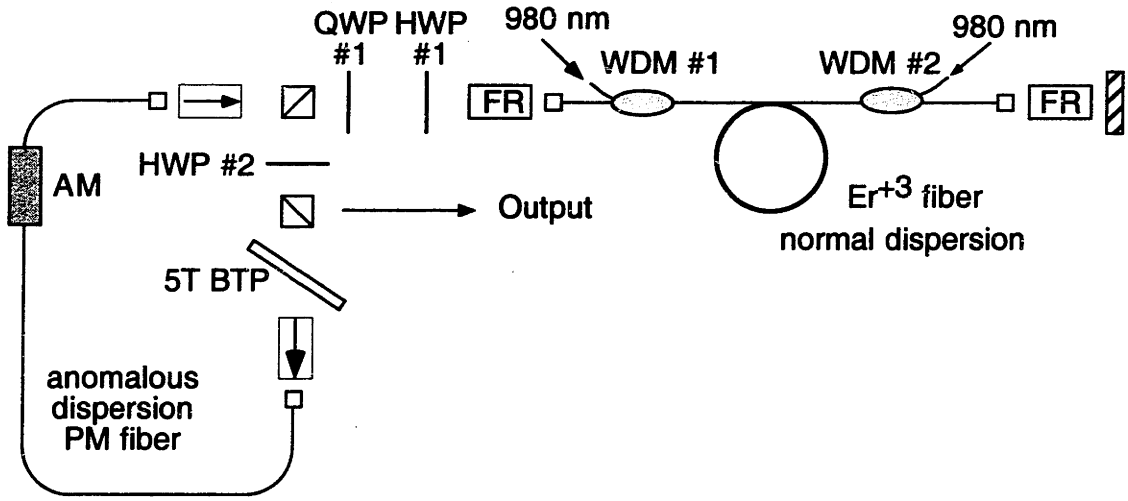

Figure 6-2: Stretched-pulse sigma cavity. WDM, Wavelength Division Multiplexer; FR, Faraday Rotator; BTP, Birefringent Tuning Plate; AM, Amplitude Modulator; QWP, Quarter Wave Plate; HWP, Half Wave Plate; PM, Polarization Maintaining. 980-nm pump is injected either through WDM #1 or WDM #2, but not both

7.50 m of standard PM panda fiber with an estimated dispersion of -20 ps^2/km, resulting in a total dispersion of approximately +0.02 ps^2. The role and use of the $LiNbO_3$ amplitude modulator is discussed below. The dominant effect in both ring and sigma stretched-pulse fiber lasers is produced by opposing fiber sections of strongly normal and anomalous dispersion, so the sigma cavity was expected to behave in a manner similar to ring configurations. An unwrapped version of the sigma cavity given in Fig. 6-3 demonstrates the similarity to previous ring cavity designs. The short lengths and small anomalous dispersion (-7 ps^2/km) of FlexCor fiber in the WDM fiber allowed their dispersive effects to be neglected with respect to the normal dispersion erbium-doped fiber. The locations of the pulse-width minima are an important characteristic of stretched-pulse fiber lasers. In both cavity designs, a consideration of only the dispersion imbalance indicates that, at pulse start-up, the two pulse-width minimum positions should be located at the centers of the normal and anomalous dispersion fiber sections. When the pulse-width minima are at these locations, the nonlinearity and thus the P-APM are maximized. These positions will then shift depending on the operating conditions. In particular, actual stretched-pulse lasers have gain in the normal dispersion (erbium-doped) fiber, and an output coupler is placed after this section as indicated in Fig. 6-3. Both the erbium-doped fiber and the output coupler break the symmetry of

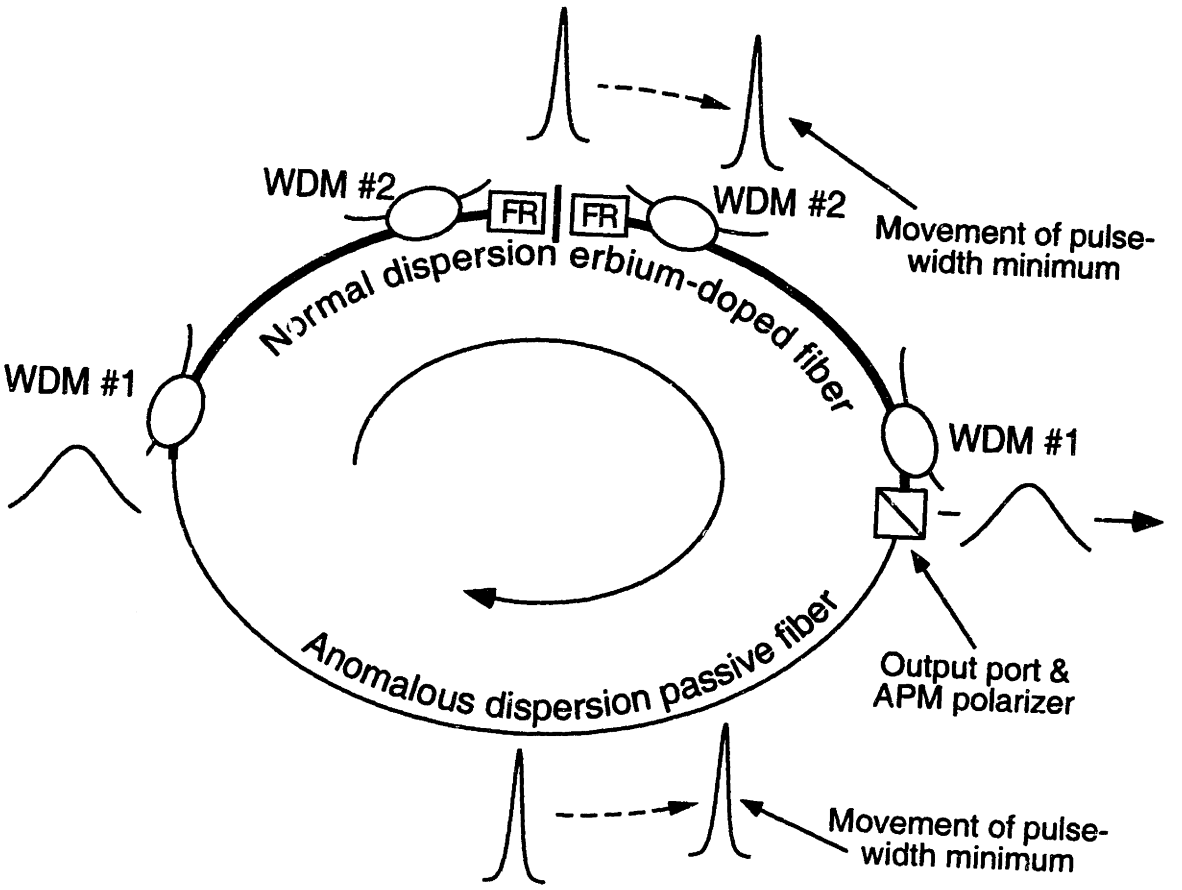

Figure 6-3: Unwrapped sigma cavity showing similarity to a stretched-pulse ring cavity. Also shown are first order estimations of pulse minima and maxima locations. As discussed in the text, the locations of the pulse-width minima move in the indicated direction with increased output coupling as well as pumping configuration.

the loop and cause the pulse-width minimum positions to shift from the midpoint of the fiber sections. Strength and location of filtering also serve to further resolve these positions. Shifts of the pulse-width minimum locations in the sigma cavity were experimentally measured and are presented below.

A study of the pulse dynamics in stretched-pulse ring fiber lasers [124] suggested a design criterion for optimization of output power and pulse width. The key to the cavity design is placement of the APM polarizer (and possibly a variable output coupler) just after the pulse emerges from normal dispersion erbium-doped fiber as shown in Fig. 6-3. Here the highest energy pulses are available for output coupling. Due to losses from the APM polarizer and output coupler, the pulse

experiences only linear propagation in the anomalous dispersion fiber. By limiting nonlinear propagation (and thus spectral generation) to fiber with normal dispersion, a remarkably linear chirp is placed on the pulse [19] which can be easily compressed with a silicon Brewster prism sequence, a grating pair, a fiber delay line, or a chirped Bragg fiber grating. In addition, avoiding nonlinear soliton effects in the anomalous dispersion fiber prevents pulse breakup, thereby allowing higher pulse energies to be produced for a given pump level. As demonstrated by Fig. 6-3, similar design principles can be used to optimize the sigma cavity which has the added benefit of environmental stability.

When the laser reported in ref. [125] was pumped at the full capacity of the MOPA, multiple pulses were observed which were most likely caused by saturation of P-APM producing Additive Pulse Limiting (APL) [71] effects. This suggested that with properly biased P-APM, comparable single pulse energies could be obtained at reduced pump power levels. Of course, the trouble is that at such bias points, self-starting operation is unlikely. Typical self-starting 980-nm pump thresholds for soliton fiber ring lasers are approximately 40 mW [132], while thresholds for stretched-pulse ring lasers range from 250 to 300 mW [125]. Presently this latter pump level is only obtainable from a MOPA, laser-diode-multiplexed pump modules, or Ti-Sapphire source.

The sigma design is not a traveling-wave cavity through its entire length. First-order reflections from bulk elements in the linear section of the cavity can form etalons which impede self-starting via mode-pulling [132]. Spatial hole-burning in the erbium-doped fiber is an additional hindrance for self-starting [133]. To overcome these obstacles and directly obtain a high energy pulse state with diode pump levels of 200 mW, a fiber pigtailed $LiNbO_3$ traveling-wave modulator was included in the ring section of the cavity for assistance with pulse start-up. After mode-locking was initiated by turning on the modulator and adjusting the wave-plates and filter, the modulator was turned off and the laser operated with a single pulse per round-trip. This procedure allowed the P-APM bias to be set to avoid the saturated regime. The modulator was driven at the third cavity harmonic (approximately 51 MHz) as our RF oscillator has a lower cut-off frequency of 50 MHz. For pulse start-up the modulation frequency must be set to within 0.5 kHz of the third cavity harmonic, and the modulation depth required was approximately 25 %. Instead of using an adjustable, free-running oscillator to drive the modulator, a regenerative RF drive that automatically selects the proper modulation frequency [75] could be implemented.

6.2.1 Operating Characteristics

With 200 mW of pump power injected into WDM #1, WDM #2 terminated with a 12-degree angle-polish, and HWP #2 set to couple out approximately 80 %, a pulsed state was obtained with average output power of 20 mW corresponding to a pulse energy of 1.2 nJ. The spectrum shown in Fig. 6-4 had a width of 50.2 nm and was associated with an uncompressed pulse width of 1.44

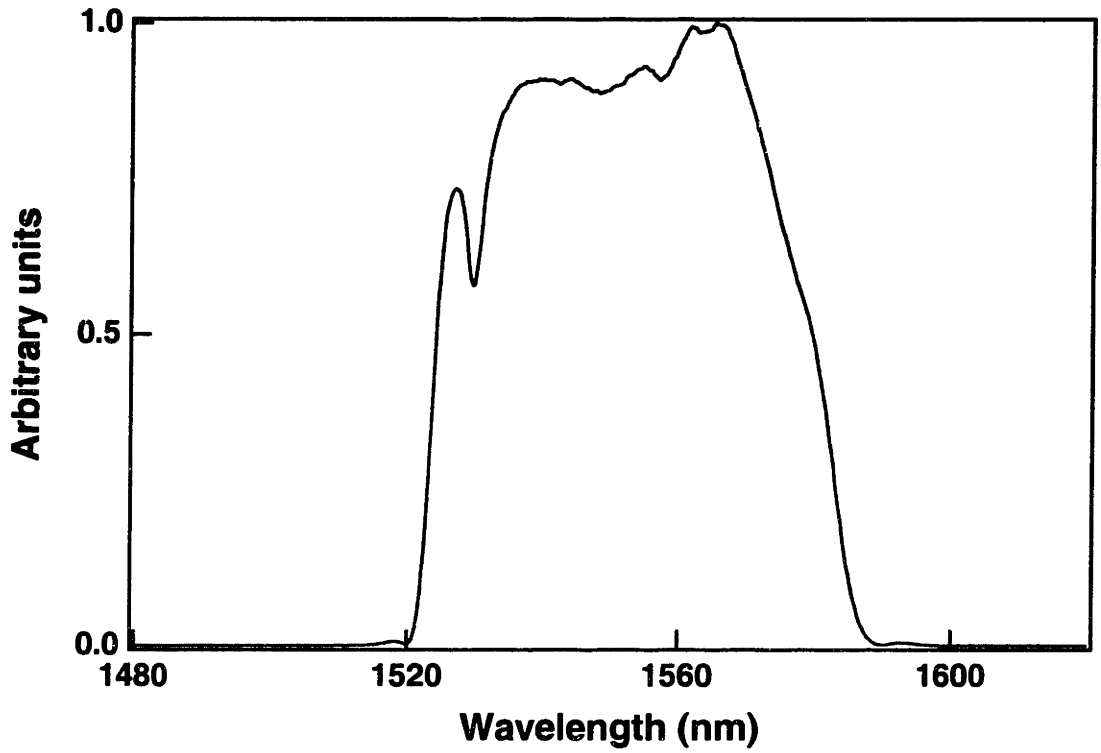

Figure 6-4: Typical pulse spectrum produced by stretched-pulse sigma laser with $\Delta\lambda$ = 50.2 nm. The uncompressed pulse width was 1.44 ps. The corresponding autocorrelation of the compressed pulse is shown in Fig. 6-5.

ps. It is important to note that the spectrum at the output port represented the true intra-cavity pulse rather than the rejected pulse from the APM polarizer. Either a grating pair or a silicon Brewster prism sequence was used for compression of the chirped output pulses. Compression via a grating pair produced typical pulse widths of 96-106 fs, assuming a sech shape. Although a Gaussian pulse shape is predicted in the stretched-pulse theory [134], a sech shape better approximates the pulse produced by this laser. A grating-compressed pulse of 104 fs is shown in Fig. 6-5 along with a sech fit. The time-bandwidth product was 0.65 while only 7 % of the energy was in

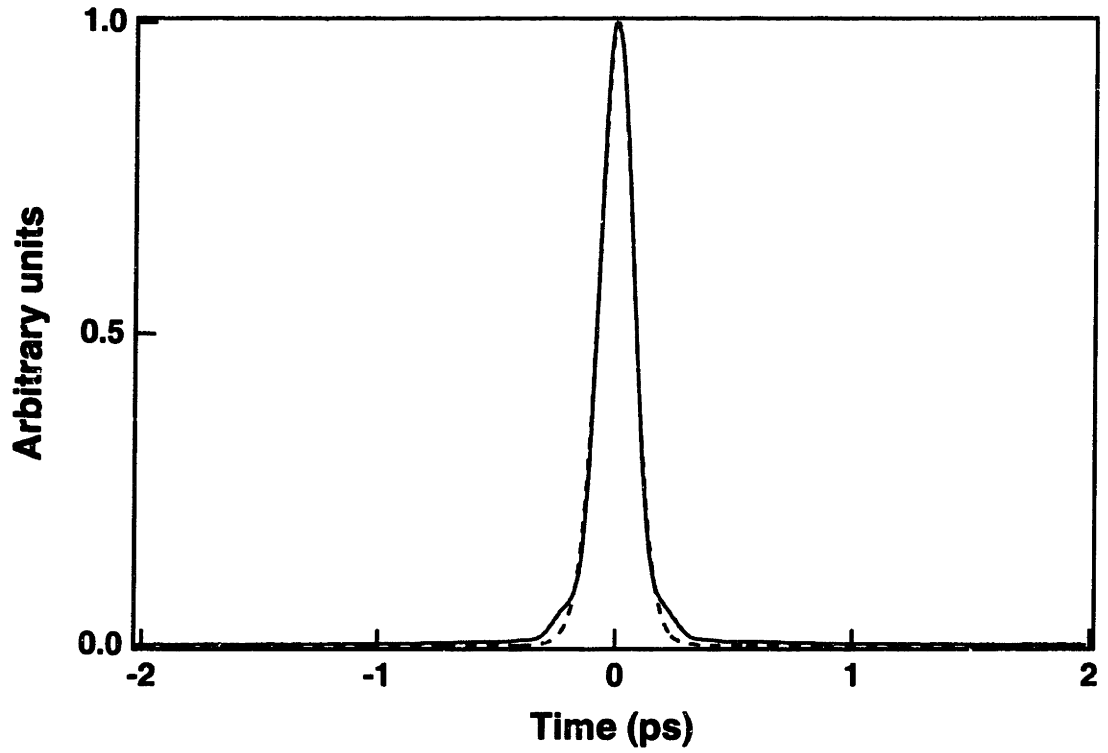

Figure 6-5: Autocorrelation of pulse generated by stretched-pulse sigma laser that was compressed by a grating pair to 104 fs. Dotted line is sech fit. The corresponding spectrum is shown in Fig. 6-4.

the non-sech component of the pulse wings after compression, indicating that a large amount of nonlinear (uncompressible) chirp was located in the center of the pulse. Grating compression consistently yielded pulses about 30 % shorter than pulses obtained with prism compression. This discrepancy was most likely due to spatial filtering of the spectrum which may occur when using a silicon prism sequence because of the large Brewster angle and the wide prism separation (15 to 19 cm) necessary for sufficient negative dispersion compensation.

Increasing the pump power to 320 mW raised the pulse energy to 1.8 nJ, while the spectrum and compressed pulse remained nearly identical to Figs. 6-4 and 6-5. Beyond this pumping level, the pulse energy remained clamped at 1.8 nJ. As mentioned previously, obtaining this level of output pulse energy required the output coupler to extract approximately 80 to 85 % of the intra-cavity power.

Environmental stability was verified by imposing local temperature changes of 35 degrees Celsius at various points on the fiber with a heat gun. Even under these conditions the sigma laser remained stably mode-locked. Overall turn-key operation with the sigma laser in the high output power (1.2 nJ pulse) state was observed over a period of months.

6.2.2 Pulse Dynamics

In the stretched-pulse ring cavity, as output coupling was increased, the spectral width of the pulse remained roughly constant, suggesting that the round-trip nonlinear phase shift also remained constant. However, the uncompressed pulse width that emerged from the output port decreased significantly [135]. This indicated that the pulse-width minimum position shifted further into the erbium-doped fiber. By shifting in this manner the pulse received more gain before reaching a minimum pulse width, thereby compensating the higher output coupling (i.e. higher cavity loss) to maintain its total nonlinear phase shift and net APM action on the pulse. Given the similarities of ring and sigma cavities, it was expected that comparable intra-cavity pulse dynamics also existed in the sigma configuration. This hypothesis was confirmed by the results presented in Fig. 6-6. In the sigma cavity, with pump injected through WDM #1, the uncompressed pulse width changed from 1.8 ps to 1.3 ps, indicating the pulse-width minimum location moved almost 50 cm into the erbium-doped fiber from the symmetry point toward the output port as the output was is changed from 15 to 80 %. During this procedure the waveplates were not changed.

Further understanding of the pulse-width minimum shift was obtained by switching the pumping configuration to use only WDM #2. Under similar conditions, the reduced change in the uncompressed pulse width, plotted as triangles in Fig. 6-6, denoted that only a slight shift of the pulse-width minimum location occurred as output coupling is increased. In this case there was more gain available near the symmetry point due to the higher pump power at this location in the erbium-doped fiber. As a result, the pulse-width minimum shifted only approximately 20 cm to maintain the same net nonlinear phase shift in the cavity when the output coupling was changed from 10 to 70 %.

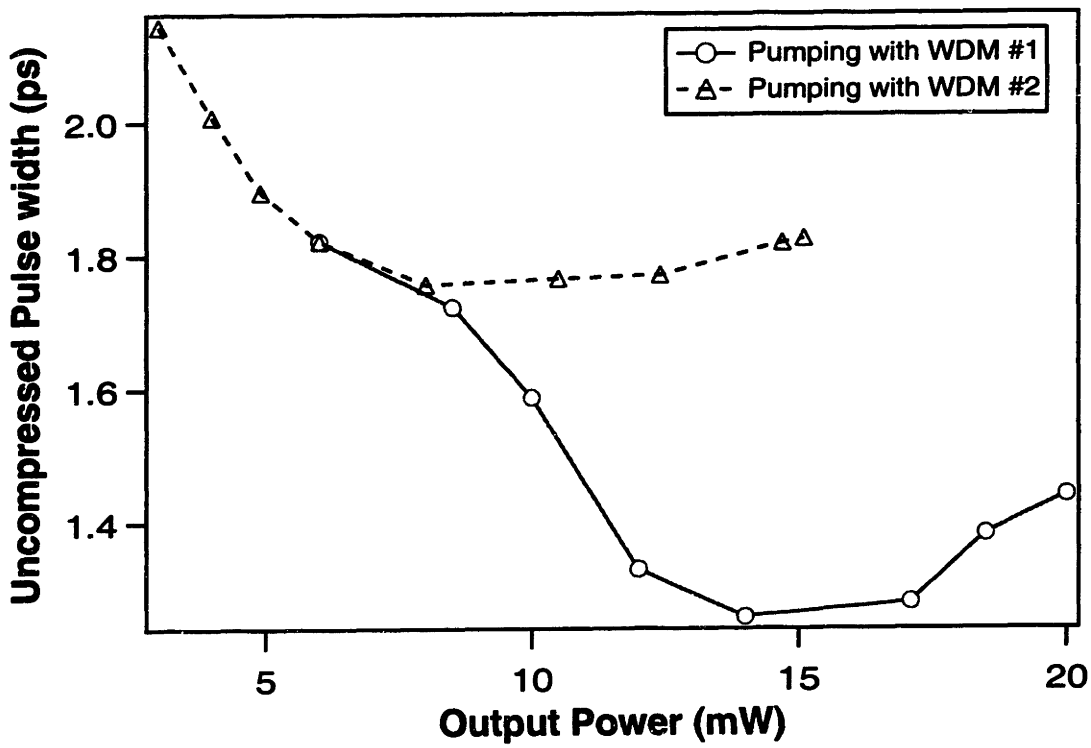

Figure 6-6: Change in uncompressed pulse-width from output port for two different pumping configurations. The location of the pulse width minimum (and hence the uncompressed pulse width that emerged from the laser) changed with output coupling in order to maintain the net APM on the pulse. The reduced change when pumping with WDM #2 supports this reasoning as there is higher gain near the pulse-width-minimum location with this pumping configuration.

6.2.3 Spectral Modulation

In each pump configuration the spectral width at the output port remained approximately 45 to 50 nm, even as the output coupling was adjusted. With low output coupling, as shown in Fig. 6-7, the spectrum exhibited a modulated structure in both pumping configurations. The likely cause of the spectral structure is nonlinear effects in the anomalous dispersion fiber. To investigate such a possibility the soliton order (N) of the pulse injected into the anomalous dispersion fiber after the output coupler was calculated. N is given by [19],

$$N = \sqrt{\frac{2\pi n_2 P_p \tau_o^2}{\lambda_o A_{eff} |\Delta k''|}} \tag{6-1}$$

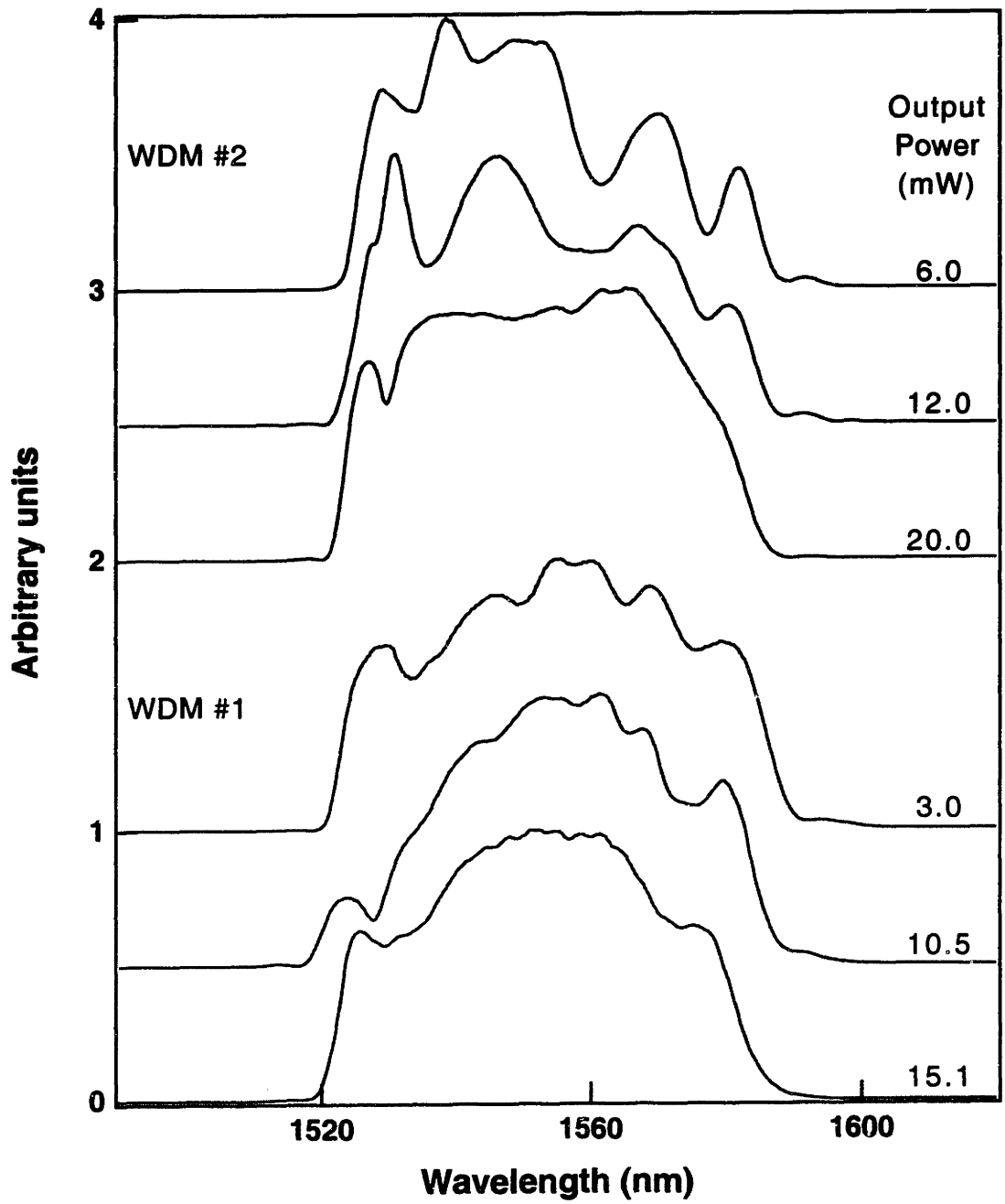

Figure 6-7: Output port pulse spectra at different output powers with pump injected by WDM #1 (lower set of traces) and with pump injected by WDM #2 (upper set of traces). At low output coupling nonlinear propagation in anomalous dispersion fiber led to higher order soliton effects that caused spectral distortion.

where n_2 is the nonlinear index, P_p is the peak power, τ_o is the transform-limited pulse width, λ_o is the central wavelength, and A_{eff} is the effective mode area. With high output coupling in either pumping configuration, eqn. (6-1) gives $N < 1$. With low output coupling (an output power of 6.0 mW for WDM #1 and 3.0 mW for WDM #2), $N \approx 2.5$ indicating that the pulse energy injected into the anomalous dispersion fiber was large enough for the pulse to produce higher order soliton effects. This is the probable cause of the spectral modulation at low output coupling. The cleanest spectra were obtained by using the highest possible output coupling (80 to 85 %) that still sustained mode-locked operation. These results confirm that in an optimally designed/ operated stretched-pulse fiber laser, any nonlinear propagation in the anomalous dispersion section of the laser should be avoided.

6.3 Resonant Sidebands in Stretched-pulse Lasers with Net Normal Dispersion[15]

In past investigations of stretched-pulse fiber lasers [124] there has been a notable absence of resonant sidebands which occur in soliton lasers [105] and long-distance soliton communication systems [106]. A number of possible reasons for this condition have been proposed including the Gaussian-like shape of the stretched-pulsed spectrum which, due to a faster decay in the spectral wings as compared with a soliton (sech) pulse, could lead to reduced (or nonexistent) sideband formation. Work completed for this thesis revealed the presence of weak spectral sideband-like structure in a stretched-pulse laser operating with net normal dispersion. The existence of sidebands is important as they could be a factor in limiting the performance of both the stretched-pulse fiber laser and related dispersion-managed soliton transmission systems. In these following sections a theoretical model, experimental evidence, and confirmation via numerical simulations are given for resonant sideband formation in stretched-pulse fiber lasers operating with net normal (non-soliton) dispersion.

15. Results reported in this section were obtained in collaboration with Dr. Y. Chen and they appear in [136].

6.3.1 Theoretical Formulation

Resonant sideband generation due to periodic perturbations that is discussed in Section 5.1.1 is a well known characteristic in soliton systems. However, this phenomenon is not unique to solitons. It occurs whenever a steady-state excitation (in this case a pulse) is perturbed so that the excitation emits radiation while readjusting itself to the steady-state. Coherent superposition of this radiation occurs when the round-trip phase delays of the primary excitation and of the radiation produced at perturbation points are modulo 2π. This process leads to sideband formation. To predict the formation of sidebands, the phase shifts for both the linear and nonlinear components must be known. Identical to soliton fiber lasers, the linear waves in a stretched-pulse fiber laser experience a per-round-trip phase dispersion of,

$$\phi_{lin} = \frac{1}{2}|\Delta k''|\Delta\omega^2 L_c \tag{6-2}$$

where $\Delta k''$ is the average net dispersion of the cavity, $\Delta\omega$ is the offset from the center frequency, and L_c is the cavity length. In the laser cavity with which the experiments were performed the third order dispersion is small enough that it can be neglected.

As shown in Section 5.1.1 the nonlinear phase shift per round-trip for a soliton in net anomalous dispersion, calculated from the soliton area theorem, is,

$$\phi_{sol} = \delta|A_o|^2 L_c = \frac{1}{2}\frac{|\Delta k''|}{\tau_s^2} L_c \tag{6-3}$$

In order to calculate the phase shift for stretched pulses a similar area theorem for stretched pulses (and dispersion-managed solitons) can be derived[16] using variational techniques [137]. The resulting phase shift per-pass is,

$$\phi_{sp} = \frac{1}{2}\Lambda\frac{|\Delta k''|}{\tau_o^2} L_c \tag{6-4}$$

16. This derivation was completed by Dr. Y. Chen and Prof H.A. Haus.

where τ_o is the Gaussian pulse width at a pulse width minimum and Λ is a correction factor to account for the pulse stretching and compressing. Λ is a function of the pulse width and the dispersion map characteristics. The explicit form of Λ is [138],

$$\Lambda = 0.88\text{arcsinh}\left\{\frac{L_c|k_o''|}{4\tau_o^2}\right\}\frac{4\tau_o^2}{L_c|k_o''|}E \tag{6-5}$$

where k_o'' is the uniform dispersion in one segment. In this formulation $|k_o''| \gg |\Delta k''|$. E is,

$$E = \frac{\tau_o}{\Delta k''}\int_0^{L_c} k''(z)\frac{1-\beta^2}{\tau^4(z)}dz\left[\int_0^{L_c}\frac{1}{\tau^3(z)}dz\right]^{-1} \tag{6-6}$$

where $k''(z)$ is the dispersion map, β is the chirp parameter, and $\tau(z)$ is z-dependent pulse width.

Due to the alternating broadening and compression they experience, stretched pulses have a z-dependent phase profile across their spectra which, at times, is nonuniform. But this phase profile is not relevant when calculating the nonlinear phase shift per round-trip of the stretched pulse to evaluate sideband formation. Rather, on successive round-trips all spectral components of a self-consistent stretched pulse will received an identical phase shift ϕ_{sp} (hence the frequency independence of ϕ_{sp}). Sidebands are formed when the phase difference between this phase shift and the radiative (linear) waves is a multiple of 2π,

$$\phi_{lin} - \phi_{sp} = \frac{L_c}{2}\left[\Delta k''\Delta\omega^2 - \frac{\Lambda|\Delta k''|}{\tau_o^2}\right] = \pm 2\pi m \tag{6-7}$$

The phase matching diagram showing both ϕ_{lin} and ϕ_{sp} as a function of $\Delta\omega$ measured from the central frequency of the pulse is given in Fig. 6-8. Due to the net normal dispersion, no particular periodicity of the perturbation is required to satisfy eqn. (6-7), since the Kerr phase delay of the pulse can exactly match the dispersion delay of the linear radiation for any L_c at $m = 0$. This

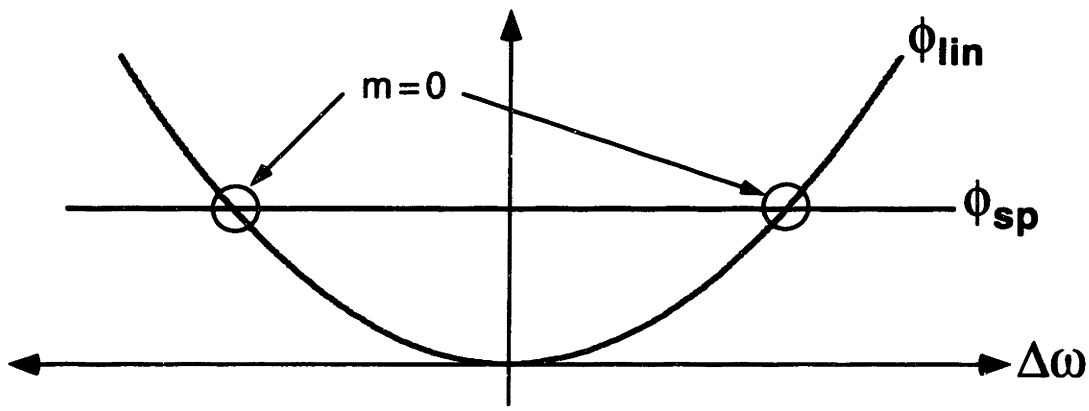

Figure 6-8: Phase per-pass diagram of linear dispersive waves and pulses in a stretched-pulse fiber laser operating with net normal dispersion.

condition is not possible in a soliton laser unless there is strong third order dispersion [139]. The position of the $m = 0$ sideband is given by,

$$\Delta\omega = \frac{\sqrt{\Lambda}}{\tau_o} \tag{6-8}$$

In the experimental investigation, Λ varied by approximately 20 % (mainly caused by the τ_o dependence) and thus it can be taken as a constant. As a result, the sideband position varied approximately as the inverse of the pulse width.

6.3.2 Experimental Results

The prediction of eqn. (6-8) was experimentally confirmed using a stretched-pulse laser operating in the net normal dispersion regime. The stretched-pulse laser used to study sideband generation is shown in Fig. 6-9.[17] It was a standard stretched-pulse design [124], [62] except that intracavity prisms provided anomalous dispersion compensation. Similar to other stretched-pulse lasers, the dispersion of both the erbium-doped fiber (0.12 ps^2) and prisms (–0.06 to –0.12 ps^2) was large.

17. This laser was constructed with help from Lynn Nelson and Siegfried Fleischer.

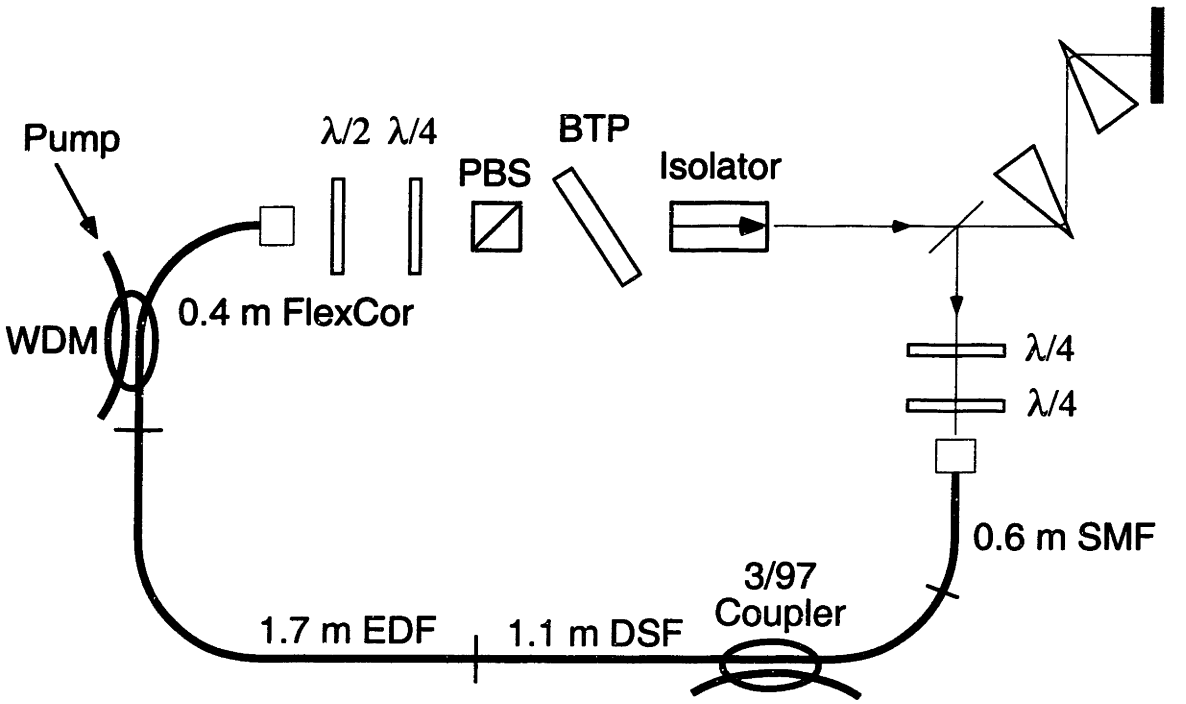

Figure 6-9: Cavity of stretched-pulse fiber laser using prisms for anomalous dispersion compensation. BTP, birefringent tuning plate; WDM, wavelength-division-multiplexer; PBS, polarizing beam splitter; SMF, single mode fiber; DSF, dispersion-shifted fiber; EDF, erbium-doped fiber.

By using intra-cavity prisms instead of fiber for anomalous dispersion compensation, the net dispersion of the cavity can be varied without changing fiber lengths. Measurements of the pulse spectra were taken at three different points in the cavity: from a 3/97 coupler placed just before the erbium-doped fiber, the P-APM rejection port from the PBS, and the residual reflection from the BTP. Similarly to other studies [124], the spectral width emerging from the P-APM rejection port depended strongly on the net dispersion in the cavity. In this case the pump level is not altered, leading to a relatively constant output power. Over a net dispersion range of 0.02 to 0.055 ps^2 when the Time-Bandwidth Product (TBP), calculated using the externally compressed pulse width, remained almost invariant. This characteristic will be important later in this chapter when experimental results are compared numerical simulations. The behavior of these parameters is summarized in Fig. 6-10.

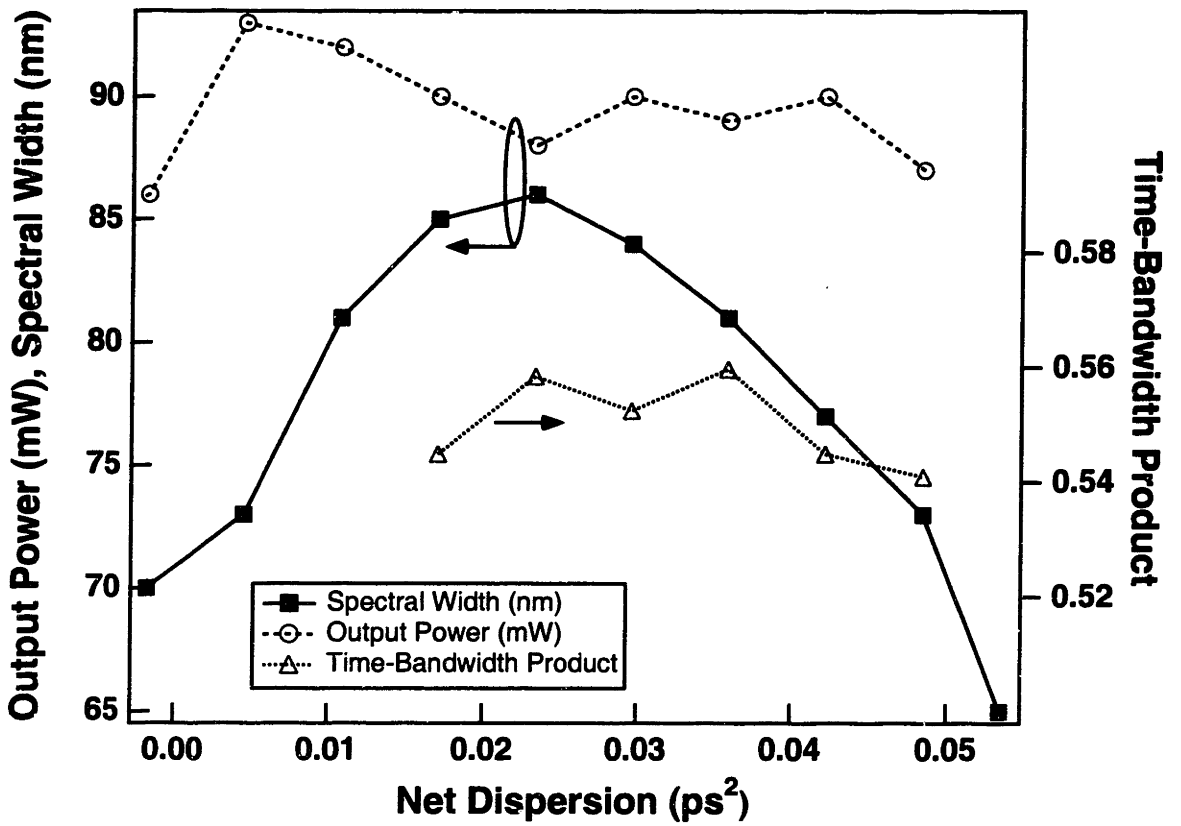

Figure 6-10: Changes in spectral width, output power, and time-bandwidth product of pulses emerging from the P-APM rejection port as a function of net cavity dispersion. In this set of measurements the pump power and waveplates were not changed.

Evidence of sidebands appeared at each of the three ports. The optical spectra of the mode-locked pulses at these three ports are shown in Fig. 6-11 for two values of net dispersion. The sidebands are most easily distinguished at the 3/97 coupler before the spectrum is broadened in the erbium-doped fiber via SPM. Figure 6-12 displays a series of spectra from this port as the net cavity dispersion is increased. In order to minimize the perturbations from trace to trace, the waveplates were not adjusted as the prism separation was increased. On the two highest dispersion settings (0.048 ps^2 and 0.052 ps^2), the filter was adjusted slightly to attenuate the CW spike at 1532 nm. There is a distinct sideband on the long wavelength side that moves toward the center as the net dispersion is increased. The sources of radiation that form the sidebands were perturbations of the pulse, particularly those due to the periodic gain and loss. This point is supported by the numerical simulations reported below. There was additional spectral structure on both sides of

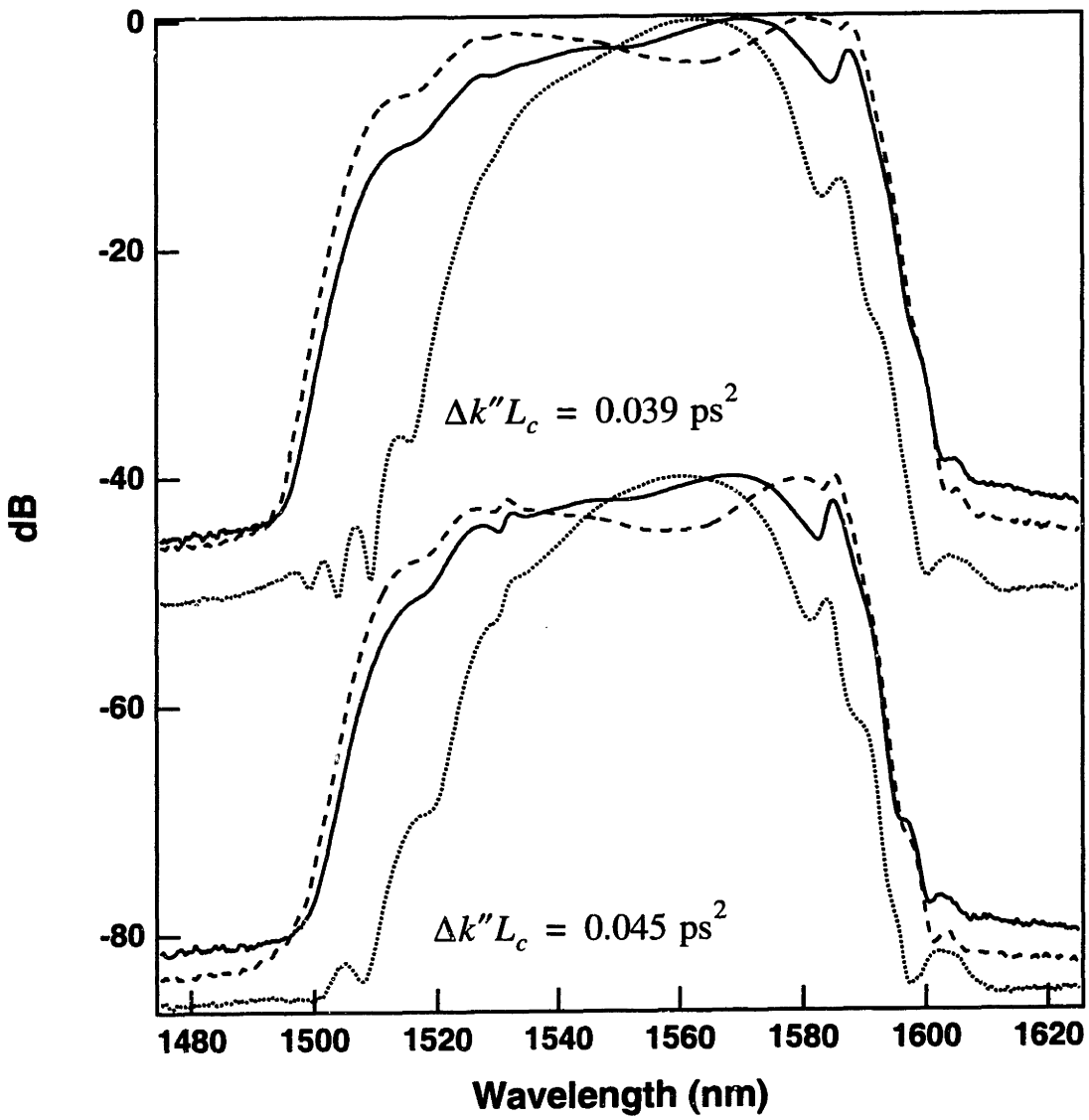

Figure 6-11: Spectra from the P-APM rejection port (dashed line), reflection off the BTP (solid line) and 3/97 coupler (dotted line) for two different values of net cavity dispersion (0.039 ps^2 and 0.045 ps^2). At each of the three ports there is evidence of m=0 sideband on the long wavelength side.

the spectra which resembles additional resonant sidebands. However, the behavior of these extremely low-level sidebands as the net dispersion is varied is not as clear.

According to eqn. (6-8), when Λ is taken to be constant, the sideband position depends linearly on the inverse minimum pulse width. As indicated in Fig. 6-10, the TBP remained approxi-

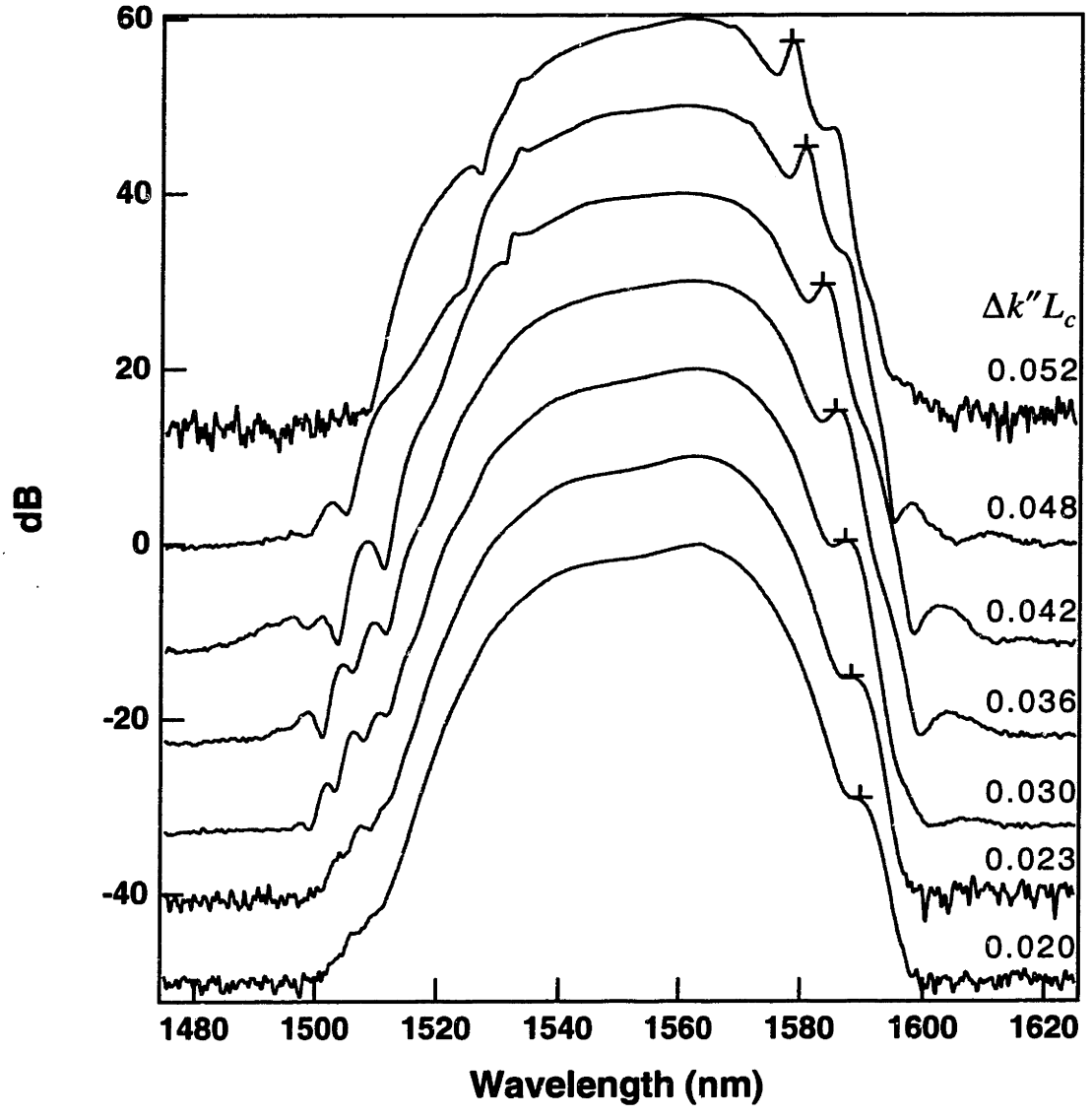

Figure 6-12: Spectra from 3/97 coupler for different values of net dispersion. The strength of net normal cavity dispersion for each trace is given on the right-hand side in units of ps^2. The crosses mark the movement of the m = 0 sideband. The first moment for all spectra is 1548 nm and this is taken as $\Delta\omega = 0$.

mately constant when the dispersion was varied which meant the sideband position depended linearly on the spectral width. Figure 6-13 plots the experimentally determined sideband position as a function of the spectral width (along with a linear fit of the experimental data). The spectral width was chosen as the independent parameter when comparing the experimental measurements

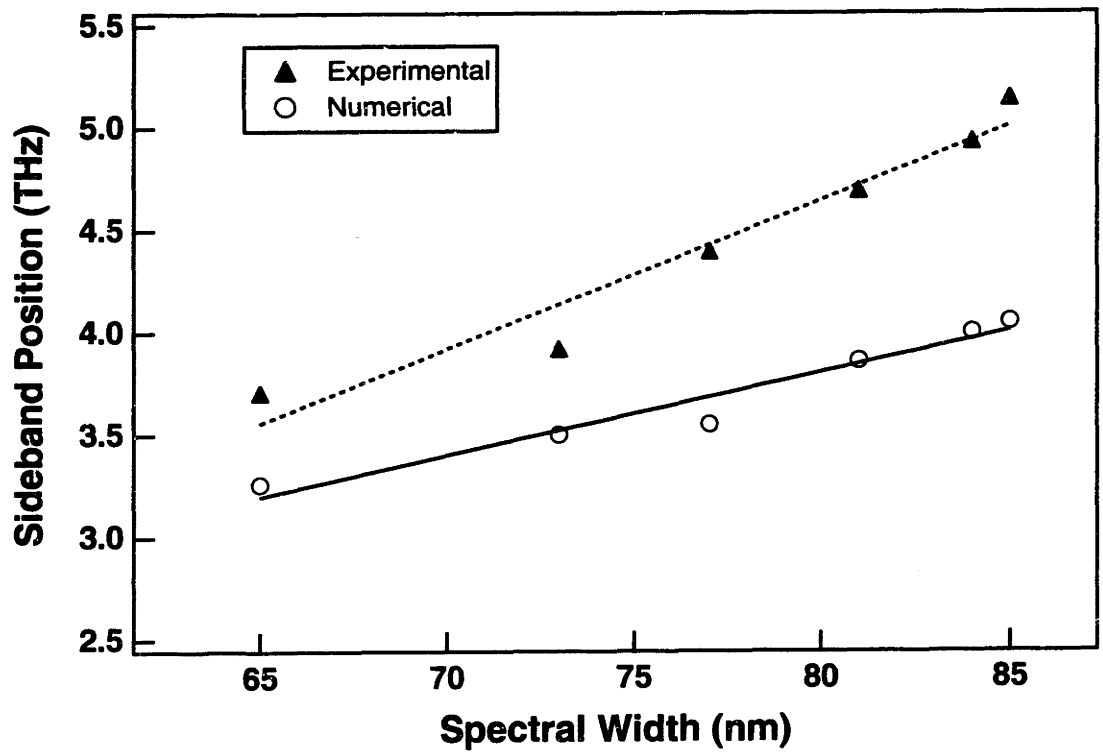

Figure 6-13: Experimental (triangles) and numerical (open circles) results for the m=0 sideband position as a function of spectral width. A linear fit, predicted theoretically by eqn. (6-8), is shown for both sets of data.

with numerical simulations and theoretical results as it was a more direct measure of the pulse width minimum (and hence the nonlinear phase shift) than the externally compressed pulse width.

6.3.3 Numerical Simulations

A full numerical simulation of the laser was completed by Dr. Y. Chen as an additional confirmation for sideband formation and behavior. The simulations were based on the nonlinear Schrödinger equation,

$$-j\frac{\partial u}{\partial z}+\frac{k''(z)}{2}\frac{\partial^2 u}{\partial t^2}+\delta|u|^2u = 0 \tag{6-9}$$

where u is the slowly varying pulse envelope and δ is the nonlinear coefficient. The dispersion map $k''(z)$ varied with amplitude ± 70 ps^2/km with net normal dispersion. Equation (6-9)

describes nondissipative propagation. In the simulations sidebands appeared because the initial (launched) pulse shed radiation as it formed a steady-state solution with a spectral signature enhanced by the phase-matching condition of eqn. (6-8). Simulations that included periodic gain and loss perturbations (a model that was closer to the actual laser) showed an increase in the amplitude of the sidebands but their position did not change. This result indicates the sidebands are formed via the resonant process illustrated in Figure 6-8, rather than a parametric process [140] involving a gain-loss periodicity. Furthermore, a calculation of the parametric sideband position predicts a spacing at least 6.5 times larger than observed experimentally or numerically.

The simulations were performed using the laser cavity parameters for various experimentally measured spectral widths (as given in Fig. 6-10) and the corresponding net normal dispersion values. The resulting (numerically determined) sideband positions are shown in Fig. 6-13 by open circles. For each data point the pulse energy was adjusted to a common value which is supported by the constant output power results shown in Fig. 6-10. The trend in the numerical simulations agreed with experimental results.

6.3.4 Characteristics of Resonant Sidebands in Stretched-Pulse Fiber Lasers

As there is no periodicity requirement to make-up the phase difference between the pulse and the radiation at $m = 0$, it might be expected that sideband generation in stretched-pulse lasers could be excessive. However, the phase and amplitude of a stretched pulse change continuously in one round-trip. For multiple perturbations the initial phases of the locally produced dispersive waves can be different. Thus, constructive interference only necessarily occurs between radiation produced at the same point in the cavity on successive round-trips. Dispersive waves produced at different points may not interfere constructively with each other. For this reason sideband generation is not catastrophic and may actually be quite weak.

Soliton sideband generation due to periodic perturbation determines the maximum amplifier spacing in long distance soliton transmission [106]. Recently, a technique closely related to the stretched-pulse principle in fiber lasers has emerged within the context of RZ long distance transmission systems. Extensive work by a number of groups has demonstrated that so-called dispersion-allocated or dispersion-managed soliton transmission networks offer a number of advantages

over pure soliton systems including longer amplifier spacing, reduced Gordon-Haus jitter and collision-induced jitter, and increased power margins [141], [142], and [143]. Sideband generation in this new type of transmission system with net normal dispersion is important in the new thrust of long distance dispersion-managed pulse propagation. For full and efficient utilization of erbium-doped fiber bandwidth, allocated WDM channels will probably be placed in both regimes of net anomalous and net normal dispersion. The energy loss to the sidebands will have to be taken into account in the design of any long distance fiber communication systems utilizing the regime of net normal dispersion.

Chapter 7

Conclusion/Future Work

A summary of the different devices investigated for this thesis is given in the following sections. Possible avenues of future work for the optical fiber ring buffer, soliton waveguide laser, and resonant sidebands in stretched-pulse fiber lasers are also discussed.

7.1 Soliton Stability in Actively Mode-locked Fiber Lasers

The stability region for pulses in a harmonically mode-locked fiber ring laser with soliton pulse compression was mapped out and compared with theoretical predictions. Soliton compression yielded pulses that were a factor of 4.4 shorter than those predicted by standard active mode-locking theory.

7.2 Asynchronous Phase-modulated Optical Fiber Ring Buffer

Successful loading, storage, and unloading of 5 Gbit/sec packets from an asynchronous phase-modulated optical fiber ring buffer was demonstrated. Introduction of a CW holding beam extended the storage time to at least 157 μs or 1600 circulations. Limitations with the diagnostic equipment prevented an observation of the packet envelope beyond this limit as well as a confirmation of maintenance of the individual bits in the packets beyond 44.3 μs (450 circulations). Asynchronous packet storage dynamics were explored and tolerances on the position of the loaded packets relative to buffer's phase modulation were investigated. Possible extensions of this work could involve increasing the bit-rate of the buffer, possibly by using all-optical phase modulation, developing new techniques to observe longer packet storage times, and performing bit-error rate tests on the stored packets.

7.3 Soliton Fiber Lasers Incorporating Waveguide Amplifiers

Two types of soliton fiber lasers incorporating a waveguide amplifier were reported. In the first laser, a passively mode-locked soliton ring fiber laser was investigated that used P-APM as the mode-locking mechanism. The resulting short cavity (1.3 m of fiber) simultaneously reduced three parasitic effects that have limited the performance of P-APM soliton fiber lasers: multi-pulsing behavior, resonant sideband formation and saturation of the P-APM mechanism. These improvements enabled generation of 116 fs solitons with a pulse energy of 130 pJ at a fundamental repetition rate of 130 MHz. By reducing the pump power to 290 mW, a 156 fs pulse was obtained with small pedestal containing 5 % of the pulse energy. Clearly, a reduction in pump power requirements would broaden the possible applications for this laser. Such improvements as low-loss pig-tailed fibers and an amplifier length optimized for higher pump powers would reduce the threshold.

As an alternate solution, a second cavity design was also investigated that employed a semiconductor saturable absorber mirror (SESAM) to obtain mode-locking. An unstable "mode-locked" state was obtained from preliminary work on short (< 0.3 m) linear cavities using SESAM devices. Possible further work on this research topic is discussed at the end of Chapter 5.

7.4 Studies of Stretched-Pulse Fiber Lasers

Two investigations into stretched-pulse fiber lasers were also pursued. An environmentally stable, diode-pumped stretched-pulse fiber laser that delivered 1.8 nJ pulses with a spectral width of 50 nm and a compressed duration of sub-100 fs was demonstrated. A sigma cavity design was used for this laser. Use of a modulator for assistance with pulse start-up allowed the P-APM bias point to be set to maximize the output pulse energy and reduced 980-nm pump power requirements to 200 mW. The effects of high (> 80 %) output coupling on intra-cavity pulse dynamics are observed to depend on the pumping configuration for the sigma cavity. The highest possible output coupling (while still retaining mode-locked operation) was found to maximize the output pulse energy and generate the cleanest, broadest spectrum for optimal pulse compression.

Finally, an observation of the zeroth-order resonant sideband in a stretched-pulse ring fiber laser with net normal dispersion (and insignificant third order dispersion) was reported. A theoret-

ical prediction of the sideband position as a function of pulse width and net dispersion was confirmed with both experimental results and a full numerical simulation of the fiber laser. An interesting topic of future work would be to investigate why resonant sidebands are much weaker in stretched-pulse fiber lasers as compared to soliton lasers. It is possible that the stretching and compressing of the pulse disrupts the phase-matching condition at the $m = 0$ sideband. Another possibility is that the stretched-pulse generates much less radiation when it is perturbed. In order to further refine these explanations, additional numerical and experimental work will be necessary.

References

[1] T. Miya, Y. Terunuma, T. Hosaka, and T. Miyashita, "Ultimate low-loss single-mode fibre at 1.55 μm," *Electron. Lett.*, vol. 15, p. 106, 1979.

[2] R. Mears, L. Reekie, I. Jauncey, and D. Payne, "Low-noise erbium-doped fibre amplifier operating at 1.54 μm," *Electron. Lett.*, vol. 23, p. 1026, 1987.

[3] S. Aisawa, T. Sakamoto, M. Fukui, J. Kani, M. Jinno, and K. Oguchi, "Ultra-wideband, long distance WDM demonstration of 1 Tbit/s (50*20 Gbit/s), 600 km transmission using 1550 and 1580 nm wavelength bands," *Electron. Lett.*, vol. 34, p. 1127, 1998.

[4] A. K. Srivastava, Y. Sun, J. W. Sulhoff, C. Wolf, M. Zirngibl, R. Monnard, A. R. Chraplyvy, A. A. Abraamov, R. P. Espindola, T. A. Strasser, J. R. Pedrazzani, A. M. Vengsarkar, J. L. Zyskind, J. Zhou, D. A. Ferrand, P. F. Wysocki, J. B. Judkinds, S. W. Granlund, and Y. P. Li, "1 TB/s transmission of 100 WDM 10 Gb/s channels over 400 km of TrueWave fiber," Optical Fiber Communications, PD10, San Jose, CA, 1998.

[5] P. Morton, "High speed 1.55 μm lasers for fiber optic transmission," *International J. of High Speed Electron. and Systems*, vol. 8, p. 457, 1997.

[6] M. Zirngibl, C. Doerr, and C. Joyner, "Demonstration of a splitter router based on a chirped waveguide grating router," *IEEE Photonics Technol. Lett.*, vol. 10, p. 87, 1998.

[7] M. Zirngibl, C. Joyner, C. Doerr, L. Stulz, and H. Presby, "An 18-channel multifrequency laser," *IEEE Photonics Technol. Lett.*, vol. 8, p. 870, 1996.

[8] B. Nelson, K. Blow, P. Constantine, N. Doran, J. Lucek, I. Marshall, and K. Smith, "All-optical Gbit/s switching using nonlinear optical loop mirror," *Electron. Lett.*, vol. 27, p. 704, 1991.

[9] K. L. Hall and K. A. Rauschenbach, "100-Gbit/s bitwise logic," *Opt. Lett.*, vol. 23, p. 1271, 1998.

[10] C. Kolleck and U. Hempelmann, "All-optical wavelength conversion of NRZ and RZ signals using a nonlinear optical loop mirror," *J. of Lightwave Technol.*, vol. 15, p. 1906, 1997.

[11] M. Dennis, M. Arend, and I. Duling, "Soliton loop mirror demultiplexer using orthogonally polarized signal and control," *IEEE Photonics Technol. Lett.*, vol. 8, p. 906, 1996.

[12] N. Patel, K. Hall, and K. Rauschenbach, "Optical rate conversion for high-speed TDM networks," *IEEE Photonics Technol. Lett.*, vol. 9, p. 1277, 1997.

[13] K. Tamura, E. Yoshida, and M. Nakazawa, "Generation of 10 GHz pulse trains at 16 wavelengths by spectrally slicing a high power femtosecond source," *Electron. Lett.*, vol. 32, p. 1691, 1996.

[14] R. A. Barry, V. W. S. Chan, K. L. Hall, E. S. Kintzer, J. D. Moores, K. A. Rauschenbach, E. A. Swanson, L. E. Adams, C. R. Doerr, S. G. Finn, H. A. Haus, E. P. Ippen, W. S. Wong, and M. Haner, "All-Optical Network Consortium-Ultrafast TDM networks," *IEEE J. on Sel. Areas in Comm.*, vol. 14, p. 999, 1996.

[15] H. Takara, S. Kawanishi, A. Yokoo, S. Tomaru, T. Kitoh, and M. Saruwatari, "100 Gbit/s optical signal eye-diagram measurement with optical sampling using organic nonlinear optical crystal," *Electron. Lett.*, vol. 32, p. 2256, 1996.

[16] L. Boivin, M. Nuss, W. Knox, and J. Stark, "206-channel chirped-pulse wavelength-division multiplexed transmitter," *Electron. Lett.*, vol. 33, p. 827, 1997.

[17] P. Leisching, A. Mycielski, and T. Elsaesser, "Ultrafast nonlinear optics in semimagnetic $Hg_{0.6}Mn_{0.4}Te$ at 1.55 μm," International Quantum Electron. Conference '98, p. 52, San Franscisco, 1998.

[18] B. E. Bouma, L. E. Nelson, G. J. Tearney, D. J. Jones, M. E. Brezinski, and J. G. Fujimoto, "Optical coherence tomographic imaging of human tissue at 1.55 μm and 1.81 μm using Er- and Tm-doped fiber sources," *J. of Biomedical Opt.*, vol. 3, p. 76, 1998.

[19] G. P. Agrawal, *Nonlinear Fiber Optics*. San Diego, CA: Academic Press Inc., 1995.

[20] A. Yariv, *Optical Electronics*, Fourth Edition ed. Philadelphia: Saunders College Publishing, 1991.

[21] A. W. Snyder and J. D. Love, *Optical waveguide theory*. London: Chapman and Hall, 1983.

[22] E. Desurvire, *Erbium-doped fiber amplifiers*. New York: John Wiley & Sons, Inc., 1994.

[23] E. Snitzer, "Optical maser action of neodymium in barium grown glass," *Phys. Rev. Lett.*, vol. 7, p. 444, 1961.

[24] F. Kapron, D. Keck, and R. Maurer, "Radiation losses in glass optical waveguides," *Applied Physics Lett.*, vol. 17, p. 423, 1970.

[25] J. Stone and C. Burrus, "Neodymium-doped silica lasers in end-pumped fiber geometry," *Applied Physics Lett.*, vol. 23, p. 388, 1973.

[26] H. Po, E. Snitzer, R. Tumminelli, L. Zenteno, F. Hakimi, N. M. Cho, and T. Haw, "Double clad high brightness Nd fiber laser pumped by GaAlAs phased array," Optical Fiber Communications, p. PD7, 1989.

[27] M. Muendel, "Optimal inner cladding shapes for double-clad fiber lasers," CLEO '96, p. 544, Anaheim, CA, 1996.

[28] M. Muendel, "High-power fiber laser studies at the Polaroid Corporation," Proceedings of the SPIE - The International Soc. for Optical Engineering, p. 21, San Jose, CA, 1998.

[29] S. G. Kosinski and D. Inniss, "High-power fiber lasers," CLEO '98, p. 78, San Francisco, CA, 1998.

[30] G. Nykolak, P. C. Becker, J. Shmulovich, Y. H. Wong, D. J. DiGiovanni, and A. J. Bruce, "Concentration-dependent $^4I_{13/2}$ lifetimes in Er^{3+}-doped fibers and Er^{3+}-doped planar waveguides," *IEEE Photonics Technol. Lett.*, vol. 5, p. 1014, 1993.

[31] D. Barbier, *private communication.*

[32] M. Federighi and F. D. Pasquale, "The effect of pair-induced energy transfer on the performance of silica waveguide amplifiers with high Er^{3+}/Yb^{3+} concentrations," *IEEE Photonics Technol. Lett.*, vol. 7, 1995.

[33] F. D. Pasquale and M. Federighi, "Improved gain characeristics in high-concentration Er^{3+}/Yb^{3+} codoped glass waveguide amplifiers," *IEEE J. Quantum Electron.*, vol. 30, p. 2127, 1994.

[34] D. Barbier, M. Rattay, F. Saint Andre, G. Clauss, M. Trouillon, A. Kevorkian, J. M. P. Delavaux, and E. Murphy, "Amplifying four-wavelength combiner, based on Erbium/ Ytterbium-doped waveguide amplifiers and integrated splitters," *IEEE Photonics Technol. Lett.*, vol. 9, p. 315, 1997.

[35] T. Izawa and S. Sudo, *Optical Fibers: Materials and Fabrication.* Dordrecht, Holland: D. Reidel Publishing Company, 1987.

[36] K. R. Tamura, "Additive pulse mode-locked erbium-doped fiber lasers," *Ph.D. in Electrical Engineering*, Boston: MIT, 1994.

[37] W. Knox, "In situ measurement of complete intracavity dispersion in an operating Ti:Sapphire femtosecond laser," *Opt. Lett.*, vol. 17, p. 514, 1992.

[38] R. Fork, O. Martinez, and J. Gordon, "Negative dispersion using pairs of prisms," *Opt. Lett.*, vol. 9, p. 150, 1984.

[39] O. Martinez, J. Gordon, and R. Fork, "Negative group-velocity dispersion using refraction," *J. of the Opt. Soc. of Amer. A (Opt. and Image Science)*, vol. 1, p. 1003, 1984.

[40] L. E. Nelson, "Mode-Locking of Thulium-doped and Erbium-doped Fiber lasers," *Ph.D. in Electrical Engineering*, Boston: MIT, 1997.

[41] H. Haus and W. Wong, "Solitons in optical communications," *Reviews of Modern Physics*, vol. 68, p. 423, 1996.

[42] H. A. Haus, "Optical fiber solitons, their properties and uses," *Proceedings of the IEEE*, vol. 81, p. 970, 1993.

[43] A. Hasegawa and F. Tappert, "Transmission of stationary nonlinear optical pulses in dispersive dielectric fibers. II. Anomalous dispersion," *Applied Physics Lett.*, vol. 23, p. 171, 1973.

[44] L. Mollenauer, R. Stolen, and J. Gordon, "Experimental observation of picosecond pulse narrowing and solitons in optical fibers," *Physical Review Lett.*, vol. 45, p. 1095, 1980.

[45] V. E. Zakharov and A. B. Shabat, "Interaction between solitons in a stable medium," *Soviet Physics - JETP*, vol. 37, p. 823, 1972.

[46] A. Hasegawa, *Optical solitons in fibers*, vol. 116. Berlin: Springer-Verlag, 1989.

[47] A. Hasegawa and Y. Kodama, *Solitons in optical communications*, vol. 7. Oxford: Clarendon Press., 1995.

[48] L. F. Mollenauer, J. P. Gordon, and M. N. Islam, "Soliton propagation in long fibers with periodically compensated loss," *IEEE J. Quantum Electron.*, vol. 22, p. 157, 1986.

[49] H. A. Haus, E. P. Ippen, and K. Tamura, "Additive-Pulse Modelocking in Fiber Lasers," *IEEE J. Quantum Electron.*, vol. 30, p. 200, 1994.

[50] P. D. Maker and R. W. Terhune, "Study of optical effects due to an induced polarization third order in the electric field strength," *Physical Review Lett.*, vol. 12, p. 507, 1964.

[51] R. H. Stolen, J. Botineau, and A. Ashkin, "Intensity discrimination of optical pulses with birefringent fibers," *Opt. Lett.*, vol. 7, p. 512-514, 1982.

[52] M. N. Islam, C. E. Soccolich, J. Gordon, and U. C. Paek, "Soliton intensity-dependent polarization rotation," *Opt. Lett.*, vol. 15, p. 21-23, 1990.

[53] M. Hofer, M. E. Fermann, F. Haberl, M. H. Ober, and A. J. Schmidt, "Mode locking with cross-phase and self-phase modulation," *Opt. Lett.*, , p. 502, 1991.

[54] E. Ippen, H. Haus, and L. Liu, "Additive pulse mode locking," *J. of the Opt. Soc. of Amer. B (Optical Physics)*, vol. 6, p. 1736, 1989.

[55] H. Haus, J. Fujimoto, and E. Ippen, "Structures for additive pulse mode locking," *J. of the Opt. Soc. of Amer. B (Optical Physics)*, vol. 8, p. 2068, 1991.

[56] I. Duling, "Subpicosecond all-fibre erbium laser," *Electron. Lett.*, vol. 27, p. 544, 1991.

[57] D. J. Richardson, R. I. Laming, D. N. Payne, M. W. Phillips, and V. J. Matsas, "320 fs soliton generation with passively mode-locked erbium fibre laser," *Electron. Lett.*, vol. 27, p. 730, 1991.

[58] M. Zirngibl, L. W. Stulz, J. Stone, J. Hugi, D. DiGiovanni, and P. B. Hansen, "1.2 ps pulses from passively mode-locked laser diode pumped Er^{+3} fibre ring laser," *Electron. Lett.*, vol. 27, p. 19, 1991.

[59] E. A. DeSouza, C. E. Soccolich, W. Pleibel, R. H. Stolen, M. N. Islam, J. R. Simpson, and D. J. DiGiovanni, "Saturable absorber mode-locked polarization maintaining erbium-doped fibre laser," *Electron. Lett.*, vol. 29, p. 447, 1993.

[60] M. Nakazawa, E. Yoshida, and Y. Kimura, "Generation of 98 fs optical pulses directly from an erbium-doped fibre ring laser at 1.57 μm," *Electron. Lett.*, vol. 29, p. 63, 1993.

[61] D. J. Jones, H. A. Haus, and E. P. Ippen, "Subpicosecond solitons in an actively mode-locked fiber laser," *Opt. Lett.*, vol. 21, p. 1818, 1996.

[62] L. E. Nelson, D. J. Jones, K. Tamura, H. A. Haus, and E. P. Ippen, "Ultrashort-pulse fiber ring lasers," *Appl. Phys. B*, vol. 65, p. 277, 1997.

[63] A. Siegman, *Lasers*. Mill Valley, CA: University Science Books, 1986.

[64] I. P. Alcock, A. I. Ferguson, D. C. Hanna, and A. C. Tropper, "Mode-locking of a neodymium-doped monomode fibre laser," *Electron. Lett.*, vol. 22, p. 268, 1986.

[65] G. Geister and R. Ulrich, "Neodymiym-fibre laser wth integrated-optic mode locker," *J. Opt. Commun*, vol. 68, p. 187, 1988.

[66] D. C. Hanna, A. Kazer, M. W. Phillips, D. P. Shepherd, and P. J. Suni, "Active mode-locking of an Yb:Er fibre laser," *Electron. Lett.*, vol. 25, p. 95, 1989.

[67] J. D. Kafka, T. Baer, and D. W. Hall, "Mode-locked erbium-doped fibre laser with soliton pulse shaping," *Opt. Lett.*, vol. 14, p. 1269, 1989.

[68] A. Takada and H. Miyazawa, "30-GHz picosecond pulse generation from actively mode-locked erbium-doped fibre laser filters," *Electron. Lett.*, vol. 26, p. 216, 1990.

[69] E. Yoshida, Y. Kimura, and M. Nakazawa, "Laser diode-pumped femtosecond erbium-doped fiber laser with a sub-ring cavity for repetition rate control," *Appl. Phys. Lett.*, vol. 60, p. 932, 1992.

[70] G. T. Harvey and L. F. Mollenauer, "Harmonically mode-locked fiber ring laser with an internal Fabry-Perot stabilizer for soliton transmission," *Opt. Lett.*, vol. 18, p. 107, 1993.

[71] C. R. Doerr, H. A. Haus, E. P. Ippen, M. Shirasaki, and K. Tamura, "Additive-pulse limiting," *Opt. Lett.*, vol. 19, p. 31, 1994.

[72] M. Nakazawa, K. Tamura, and E. Yoshida, "Supermode noise suppression in a harmonically mode-locked fibre laser by self phase modulation and spectral filtering," *Electron. Lett.*, vol. 32, p. 461, 1996.

[73] K. Tamura and M. Nakazawa, "Pulse energy equalization in harmonically FM mode-locked lasers with slow gain," *Opt. Lett.*, vol. 21, p. 1930, 1996.

[74] X. Shan, D. Cleland, and A. Ellis, "Stabilising Er fibre soliton laser with pulse phase locking," *Electron. Lett.*, vol. 28, p. 182, 1992.

[75] M. Nakazawa, E. Yoshida, and Y. Kimura, "Ultrastable harmonically and regeneratively modelocked polarisation-maintaining erbium fibre ring laser," *Electron. Lett.*, vol. 30, p. 1603, 1994.

[76] K. Tamura and M. Nakazawa, "Dispersion-tuned harmonically mode-locked fiber ring laser for self-synchronization to an external clock," *Opt. Lett.*, vol. 24, p. 1984, 1996.

[77] C. R. Doerr, H. A. Haus, and E. P. Ippen, "Asynchronous soliton modelocking," *Opt. Lett.*, vol. 19, p. 1958, 1994.

[78] H. A. Haus, D. J. Jones, E. P. Ippen, and W. S. Wong, "Theory of Soliton Stability in Asynchronous Modelocking," *IEEE J. Lightwave Technol.*, vol. 14, p. 622, 1996.

[79] P. V. Mamyshev and L. F. Mollenauer, "Stability of soliton propagation with sliding-frequency guiding filters," *Opt. Lett.*, vol. 19, p. 2083, 1994.

[80] D. J. Kuizenga and A. E. Siegman, "FM and AM Mode Locking of the Homogeneous Laser-Part I: Theory," *IEEE J. Quantum Electron.*, vol. 6, p. 694, 1970.

[81] H. A. Haus and Y. Silberberg, "Laser Mode Locking with Addition of Nonlinear Index," *IEEE J. Quantum Electron.*, vol. 22, p. 325, 1986.

[82] O. E. Martinez, R. L. Fork, and J. P. Gordon, "Theory of passively mode-locked lasers including self-phase modulation and group-velocity dispersion," *Opt. Lett.*, vol. 9, p. 156, 1984.

[83] M. W. Phillips, A. I. Ferguson, and D. C. Hanna, "Frequency-modulation mode locking of a Nd+3-doped fiber laser," *Opt. Lett.*, vol. 14, p. 219, 1989.

[84] D. Burns and W. Sibbett, "Controlled amplifier mode-locked Erbium fiber ring laser," *Electron. Lett.*, vol. 26, p. 505, 1990.

[85] R. P. Davey, N. Langford, and A. I. Ferguson, "Subpicosecond pulse generation from Erbium doped fiber laser," *Electron. Lett.*, vol. 27, p. 726, 1991.

[86] K. Smith, J. R. Armitage, R. Wyatt, and N. J. Doran, "Erbium fiber soliton laser," *Electron. Lett.*, vol. 26, p. 1149, 1990.

[87] F. X. Kartner, D. Kopf, and U. Keller, "Solitary-pulse stablization and shortening in actively mode-locked lasers," *J. Opt. Soc. Am. B*, vol. 12, p. 486, 1995.

[88] H. A. Haus and A. Mecozzi, "Long term storage of a bit stream of solitons," *Opt. Lett.*, vol. 17, p. 1500, 1992.

[89] H. A. Haus and A. Mecozzi, "Noise of Mode-Locked Lasers," *IEEE J. Quantum Electron.*, vol. 29, p. 983, 1993.

[90] K. Tamura, C. R. Doerr, H. A. Haus, and E. P. Ippen, "Soliton fiber ring laser stablization and tuning with a broad intracavity filter," *IEEE Photonics Technol. Lett.*, vol. 6, p. 697, 1994.

[91] D. J. Jones, K. L. Hall, H. A. Haus, and E. P. Ippen, "Asynchronous phase-modulated optical fiber ring buffer," *Opt. Lett.*, vol. 23, p. 177, 1998.

[92] R. Langenhorst, M. Eiselt, W. Pieper, and G. Grosskopf, "Fiber loop optical buffer," *IEEE J. Lightwave Technol.*, vol. 14, p. 324, 1996.

[93] C. R. Doerr, W. S. Wong, H. A. Haus, and E. P. Ippen, "Additive-pulse mode-locking/ limiting storage ring," *Opt. Lett.*, vol. 19, p. 1747, 1994.

[94] K. L. Hall and K. A. Rauschenbach, "All-optical buffering of 40-Gb/s data packets," *IEEE Photonics Tech. Lett.*, vol. 10, p. 442, 1998.

[95] J. D. Moores, W. S. Wong, and K. L. Hall, "50-Gbit/s optical pulse storage ring using novel rational harmonic modulation," *Opt. Lett.*, vol. 20, p. 2547, 1995.

[96] G. D. Bartolini, D. K. Serkland, P. Kumar, and W. L. Kath, "All-optical storage of a picosecond-pulse packet using parametric amplification," *IEEE Photonics Technol. Lett.*, vol. 9, p. 1020, 1997.

[97] A. Mecozzi, W. L. Kath, P. Kumar, and C. G. Goedde, "Long-term storage of a soliton bit stream by use of phase-sensitive amplification," *Opt. Lett.*, vol. 19, p. 2050, 1994.

[98] R. Lang and K. Kobayashi, "Suppression of the relaxation oscillation in the modulated output of semiconductor lasers," *IEEE J. Quantum Electron.*, vol. 12, p. 194, 1976.

[99] E. A. Golovchenko, A. N. Pilipetskii, C. R. Menyuk, J. Gordon, and L. Mollenauer, "Soliton propagation with up- and down-sliding-frequency guiding filters," *Opt. Lett.*, vol. 20, p. 539, 1995.

[100] M. E. Fermann, A. Galvanauskas, G. Sucha, and D. Harter, "Fiber-lasers for ultrafast optics," *Appl. Phys. B*, vol. 65, p. 259, 1997.

[101] I. N. Duling, *Compact Sources of Ultrashort Pulses*. Cambridge, UK: Cambridge University Press, 1995.

[102] B. Collings, K. Bergman, S. Cundiff, S. Tsuda, J. Kutz, J. Cunningham, W. Jan, M. Koch, and W. Knox, "Short cavity erbium ytterbium fiber lasers mode-locked with a saturable Bragg reflector," *IEEE J. of Sel. Top. in Quantum Electron.*, vol. 3, p. 1065, 1997.

[103] K. Shuto, K. Hattori, T. Kitagawa, Y. Ohmori, and M. Horiguchi, "Erbium-doped phosphosilicate glass waveguide amplifier fabricated by PECVD," *Electron. Lett.*, vol. 29, p. 139, 1993.

[104] R. N. Ghosh, J. Shmulovich, C. F. Kane, M. R. X. de Barros, G. Nykolak, A. J. Bruce, and P. C. Becker, "8-mW threshold Er-doped planar waveguide amplifier," *IEEE Photonics Technol. Lett.*, vol. 8, p. 518, 1996.

[105] S. M. J. Kelly, "Characteristic sideband instability of periodically amplified average soliton," *Electron. Lett.*, vol. 28, p. 806, 1992.

[106] J. P. Gordon, "Dispersive perturbations of solitons of the nonlinear Schroedinger equation," *J. Opt. Soc. Amer. B*, vol. 9, p. 91, 1992.

[107] S. M. J. Kelly, K. Smith, K. J. Blow, and N. J. Doran, "Average soliton dynamics of a high-gain erbium fiber laser," *Opt. Lett.*, vol. 16, p. 1337, 1991.

[108] K. Tamura, H. A. Haus, and E. P. Ippen, "Self-starting additive pulse mode-locked erbium fibre ring laser," *Electron. Lett.*, vol. 28, p. 2226, 1992.

[109] D. Richardson, J. , R. I. Laming, D. N. Payne, M. W. Phillips, and V. Matsas, "Pulse repetition rates in passive, self-starting, femtosecond soliton fibre laser," *Electron. Lett.*, vol. 27, p. 1451, 1991.

[110] V. Matsas, T. Newson, D. Richardson, and D. Payne, "Self-starting passively mode-locked fibre ring soliton laser exploiting nonlinear polarisation rotation," *Electron. Lett.*, vol. 28, p. 1391, 1992.

[111] J. M. P. Delavaux, S. Granlund, O. Mizuhara, L. D. Tzeng, D. Barbier, M. Rattay, F. St. Andre, and A. Kevorkian, "Integrated optics Erbium-Ytterbium amplifier system in 10-Gb/s fiber transmission experiment," *IEEE Photonics Technol. Lett.*, vol. 9, p. 247, 1997.

[112] S. Lovold, P. F. Moulton, D. K. Killinger, and N. Menyuk, "Frequency tuning characteristics of a Q-switched C:MgF_2 laser," *IEEE J. of Quantum Electron.*, vol. 21, p. 202, 1985.

[113] D. J. Jones, S. Namiki, D. Barbier, H. A. Haus, and E. P. Ippen, "Passively mode-locked fiber laser using an Er-Yb co-doped planar waveguide amplifier," Optical Fiber Communications '98, p. 377, San Jose, 1998.

[114] D. J. Jones, S. Namiki, D. Barbier, H. A. Haus, and E. P. Ippen, "116-fs soliton source based on an ErYb-codoped planar waveguide amplifier," *IEEE Photonics Tech. Lett.*, vol. 10, p. 666, 1998.

[115] K. Tamura, C. R. Doerr, L. E. Nelson, H. A. Haus, and E. P. Ippen, "Technique for obtaining high-energy ultrashort pulses from an additive-pulse mode-locked erbium-doped fiber ring laser," *Opt. Lett.*, vol. 19, p. 46, 1994.

[116] U. Keller, K. J. Weingarten, F. X. Kartner, D. Kopf, B. Braun, I. D. Jung, R. Fluck, C. Honninger, M. N., and J. Aus der Au, "Semiconductor saturable absorber mirrors (SESAM's) for femtosecond to nanosecond pulse generation in solid-state lasers," *IEEE J. of Sel. Top. in Quantum Electron.*, vol. 2, p. 435, 1996.

[117] S. Tsuda, W. H. Knox, S. T. Cundiff, W. Y. Jan, and J. E. Cunningham, "Mode-locking ultrafast solid-state lasers with saturable bragg reflectors," *IEEE J. of Sel. Top. in Quantum Electron.*, vol. 2, p. 454, 1996.

[118] M. H. Ober, M. Hofer, U. Keller, and T. H. Chiu, "Self-starting diode-pumped femtosecond Nd fiber laser," *Opt. Lett.*, vol. 18, p. 1532, 1993.

[119] F. X. Kartner, L. R. Brovelli, D. Kopf, M. Kamp, I. Calasso, and U. Keller, "Control of solid-state laser dynamics by semiconductor devices," *Optical Engineering*, vol. 34, p. 2024, 1995.

[120] K. Tamura, E. P. Ippen, H. A. Haus, and L. E. Nelson, "77-fs pulse generation from a stretched-pulse mode-locked all-fiber ring laser," *Opt. Lett.*, vol. 18, p. 1080, 1993.

[121] M. C. Nuss, W. H. Knox, and U. Koren, "Scalable 32 channel chirped-pulse WDM source," *Electron. Lett.*, vol. 32, p. 1311, 1996.

[122] G. Lenz, W. Gellermann, D. J. Dougherty, K. Tamura, and E. P. Ippen, "Femtosecond fiber laser pulses amplified by a KCl:Tl+ color-center amplifier for continuum generation in the 1.55 micron region," *Opt. Lett.*, vol. 21, p. 137, 1996.

[123] M. Hofer, M. H. Ober, F. Haberl, M. E. Fermann, E. R. Taylor, and K. P. Jedrzejewski, "Regenerative Nd:glass amplifier seeded with a Nd:fiber laser," *Opt. Lett.*, vol. 17, p. 807, 1992.

[124] K. Tamura, E. P. Ippen, and H. A. Haus, "Pulse dynamics in stretched-pulse fiber lasers," *Appl. Phys. Lett.*, vol. 67, p. 158, 1995.

[125] L. E. Nelson, S. B. Fleischer, G. Lenz, and E. P. Ippen, "Efficient frequency doubling of a femtosecond fiber laser," *Opt. Lett.*, vol. 21, p. 1759, 1996.

[126] D. J. Jones, L. E. Nelson, H. A. Haus, and E. P. Ippen, "Diode-pumped environmentally stable stretched-pulse fiber laser," *IEEE J. of Sel. Top. in Quantum Electron.*, vol. 3, p. 1076, 1997.

[127] D. J. Jones, H. A. Haus, L. E. Nelson, and E. P. Ippen, "Stretched-pulse generation and propagation," *IEICE Transations of Electron.*, vol. E81-C, p. 180, 1998.

[128] M. E. Fermann, L. M. Yang, M. L. Stock, and M. J. Andrejco, "Environmentally stable Kerr-type mode-locked erbium fiber laser producing 360 fs pulses," *Opt. Lett.*, vol. 19, p. 43, 1994.

[129] M. Martinelli, "A universal compensator for polarization changes induced by birefringence on a retracing beam," *Opt. Communications*, vol. 72, p. 341, 1989.

[130] T. F. Carruthers, I. N. Duling, and M. L. Dennis, "Active-passive modelocking in a single-polarisation erbium fibre laser," *Electron. Lett.*, vol. 30, p. 1051, 1994.

[131] T. F. Carruthers and I. N. Duling, "10-GHz, 1.3-ps erbium fiber laser employing soliton pulse shortening," *Opt. Lett.*, vol. 21, p. 1927, 1996.

[132] K. Tamura, J. Jacobson, E. P. Ippen, H. A. Haus, and J. G. Fujimoto, "Unidirectional ring resonators for self-starting passively mode-locked lasers," *Opt. Lett.*, vol. 18, p. 220, 1993.

[133] F. Krasuz and T. Brabec, "Passive mode locking in standing wave laser resonators," *Opt. Lett.*, vol. 18, p. 888, 1993.

[134] H. A. Haus, K. Tamura, L. E. Nelson, and E. P. Ippen, "Stretched-pulse additive pulse mode-locking in fiber ring lasers: theory and experiment," *IEEE J. Quantum Electron.*, vol. 31, p. 591, 1995.

[135] K. Tamura and M. Nakazawa, "Optimizing power extraction in stretched-pulse fiber ring lasers," *Appl. Phys. Lett.*, vol. 67, p. 3691, 1995.

[136] D. J. Jones, Y. Chen, H. A. Haus, and E. P. Ippen, "Resonant sideband generation in stretched-pulse fiber lasers," *Opt. Lett.*, vol. 23, p. 1535, 1998.

[137] Y. Chen and H. A. Haus, "Dispersion-managed 'solitons" in net positive dispersion regime," to appear in *J. Opt. Soc. Am. B.*

[138] Y. Chen and H. A. Haus, *private communication.*

[139] M. L. Dennis and I. N. Duling, "Third-order dispersion in femtosecond fiber lasers," *Opt. Lett.*, vol. 19, p. 1750, 1994.

[140] F. Matera, A. Mecozzi, M. Romagnoli, and M. Settembre, "Sideband instability induced by periodic power variations in long-distance fiber links," *Opt. Lett.*, vol. 18, p. 1499, 1993.

[141] J. H. B. Nijhof, N. J. Doran, W. Forysiak, and F. M. Knox, "Stable soliton-like propagation in dispersion managed systems with net anomalous, zero and normal dispersion," *Electron. Lett.*, vol. 33, p. 1726, 1997.

[142] V. S. Grigoryan and C. R. Menyuk, "Dispersion-managed solitons at normal average dispersion," *Opt. Lett.*, vol. 23, p. 609, 1998.

[143] M. Nakazawa, H. S. A. Kubota, and K. Tamura, "Marked increase in the power margin through the use of a dispersion-allocated soliton," *IEEE Photonics Technol. Lett.*, vol. 8, p. 1088, 1996.

THESIS PROCESSING SLIP

FIXED FIELD: ill. _____ name _____

index _____ biblio _____

▶ **COPIES:** (Archives) Aero Dewey (Eng) Hum

Lindgren Music Rotch Science

TITLE VARIES: ▶☐ _____

_____

_____

NAME VARIES: ▶☐ _____

_____

IMPRINT: **(COPYRIGHT)** _____

_____

▶ **COLLATION:** 116 ℓ _____

_____

▶ **ADD: DEGREE:** _____ ▶ **DEPT.:** _____

SUPERVISORS: _____

_____

_____ _____ _____

_____ _____ _____

_____ _____ _____

_____ _____ _____

_____ _____ _____

_____ _____ _____

_____ _____ _____

NOTES:

_____ cat'r: _____ date:

page:

▶ **DEPT:** E. E. ▶ F50

▶ **YEAR:** 1999 ▶ **DEGREE:** Ph. D.

▶ **NAME:** JONES, David John

_____